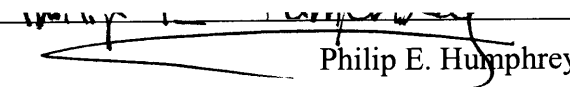


## AN ABSTRACT OF THE THESIS OF

Heiko Thömen for the degree of Doctor of Philosophy in Forest Products presented on May 23, 2000. Title: Modeling the Physical Processes in Natural Fiber Composites During Batch and Continuous Pressing.

Signature redacted for privacy.

Abstract approved:

  
Philip E. Humphrey

A three-dimensional model based on fundamental principles to simulate heat and mass transfer and mat densification during hot pressing of wood-based composites is presented. Mechanisms included in the analysis are water vapor and air transfer by gas convection and molecular gas diffusion, conductive and convective heat transfer, and sorptive effects, as well as densification of the material and development of internal stresses. The implementation of the model enables one to simulate the local evolution of temperature, moisture content, vapor and air pressure, density and internal stresses, as well as overall heat and gas flow patterns.

The model consists of a set of constitutive flux equations that are coupled by local energy and mass balances, combined with a one-dimensional rheological model. Non-linear dependencies of the material and gas properties are accounted for. A particular modeling approach is developed and implemented to simulate the pressing process not only in batch but also in continuous presses.

The numerical results of the model are in good agreement with those of experiments performed in a large-size laboratory press and an industrial continuous press. A small selection of topics important during hot pressing is given particular attention by means of model predictions. Among these are considerations of the importance of different heat transfer mechanisms and how they vary over space and time, and changes in gas composition inside the mat throughout the process.

The model may be used in the future to optimize the manufacture of existing natural fiber composites and to aid in the development of new products and technology for their production.

**MODELING THE PHYSICAL PROCESSES IN NATURAL FIBER COMPOSITES  
DURING BATCH AND CONTINUOUS PRESSING**

by

**HEIKO THÖMEN**

**A THESIS**

submitted to

Oregon State University

in partial fulfillment of  
the requirements for the  
degree of

Doctor of Philosophy

Presented May 23, 2000  
Commencement June 2001

Doctor of Philosophy thesis of Heiko Thömen presented on May 23, 2000

APPROVED:

Signature redacted for privacy.

---

Major Professor, representing Forest Products

Signature redacted for privacy.

---

Head of Department of Forest Products

Signature redacted for privacy.

---

Dean of Graduate School

I understand that my thesis will become part of the permanent collection of Oregon State University libraries. My signature below authorizes release of my thesis to any reader upon request.

Signature redacted for privacy.

---

Heiko Thömen, Author

## ACKNOWLEDGMENT

Foremost, I wish to thank Phil Humphrey, my advisor, for his guidance, support, and friendship. This work would not have been possible without his knowledge, ideas, and his patience.

Thanks are also due to Dr. Andreas Steffen with whom I have greatly enjoyed working over the past several years. His professional capabilities and organizational talent were essential for the successful realization of this research. My special thanks are extended to Prof. Dr. A. Frühwald for continually supporting me during the course of my doctorate.

I think back with gratitude to Günter Schneider who helped me to get started with the programming as well as my life in Corvallis. Numerous others both in Germany and the United States have provided useful suggestions, valuable criticism, and interesting discussions about my research.

Furthermore, I would like to express my thanks to all my dear friends for giving me company and support, especially at difficult times, and who made the last four years a wonderful time.

Lastly, I thank Angela for her love, understanding and motivation, and without whom I would have never enjoyed the music so much.

## TABLE OF CONTENTS

<b>1. INTRODUCTION</b> .....	1
<b>1.1 BACKGROUND</b> .....	1
<b>1.2 OBJECTIVES</b> .....	3
<b>2. LITERATURE REVIEW</b> .....	5
<b>2.1 INTRODUCTION</b> .....	5
<b>2.2 EFFECT OF DENSITY PROFILE ON PANEL PROPERTIES</b> .....	6
<b>2.3 MECHANISMS OPERATIVE DURING PRESSING</b> .....	8
2.3.1 MOISTURE MOVEMENT AND HEAT TRANSFER.....	8
2.3.1.1 Introduction.....	8
2.3.1.2 Heat conduction .....	12
2.3.1.3 Gas convection.....	15
2.3.1.4 Gas diffusion.....	18
2.3.1.5 Hygroscopic relationships.....	24
2.3.2 MAT DENSIFICATION AND STRESS RELAXATION .....	28
2.3.2.1 Introduction.....	28
2.3.2.2 Rheological behavior of wood-furnish mats.....	30
2.3.2.3 Factors influencing rheological behavior.....	34
2.3.2.4 Factors affecting cross-sectional density profile.....	39
2.3.2.5 Modeling cross-sectional density profiles .....	41
<b>2.4 INTEGRATED MODELS</b> .....	42
<b>3. MODEL DESCRIPTION</b> .....	48
<b>3.1 INTRODUCTION</b> .....	48
<b>3.2 MODEL DEVELOPMENT</b> .....	49
3.2.1 PROBLEM STATEMENT AND ASSUMPTIONS .....	49
3.2.1.1 The modeling system .....	49
3.2.1.2 Mass transfer.....	50
3.2.1.3 Supply and transfer of heat .....	51
3.2.1.4 Equilibrium assumptions .....	52
3.2.1.5 Rheology.....	54
3.2.1.6 Physical properties .....	55
3.2.1.7 Summary of important assumptions .....	55
3.2.2 MATHEMATICAL FORMULATION .....	56
3.2.2.1 Mass transfer.....	56

3.2.2.2	Heat transfer.....	58
3.2.2.3	Sorption equilibrium.....	60
3.2.2.4	Thermodynamic relationships.....	60
3.2.2.5	Mat densification and stress relaxation.....	62
3.2.3	INITIAL AND BOUNDARY CONDITIONS.....	69
3.2.3.1	Initial conditions.....	69
3.2.3.2	Boundary conditions.....	70
<b>3.3</b>	<b>PHYSICAL PROPERTIES.....</b>	<b>73</b>
3.3.1	MATERIAL PROPERTIES.....	73
3.3.1.1	Permeability.....	74
3.3.1.2	Obstruction factor for molecular diffusion.....	75
3.3.1.3	Thermal conductivity.....	76
3.3.1.4	Specific heat.....	77
3.3.1.5	Hygroscopicity.....	79
3.3.1.6	Heat of sorption and heat of evaporation.....	80
3.3.1.7	Rheological data.....	80
3.3.2	PROPERTIES OF VAPOR-AIR MIXTURES.....	85
3.3.2.1	Viscosity.....	85
3.3.2.2	Molecular diffusion coefficient.....	86
<b>3.4</b>	<b>NUMERICAL PROCEDURE.....</b>	<b>87</b>
3.4.1	CLASSIFICATION OF THE EMPLOYED NUMERICAL METHOD.....	87
3.4.2	UNDERLYING CONCEPT FOR HEAT AND MASS TRANSFER.....	88
3.4.3	GRID AND TIME STEPS.....	89
3.4.4	STABILITY.....	91
3.4.5	SEQUENCE OF COMPUTATION.....	93
3.4.5.1	Conductive heat flow.....	93
3.4.5.2	Inner time loop.....	94
3.4.5.3	Rheology.....	96
3.4.5.4	Update variables of state.....	97
3.4.6	MODEL IMPLEMENTATION.....	98
<b>4.</b>	<b>THE CONTINUOUS PRESS.....</b>	<b>99</b>
<b>4.1</b>	<b>INTRODUCTION.....</b>	<b>99</b>
<b>4.2</b>	<b>CHARACTERISTICS OF THE PROCESS.....</b>	<b>99</b>
<b>4.3</b>	<b>SPECIFIC ASPECTS OF CONTINUOUS PRESS MODELING.....</b>	<b>102</b>
<b>4.4</b>	<b>BOUNDARY CONDITIONS.....</b>	<b>104</b>

<b>5. PREDICTIONS OF THE MODEL</b> .....	106
<b>5.1 INTRODUCTION</b> .....	106
<b>5.2 EVALUATION OF BATCH PRESS MODEL PREDICTIONS</b> .....	106
5.2.1 SPECIFICATION OF INPUT CONDITIONS.....	107
5.2.2 PRESENTATION AND DISCUSSION OF MODEL PREDICTIONS .....	110
5.2.2.1 Surface layer ( $z = 1$ ) behavior.....	112
5.2.2.2 Intermediate layer ( $z = 4$ ) behavior.....	114
5.2.2.3 Core layer ( $z = 10$ ) behavior .....	115
5.2.2.4 Time dependent changes in layer density .....	116
5.2.3 COMPARISON OF MODEL PREDICTIONS WITH MEASUREMENTS .....	118
5.2.3.1 Temperature and gas pressure.....	119
5.2.3.2 Cross-sectional density profile.....	123
5.2.3.3 Cross-sectional moisture profile .....	125
5.2.3.4 Pressing pressure.....	126
<b>5.3 EVALUATION OF CONTINUOUS PRESS MODEL PREDICTIONS</b> .....	128
5.3.1 SPECIFICATION OF INPUT CONDITIONS.....	129
5.3.2 PRESENTATION AND DISCUSSION OF MODEL PREDICTIONS .....	131
5.3.2.1 Gas pressure predictions .....	131
5.3.2.2 Temperature predictions .....	133
5.3.2.3 Moisture content predictions.....	135
5.3.2.4 Density profile predictions.....	136
5.3.3 COMPARISON OF MODEL PREDICTIONS WITH MEASUREMENTS .....	138
<b>5.4 SELECTED ASPECTS OF THE PHYSICS</b> .....	140
5.4.1 HEAT TRANSFER MECHANISMS.....	140
5.4.2 AIR INSIDE THE MAT.....	144
5.4.3 CROSS-SECTIONAL GAS PRESSURE DISTRIBUTION .....	147
<b>6. CONCLUSIONS AND OUTLOOK</b> .....	151
<b>BIBLIOGRAPHY</b> .....	154
<b>APPENDICES</b> .....	165
A Measurement of the obstruction factor for molecular diffusion.....	167
B Measurements in a large-size laboratory press .....	169
C Measurements in an industrial continuous press .....	176

D	Derivation of conservation equations .....	181
E	Variation of relative humidity with wood EMC and temperature.....	186
F	Constants for Equations 3.62 and 3.65 for fiber mats .....	187



## LIST OF FIGURES

<u>Figure</u>	<u>Page</u>
2.1	Progressing zone of evaporation and condensation ..... 9
2.2	Typical temperature curves measured at surface, central plane and two intermediate positions in a particleboard pressed in a laboratory press..... 10
2.3	Typical internal gas pressure curves measured at the central plane of a 15-mm particleboard pressed in an industrial batch press ..... 11
2.4	Comparison of measurements (solid symbols) and extrapolations (×) of equilibrium moisture content at elevated temperatures for two levels of relative humidity (RH)..... 26
2.5	A typical pressing schedule in a continuous press for particleboard ..... 30
2.6	Five-element Burger-Humphrey model, representing four strain components .... 32
2.7	Cross-sectional density profile of a particleboard prior to sanding ..... 40
2.8	Main mechanisms operative within wood-furnish mats during hot pressing ..... 43
3.1	The four strain components described by the Burger-Humphrey model as a function of stress and time ..... 63
3.2	Kelvin model..... 66
3.3	Measured and extrapolated sorption isophsyrens for beech presented by Engelhardt (1979) ..... 79
3.4	Stress-density relationship during densification of a fiber mat at 80°C for four different moisture levels, calculated from Equation (3.62)..... 83
3.5	(a) Two-dimensional schematic of flow through a control region. Note: the model does operate in three dimensions. (b) Two simple profile assumptions..... 89
3.6	(a) Three-dimensional segment of model grid. (b) Locations of control regions and grid points..... 90
3.7	Diagram of adaptive time step scheme ..... 91
3.8	Exaggerated sketch of two adjacent control regions in the in-feed section of a continuous press..... 94

<u>Figure</u>	<u>Page</u>
3.9 (a) Illustration of the procedure used for equalization of total gas pressure through a cross-section of the mat. (b) Schematic showing gas pressure distributions before and after the iterative relaxation procedure .....	96
4.1 A cross-section of the center zone of a typical continuous press .....	100
4.2 Schematic of a typical continuous press .....	101
4.3 Example of an in-feed section.....	101
4.4 Schematic of the modeling mat segment passing through the continuous press .....	102
4.5 Modeling mat segment with grid clustered around reference regions.....	103
4.6 Schematic of the model boundaries .....	105
5.1 Specified pressing schedule for simulation of batch press trial 1 .....	109
5.2 Predicted temperature development within the mat at ten cross-sectional positions in the horizontal center .....	110
5.3 Predicted moisture content development within the mat at ten cross-sectional positions in the horizontal center .....	111
5.4 Predicted gas pressure development within the mat at ten cross-sectional positions in the horizontal center .....	111
5.5 Predicted density development within the mat at ten cross-sectional positions in the horizontal center .....	112
5.6 Schematic of mat with positions of temperature and gas pressure probes .....	119
5.7 Comparison of measured (a) and predicted (b) temperature and total gas pressure development within the mat .....	121
5.8 Comparison of measured (a) and predicted (b) total gas pressure in the center of the mat ( <i>P1</i> position in Figure 5.6).....	122
5.9 Comparison of cross-sectional density profile in the horizontal center of the panel.....	123
5.10 Comparison of cross-sectional moisture profile in the horizontal center of the panel.....	125
5.11 Comparison of recorded (a) and predicted (b) pressing pressure .....	127

<u>Figure</u>	<u>Page</u>
5.12 Specified pressing pressure and steel belt temperature for the continuous press standard simulation run.....	130
5.13 Predicted total gas pressure distribution within the central layer of the mat .....	132
5.14 Predicted total gas pressure distribution and gas velocities (arrows) for the first 6 meters within the central layer of the mat .....	133
5.15 Predicted temperature distribution within the central x-z plane of the mat.....	134
5.16 Predicted temperature distribution at four cross-sectional positions within the central x-z plane of the mat.....	135
5.17 Predicted moisture distribution within the central x-z plane of the mat.....	136
5.18 Predicted density profile development within the central x-z plane of the mat.....	137
5.19 Total gas pressure distributions at two horizontal positions within the central layer of the mat during pressing in a continuous press .....	138
5.20 Final cross-sectional density profiles.....	139
5.21 Predicted conductive heat flux perpendicular to the mat plane over time and cross-sectional position in the horizontal center of the mat.....	141
5.22 Predicted conductive heat flux perpendicular to the mat plane over cross-sectional position in the horizontal center of the mat .....	141
5.23 Heat energy expended to increase the local temperature in the horizontal center of the mat.....	142
5.24 Contribution of convective and conductive heating over time at the central position of the mat .....	143
5.25 (a) Gas pressure and temperature measured in the central plane 900 mm from the edge (Continuous press trial 3). (b) Predicted total gas pressure, vapor pressure and air pressure in the middle of the central plane of the mat....	146
5.26 Comparison of gas pressure predictions .....	148
5.27 Measured gas pressure development in the horizontal middle of an MDF mat at two cross-sectional positions .....	149

## LIST OF TABLES

<u>Table</u>		<u>Page</u>
2.1	Diffusion coefficients based upon a bound-water concentration gradient for particleboard perpendicular and parallel to the panel plane .....	21
3.1	Coefficients for Equation (3.50) to determine in-plane and cross-sectional permeability .....	75
3.2	Constants presented by von Haas (1998) for Equation (3.60) to calculate the rheological coefficients of the four-element Burger model for fiber mats .....	82
5.1	Input conditions for simulation of batch press trial 1 .....	108
5.2	Positions of temperature and gas pressure probes in percent of mat dimensions for batch press trial 1 .....	120
5.3	Input conditions specified for the continuous press standard simulation run.....	129
5.4	Composition of the gas mixture sampled from the core layer of a particle mat during consolidation in an industrial batch press.....	144

## LIST OF APPENDIX FIGURES

<u>Figure</u>	<u>Page</u>
A.1 Obstruction factor for molecular diffusion perpendicular to the panel surface, $k_d$ , versus density $\rho$ for MDF.....	168
B.1 Schematic of mat with positions of temperature and gas pressure probes .....	169
B.2 Pressing pressure, mat thickness, internal temperature and gas pressure, measured for batch press trial 1 .....	172
B.3 Pressing pressure, mat thickness, internal temperature and gas pressure, measured for batch press trial 2 .....	173
B.4 Pressing pressure, mat thickness, internal temperature and gas pressure, measured for batch press trial 3 .....	174
B.5 Pressing pressure, mat thickness, internal temperature and gas pressure, measured for batch press trial 4 .....	175
C.1 Pressing conditions that prevailed during continuous press trial 3.....	176
C.2 Absolute gas pressure inside the mat and temperatures, measured at two positions, for continuous press trial 1 .....	178
C.3 Absolute gas pressure inside the mat and temperatures, measured at three positions, for continuous press trial 2 .....	179
C.4 Absolute gas pressure inside the mat and temperatures, measured at three positions, for continuous press trial 3 .....	179
C.5 Absolute gas pressure inside the mat and temperatures, measured at three positions, for continuous press trial 4 .....	180

## LIST OF APPENDIX TABLES

<u>Table</u>	<u>Page</u>
B.1 Positions of temperature (T) and gas pressure (P) probes as well as mat dimensions in mm for batch press trials 1 to 4 .....	170
C.1 Some pressing conditions and positions of probes for continuous press trials 1 to 4 .....	177
E.1 Variation of relative humidity [%] with wood equilibrium moisture content (EMC) and temperature .....	186
F.1 Constants for Equations 3.62 and 3.65 for fiber mats presented by von Haas (1998).....	187

## NOMENCLATURE

The listed symbols are used throughout this dissertation unless otherwise stated. Some symbols are locally defined in the appropriate locations and are not included.

$a, b, c$	constants
$c$	specific heat [ $\text{J kg}^{-1} \text{K}^{-1}$ ]
$D_{eff}$	effective diffusion coefficient [ $\text{m}^2 \text{s}^{-1}$ ]
$D_{va}$	binary diffusion coefficient of the water vapor-air pair [ $\text{m}^2 \text{s}^{-1}$ ]
$E$	rheological coefficient to describe elastic material behavior [Pa]
$H_{ev}$	latent heat of evaporation [ $\text{J kg}^{-1}$ ]
$H_l$	latent (or differential) heat of sorption from the liquid state [ $\text{J kg}^{-1}$ ]
$H_v$	latent (or differential) heat of sorption from the vapor state [ $\text{J kg}^{-1}$ ]
$j$	mass flux [ $\text{kg m}^{-2} \text{s}^{-1}$ ]
$k_d$	obstruction factor for molecular diffusion [-]
$k_p$	permeability coefficient [ $\text{m}^2$ ]
$k_t$	thermal conductivity [ $\text{W m}^{-1} \text{K}^{-1}$ ]
$l$	spatial variable or length [m]
$m$	mass [kg]
$m_{ev}$	evaporation rate [ $\text{kg m}^{-3} \text{s}^{-1}$ ]
$M$	molecular mass [ $\text{kg mol}^{-1}$ ]
$p$	gas pressure [Pa]
$q$	conductive heat flux [ $\text{J m}^{-2} \text{s}^{-1}$ ]
$Q$	energy [J]
$Q^*$	specific rate of heating [ $\text{J kg}^{-1} \text{s}^{-1}$ ]
$r$	rate of generation [ $\text{kg m}^{-3} \text{s}^{-1}$ ]
$R$	gas constant [ $\text{J mol}^{-1} \text{K}^{-1}$ ]
$t$	time [s]
$T_{(abs)}$	temperature [ $^{\circ}\text{C}$ ] or absolute temperature [K]
$u$	moisture content on a dry weight basis [-] or [%]
$u_i$	mass ratio of component $i$ [-]

$V$	rheological coefficient to describe viscous material behavior [Pa s]
$V$	volume [m <sup>3</sup> ]
$x, y, z$	spatial variables

## GREEK SYMBOLS

$\varepsilon$	strain [-]
$\eta$	dynamic viscosity [Pa s]
$\rho$	density [kg m <sup>-3</sup> ]
$\varphi$	relative humidity [-] or [%]
$\phi$	void fraction [-]
$\sigma$	stress [Pa]

## SUBSCRIPTS

0	initial
a	air
b	bound water
de	delayed elastic
el	elastic
i	inner
p	primary
pmf	plastic and micro-fracture
u	at given moisture content
v	vapor
vi	viscous
w	dry wood
$x, y, z$	spatial position or coordinate direction



**SUPERSCRIPTS**

c	convection
d	diffusion

**ABBREVIATIONS**

EMC	equilibrium moisture content
MDF	medium density fiberboard
OSB	oriented strandboard
PMF	plastic and micro-fracture

**GRADIENT OPERATOR**

$$\nabla = \hat{x} \frac{\partial}{\partial x} + \hat{y} \frac{\partial}{\partial y} + \hat{z} \frac{\partial}{\partial z} \text{ with } \hat{x}, \hat{y}, \hat{z} \text{ as unit vectors}$$

To my parents

# MODELING THE PHYSICAL PROCESSES IN NATURAL FIBER COMPOSITES DURING BATCH AND CONTINUOUS PRESSING

## 1. INTRODUCTION

### 1.1 BACKGROUND

Industrial manufacture of wood-based composites produced in the so-called 'dry process' started in the middle of the twentieth century<sup>1</sup>. The market for such composites has grown steadily over the last decades, and the growth has gone along with a diversification within this product group. Today, particleboard, medium density fiberboard (MDF) and oriented strandboard (OSB) are the most important types. Their worldwide production reached 85.5 millions m<sup>3</sup> annually in 1998 (F.A.O. 2000).

Hot pressing of the wood-furnish mat plays a crucial role in the production process of wood-based composites. The press is the most costly part of the entire process to operate; thus it determines the maximum capacity of the production line. Moreover, the in-use properties of final products depend heavily on the conditions under which the mats are pressed. A fundamental understanding of the pressing process is therefore essential for optimizing production speed, costs and energy consumption as well as manipulating board properties, and for the development of new technologies and products.

In the press, high temperatures and compaction pressures are applied to consolidate the loosely formed mat of adhesive-treated wood constituents. Heat is transferred from the heating platens to the mat surfaces, and from there towards the central plane of the mat. The heat is required to plasticize the wood particles and to cure the adhesive bonds. As a consequence of heating, moisture also migrates in the form of vapor towards the central plane and escapes through the edges of the mat. The rheological properties of the material depend interactively on temperature and moisture content. Hence, the non-uniform temperature and moisture distribution that prevails

---

<sup>1</sup> Wood-based composites include a wide range of different product groups. Throughout this dissertation the term will be used only for particle composites produced in the dry process.

during the earlier stages of the pressing cycle causes a differential densification of the mat, establishing a cross-sectional density profile. The density profile dramatically influences the properties of the product.

Considerable efforts have been made in the past to improve the understanding of the process. The effects of most important material and pressing variables on board properties and production speed have been addressed in one or another way. The determination of simple links between single production variables and output parameters is, however, difficult for a process in which many interacting events affect each other in a rather complex way.

In order to develop a scientifically based method to quantify the impact of variations in pressing conditions on process and final product, some researchers have proposed an integrated approach that considers those variables important during hot pressing not in isolation, but simultaneously. Among the first were Kavvouras (1977) and Bolton and Humphrey (1988). With this approach, along with the rapid increase of computational power, the foundation was laid to develop process models based on fundamental principles.

Some analytical models of the hot pressing process have been presented during the last two decades. It appears to be reasonable to consider that one developed by Bolton and Humphrey (Humphrey 1982, Humphrey and Bolton 1989a), and subsequently expanded by Haselein (1998), as the most advanced one so far. This model was therefore the starting point for the present work.

The model development has to be regarded as an evolutionary process. The multitude of interacting events within the wood-furnish mat during pressing makes it impossible to include all important mechanisms from the outset. Once a model has been developed, it has to be evaluated critically, and shortcomings must be addressed and tackled; further features may be necessary to add. It was the first objective of this research to refine, re-structure and supplement the existing model to improve its flexibility and the accuracy of predictions it makes. Clearly, in a broader picture this undertaking must be seen as an intermediate step, and others will come to continue the path towards more elaborate and powerful models in the future.

All analytical models developed so far simulate a batch process in which parallel heated platens press rectangular mats at rest. However, the quantitative and economical importance of the continuous pressing process has increased steadily over the last two decades. Such technology enables the mat to be pressed continuously while moving horizontally through the press between two heated steel belts. Not only does the productivity of this relatively new technology exceed that of the batch process, but it has also opened new opportunities to better manipulate board properties in desirable ways.

Results of existing models can be transferred up to a certain degree to the continuous process, since the same physical mechanisms within the mat happen in both types of machine; but there are limitations to doing so. Not all important features of the continuous process can be simulated by modifying a conventional press model. For example, the boundary conditions change in the feed direction of the continuous press. Further, air and vapor flow at the press entry and outlet has to be considered; the gas mixture escapes not only through the sides of the mat but also through its surfaces immediately in front of and behind the press. The second objective of this research work was therefore to expand the batch press model, so that these and other features of the continuous pressing process can be simulated.

The present study is part of a cooperative effort with the Ordinariat für Holztechnologie (Universität Hamburg, Germany) and the machine-building company Siempelkamp GmbH & Co. (Krefeld, Germany). Material properties input data for the model were obtained by using techniques mainly developed at Oregon State University and expanded at Universität Hamburg. Furthermore, internal temperature and gas pressure measurements in an industrial continuous press and a 4 x 8 ft. laboratory press were carried out jointly with the project partners.

## 1.2 OBJECTIVES

The main objectives of this research may be summarized as follows:

- Refine and supplement an existing process model, and write a new program code for the upgraded model.
- Develop and implement a strategy to simulate continuously working presses.

- Validate the simulation model by comparing model predictions with measurements made in a laboratory batch press and an industrial continuous press.

## 2. LITERATURE REVIEW

### 2.1 INTRODUCTION

Since the beginning of industrial wood-based panel manufacture, most research and development efforts have focused on the technical and economic optimization of both processes and products. Performance demands on panels have increased steadily over this period, while minimization of manufacturing costs per unit output was sought simultaneously. In addition, ecological aspects gained importance during the later decades. One emphasis in this respect was, and still is, the reduction of formaldehyde emissions from urea-formaldehyde bonded panels, or the development of totally formaldehyde-free adhesive systems.

Regarding technological and economic optimization, two major goals of research can be identified. The first goal has been to achieve a better understanding of the factors that influence panel properties. This goal includes attempts to minimize raw material consumption and associated costs without impairing panel properties and to optimize the panel properties without increasing the pressing time or the production costs. Although all preceding sub-processes in the manufacturing line influence panel properties, the hot press is clearly of particular importance when investigating the relationship between process parameters and panel properties.

The second research goal has been to maximize production speed. Such maximum may be dictated by panel property requirements. This implies that the two goals are closely related. In addition, a range of other limiting factors, such as the build-up of internal gas pressure within the wood-furnish mat during hot pressing, may be of significance as well.

The cross-sectional density profile clearly plays a central role in the relationship between raw material characteristics and process variables on the one hand, and panel properties on the other. The density profile is dictated by factors such as initial structure and moisture content of the wood-furnish mat and the pressing strategy employed. Important panel properties affected by the density profile are bending and internal bond strength, dimensional stability, machinability and many more. The first section of the

literature review will give an overview of research work that was done to investigate the effect of the density profile on important panel properties.

Important mechanisms operative during mat consolidation in the hot press are heat transfer, phase change of water, moisture movement, densification of the mat, stress development, and adhesive cure. An understanding of these mechanisms and their interaction is essential if we are to address the research goals stated above. Section 2.3 of this literature review will summarize previous work that has been done to investigate and describe some of these mechanisms, while section 2.4 will concern modeling approaches that integrate the internal mechanisms to simulate important aspects of the pressing process.

## **2.2 EFFECT OF DENSITY PROFILE ON PANEL PROPERTIES**

It has long been recognized that important mechanical properties of panels are closely related to density. Maku and Hamada (1955) were among the first to study the mechanical properties of single-layer flakeboards. They showed that the relation of tensile, compressive, and shear strength, and modulus of elasticity to density can be described by exponential functions; the values of all these properties are positively correlated with density.

Strickler (1959) carried out an extensive and pioneering, though empirical, study to identify important factors that influence the panel properties. To do so, he varied target density of the panel, pressing cycle, initial moisture content of the mat, and initial cross-sectional moisture distribution. For constant pressing cycles and moisture content treatments, bending strength and internal bond strength were found to be significantly influenced by the target density. However, he wisely emphasized the complex actions and reactions that occur as the adhesive polymerizes during pressing. The adhesive polymerization is obviously influenced by factors other than density. These factors may compensate for or even reverse, for example, the positive correlation that exists between density of the center layer and internal bond strength. Strickler's study clearly demonstrated the difficulties one has when trying to determine the effect of single variables on panel properties.



Additional studies have been carried out since those of Strickler to further investigate the effect of the density of an individual layer on the localized mechanical properties of that layer (e.g., Plath and Schnitzler 1974, May 1983, Xu and Winistorfer 1995). A positive correlation was generally confirmed between density and mechanical properties provided that no other factors compensate for the density effect.

Fahrni (1956) pointed out the effect of cross-sectional density profile (typically with higher surface density and lower core density) on the bulk mechanical properties of panels. Density profiles can be manipulated by adjusting the initial moisture distribution within the mat and the pressing conditions (pressing cycle and platen temperature), or they can be realized by pressing three- or multi-layer mats. The elevated tensile strength of the more densified surface layers leads to panels with increased bending strength values compared with panels of identical average density but without a pronounced density profile. The positive correlation between density of the surface layer and bending strength was confirmed by Kollmann (1957). However, Suchsland (1967) mentioned that such a shelling effect of the surface layers does not necessarily require higher surface densities. Factors such as particle geometry and ratio of panel density to particle density could also lead to a shelling effect even if the core and surface densities are similar.

It was Keylwerth (1958) who basically established the theory about the mechanics of multi-layer flakeboards. He gave a detailed description of the physical and mechanical principles of such composites and emphasized that the resulting properties of the whole panel are related to the properties of its individual layers. In addition to elasticity and the strength properties of individual layers, the ratio of surface to core layer thickness is important in determining the properties of whole panels. Keylwerth measured the modulus of elasticity as well as tensile and compressive strengths of the single layers and found a nearly linear relationship between these properties and layer density.

The cumulative effect of layer density on overall panel properties was given some further consideration during the subsequent decades, and the theory about the mechanics of multi-layer flakeboards, established by Keylwerth (1958), was repeatedly refined. While Keylwerth treated each layer as a region of constant density and properties, Plath (1971) introduced functions that consider continuous changes throughout the cross-section. This approach allowed him a more precise calculation of overall modulus of

elasticity and shear modulus for differently shaped cross-sectional density profiles. Plath derived an equation that described the modulus of elasticity as a function of maximum (regarding the different layers) modulus of elasticity, maximum density, and a variable that characterizes the shape of the cross-sectional density profile. May (1977) described an approach that takes the micro-structure of each layer into account. He proposed the use of a moment of inertia in Keylwerth's calculations that is corrected for the void spaces within the layer.

Several authors reported an effect of the cross-sectional density profile on the dimensional stability of panels. It was suggested that a pronounced cross-sectional density profile with high densities close to the surfaces leads to improved dimensional stability since the time dependent process of water sorption is retarded by the more highly densified surface layers (e.g., Boehme 1991, Boehme 1992, Xu and Winistorfer 1995).

The layer in which the fracture during an internal bond strength test occurs is repeatedly reported to not coincide with the layer of lowest density, which usually is the central layer of the panel (Xu and Winistorfer 1995, Schulte and Frühwald 1996). Preliminary simulation results of bond strength development reported by Humphrey (1991) supported this finding. These observations demonstrate again that the density cannot be the only criterion to assess the mechanical properties of the panel.

## **2.3 MECHANISMS OPERATIVE DURING PRESSING**

### **2.3.1 Moisture movement and heat transfer**

#### ***2.3.1.1 Introduction***

Moisture movement and heat transfer within the wood-furnish mat during hot pressing are physical processes that interact with each other and with other mechanisms in a complicated way. The scientific community is still far away from a complete appreciation of these interactions. However, the more general concepts concerning moisture movement and heat transfer are reasonably well understood; they have been considered by many researchers (Rackwitz 1954, Maku et al. 1959, Strickler 1959,

Gefahrt 1977, Bolton and Humphrey 1988, Kamke and Wolcott 1991, von Haas 1998). The mechanisms of heat and moisture movement can be summarized as follows.

The mat surfaces are heated through direct contact with the hot platens by means of conduction. As a consequence of the temperature increase at the surface, water, which exists in the bound state within the cell wall substance, or which is associated with the glue, evaporates. This evaporation causes an increase of the vapor pressure in the pore spaces of the outermost layer, and consequently a gas pressure gradient towards the central plane of the mat. A convective vapor flux along this gradient occurs. The vapor carries with it its heat content. When the vapor reaches a cooler layer in the mat, some of the vapor condenses<sup>2</sup>, and its inherent heat is released. A relatively rapid temperature rise in this layer goes along with an increase of the moisture content. Once the moisture content has reached its maximum, the heat that is transferred from the surfaces to this zone by conduction starts to evaporate the moisture. By this sequence the zone of evaporation and condensation moves gradually towards the central plane (Figure 2.1).

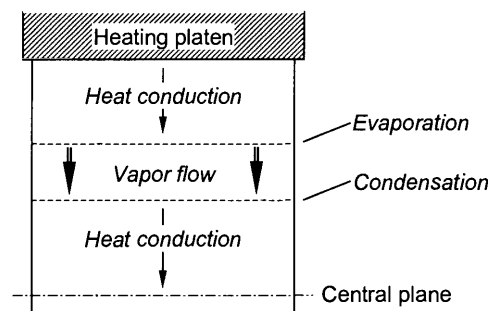


Figure 2.1. Progressing zone of evaporation and condensation. (Simplified and altered after Gefahrt 1977)<sup>3</sup>

Simultaneously with the described heat and moisture transfer from the surfaces towards the central plane of the mat, temperature and gas pressure gradients develop within its horizontal plane, and this leads to the escape of heat, moisture and air through the edges.

<sup>2</sup> The term 'condensation' is used here in a sense that includes adsorption and absorption.

<sup>3</sup> The existence of abrupt evaporation and condensation fronts is debatable, as will be discussed in section 5.2.2.2.

The temperature development at different locations can be monitored by positioning thermocouples within the loose mat before pressing. This has been done frequently in the laboratory and in the industry for all kinds of press system (e.g., Maku et al. 1959, Strickler 1959, Graser 1962, Gefahrt 1977, Kavvouras 1977). Figure 2.2 shows a typical set of such measured temperature curves for a laboratory press. After a rapid increase at the beginning, the surface temperature flattens out and approaches temperature of the hot platen. The pronounced plateau of the intermediate temperature curves at about 100°C is a consequence of condensation and evaporation of water in the respective zone. The main characteristic of the central plane temperature curve is that the temperature stays almost constant for a considerable period, before rising rapidly. The plateau at about 100°C is typical for small size laboratory presses. Due to the build-up of higher vapor pressures in industrial presses, the temperature usually continuous to rise, although decelerated, and approaches a plateau significantly higher than 100°C (see Graser 1962, Denisov and Juskov 1974, Rauch 1984). However, in practice the pressing process is usually terminated before this plateau is reached.

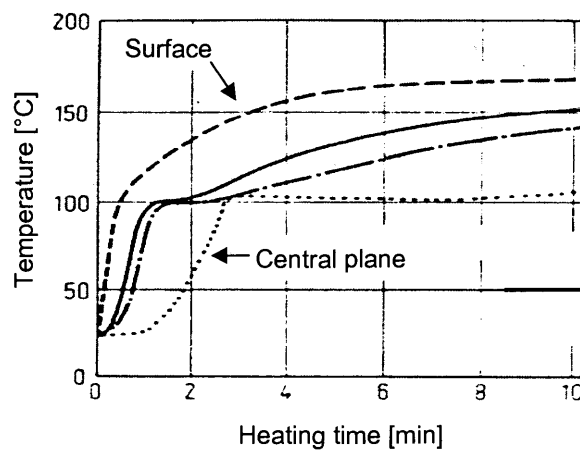


Figure 2.2. Typical temperature curves measured at surface, central plane and two intermediate positions in a particleboard pressed in a laboratory press. Platen temperature = 180 °C, initial moisture content = 10 %, density = 650 kg/m<sup>3</sup>, panel thickness = 19 mm. (Gefahrt 1977, presenting data from Meyer and Reinhardt 1976)

To determine internal gas pressure, a thin steel tube that is attached to a pressure transducer can be inserted from the side into the mat. This technique was developed and

first reported in the literature by Denisov and Sosnin (1967), and has been used by many researchers and in industrial applications since then (e.g., Kavvouras 1977, Humphrey 1982, Kamke and Casey 1988a,b). Results of a typical gas pressure measurement cycle are given in Figure 2.3. The small pressure maximum evident after 30 seconds is a consequence of compressed air when the press closes. Generation of vapor due to heating of the mat causes the subsequent major gas pressure increase. As air and vapor escape through the edges of the mat, the gas pressure drops from the horizontal center of the mat towards the edges. This can be seen from the fact that the curve for the intermediate position between center and edge of the mat lays at all times below the curve for the center.

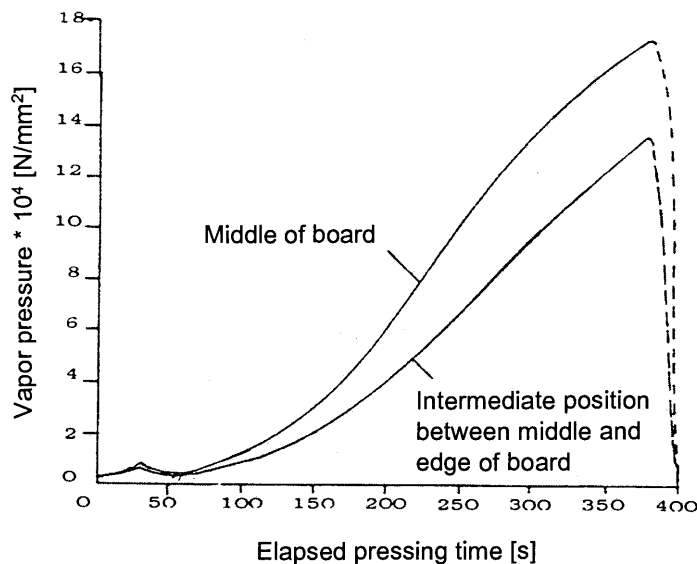


Figure 2.3. Typical internal gas pressure curves measured at the central plane of a 15-mm particleboard pressed in an industrial batch press. (Humphrey 1982)

Until recently, all gas pressure measurements reported in the literature were made in batch presses. Techniques to do such measurements in a continuous working industrial press have been developed only lately by our project group and by a Canadian group at the same time. Only some of the results of the former group have been published so far (Steffen et al. 1999).

### 2.3.1.2 Heat conduction

#### 2.3.1.2.1 General description

Conduction is the heat transfer mechanism in which energy exchange takes place in solids or in fluids at rest (i.e., no convective motion) from the region of high temperature to the region of low temperature (Ozisik 1993). The relationship between heat flow and the temperature gradient is described by Fourier's law. In its basic form this law can be written as:

$$q = -k_t \frac{dT}{dl} \quad (2.1)$$

where  $q$  denotes the conductive heat flux in  $J/(m^2 \cdot s)$ ,  $dT/dl$  the temperature gradient and  $k_t$  the thermal conductivity in  $W/(m \cdot K)$ . The minus sign reflects the fact that the heat flux occurs in the opposite direction to the temperature gradient.

The significance of conductive heat transfer varies with time and space within the mat throughout the pressing process. Gefahrt (1977) distinguishes three zones where at least part of the transferred heat is driven by conduction. These zones are the heating platen-mat interface, the outer region between the surface and the vapor front, and the inner region of the mat between the vapor front and the central plane (see Figure 2.1).

Heat conduction at the heating platen-mat interface has been described as the major heat transfer mechanism by many researchers, e.g., by Bowen (1970). Only in situations where steam or other gases are injected into (or removed from) the mat through perforated platens, may heat transfer associated with the gas flow become important (Hata et al. 1990). The role of radiation is believed to be negligible at the platen-mat interface (Strickler 1959, Humphrey and Bolton 1989a).

Some scientists describe the contact between heating platen and wood particles or between the wood particles themselves in the surface layer as poor, causing a restricted interfacial heat conduction. Strickler (1959) observed that the compaction pressure influences the temperature development in the central plane of the mat. He concluded from this that the higher compaction pressure increases the heat conduction rate at the interface. However, the effect of the compaction pressure on the core temperature may be conclusively explained simply by the higher density (and consequently higher thermal

conductivity) that was achieved when higher pressures were applied. Gefahrt (1977) introduced an interfacial heat transfer coefficient to account for poor contact between heating platen and mat. He did not describe from which observation he concluded that the contact must be poor.

Von Haas (1998) pointed out that measurements of the surface temperature are usually done with common thermocouples. These are pressed somewhat into the mat surface, so that the temperature slightly below the surface is measured rather than the actual interfacial temperature.

Although the heat transfer at the platen-mat interface is suggested by some researchers to be critical for the entire pressing process, little attention has been given to this topic so far. Clearly, for a more complete understanding of the physics at the platen-mat interface, and in particular for a quantitative description of resistance to heat conduction, further investigation is necessary.

Once the vapor front has proceeded towards the central plane, heat conduction becomes important again in the outer layers since heat has to be transferred through these layers to the zone of evaporation (Gefahrt 1977, Humphrey and Bolton 1989a). The outer layers have reached a relatively low moisture level by then so that barely any additional vapor is generated in this region that could contribute significantly to heat transfer.

Heat conduction between the vapor front and the central plane has been mentioned by Gefahrt (1977), but has been given hardly any attention by others so far. This is probably due to the fact that the amount of heat transferred by this mode was assumed to be insignificant compared to the heat that is brought in by convection at a later stage.

#### 2.3.1.2.2 Thermal conductivity measurements

A broad literature review about the effect of density, moisture content and temperature on the thermal conductivity of wood and wood-based composites has been conducted by Shao (1989). Shao herself developed an unsteady-state technique to measure the thermal conductivity of un-resinated wood fiber networks as a function of density and moisture content.

Haselein (1998) derived an equation from Shao's (1989) results that gives the thermal conductivity as a function of density and moisture content. In addition, he developed a correction term from measurements made by Kühlmann (1962) to account for the temperature effect.

Avramidis and Lau (1992) determined the thermal conductivity of wood particle networks in the density range below  $220 \text{ kg/m}^3$ , using a modified unsteady-state method that was originally developed by van der Held and van Drunen (1949) to measure the thermal conductivity of liquids. They confirmed that the thermal conductivity is usually influenced by density, moisture content and temperature in a positive way.

A method first used by Maku (1954) to measure the thermal conduction in wood was used by von Haas (1998). For different material types and moisture contents he derived polynomial functions that describe the dependency of thermal conductivity on density. Besides he carried out some orienting investigations on the effect of temperature, adhesive content, stage of curing and treatment prior to testing on thermal conductivity. Panels that were manufactured in a cold press had a 30 % lower thermal conductivity than panels pressed in a hot press. Von Haas contributed this difference to the plasticization of the material when heated, which results in larger contact areas between adjacent fibers.

Almost all measurements done so far are for mats or panels where the main fiber direction were perpendicular to the direction of heat flow. Hardly any data are available for the thermal conductivity parallel to the main fiber direction. This is due to the fact that the main fiber direction is usually parallel to the panel plane, while heat is applied to the surfaces in most experiments. However, Humphrey and Bolton (1989a) estimated from data obtained by Ward and Skaar (1963) and from their own preliminary measurements that the thermal conductivity parallel to the main fiber direction is about 50 % higher than that perpendicular. Avramidis and Lau (1992) did not explicitly comment on the fiber direction with respect to the heat source, but by the description of the experimental procedure it is likely that the wood particles were aligned parallel to the heat flow direction, as well.



### 2.3.1.3 Gas convection

#### 2.3.1.3.1 General description

In general terms, convection is of its nature a bulk motion of a liquid or a gas. The transport of the vapor-air mixture as a whole through a wood-furnish mat can be regarded as forced convection, driven by total pressure gradients that develop during pressing<sup>4</sup>.

As the mat is a capillary-porous medium with the cell wall substance as matrix and the inter-linked voids between and within the wood particles as pores, Darcy's law can be applied to describe the cross-sectional and in-plane convective flux<sup>5</sup> (Denisov 1973, Sokunbi 1978, Nketiah 1982, Bolton and Humphrey 1994). Darcy (1803 - 1858) found that the flux of a viscous fluid (which can be a liquid or a gas) in a porous medium is directly proportional to the pressure difference in the flow direction. For a gas, this relationship may be written in the form:

$$j^c = -\frac{k_p}{\eta} \frac{M}{RT_{abs}} p \frac{dp}{dl} \quad (2.2)$$

where:

$j^c$	convective mass flux [kg/(m <sup>2</sup> ·s)]
$k_p$	permeability coefficient [m <sup>2</sup> ]
$\eta$	dynamic viscosity of the gas [Pa·s]
$p$	gas pressure [Pa]
$R$	gas constant [J/(mol·K)]
$T_{abs}$	absolute temperature [K]
$M$	molecular mass [kg/mol]
$dp/dl$	gas pressure gradient [Pa/m]

It is reasonable to assume that, on a *microscopic* level, almost all of the gas flows through the void spaces between the wood particles, rather than through the pore structure within the cell walls (Lehmann 1972, Denisov et al. 1975). However, by

---

<sup>4</sup> The term 'convection' will be used throughout this work for any flow where the average velocity of all species of the gas mixture is the same. The same transport mechanism is called diffusion by some authors, referring to the mat as reference system through which the gas 'diffuses'.

<sup>5</sup> Other common terms for convective flux are viscous or Darcian flux.

applying Darcy's law, the phenomenon of gas convection is treated on a *macroscopic* level, where the mat is considered as a homogeneous continuum.

Darcy's law is only valid if the flow is laminar. In the case of turbulent flow, the flow is not proportional to the pressure gradient. Denisov et al. (1975) found a slight deviation from linearity for the transit of air through a flake mat. Von Haas et al. (1998) confirmed this finding but concluded that this deviation is small enough to enable one to describe convective flow in the mat by Darcy's law. Humphrey and Bolton (1989a) pointed out that turbulent flow may be of some significance in steam injection pressing.

Permeability is a material property that reflects the pore structure of the mat, i.e., the shape and size distribution of the pores. It is independent of the fluid (provided that the fluid does not change the pore structure) and can be expressed by the experimentally determined permeability coefficient  $k_p$ .

#### 2.3.1.3.2 Permeability measurements

Some work has been done in the past to measure the permeability of different types of wood composite mats and panels. All methods described in the literature have in common that a total pressure differential was applied to the sample, and the amount of gas flowing through the sample along the pressure gradient was measured.

As the permeability depends on the pore structure of the mat, it seems obvious that any densification will have a direct effect on the permeability. Early measurements did indeed show a strong negative correlation between density and permeability (Bowen 1970, Lehmann 1972).

During hot pressing, the density varies considerably with time and, as a consequence of the cross-sectional density profile that develops, with position within the mat. To model the hot pressing process, permeability coefficients are clearly needed that are measured for exact densities. Permeability values that were attained from measurements on panels with a pronounced density profile, and that therefore only give average values over the range of densities in the sample, cannot be used and will for that reason not be discussed here.

Denisov et al. (1975) investigated the cross-sectional permeability for one-layered flake mats. While a significant decrease of permeability with increasing density was

observed between  $300 \text{ kg/m}^3$  and  $600 \text{ kg/m}^3$ , the permeability stayed almost constant for densities above  $700 \text{ kg/m}^3$ . As such constancy for high densities appears rather unlikely by simple reasoning and contradicts the finding of Bowen (1970) and Lehmann (1972), it may be a hint that some of the gas did not flow through the sample but rather around it, causing inaccuracies of the results. Furthermore, Denisov et al. compared the results of measurements that were done with air and steam, respectively. They reported that all permeability values that were determined with steam were at least two orders of magnitude smaller than those determined with air, and conclude that this must be an effect of swelling due to higher moisture contents of the steam treated samples. However, such a pronounced effect of the moisture content is not likely. Denisov et al. apparently compared superficial permeability values and ignored the viscosity effect of the fluid on the superficial permeability when drawing their conclusions. Von Haas et al. (1998) found no moisture effect for low densities and a comparatively small moisture effect for high densities above  $900 \text{ kg/m}^3$ .

Oblivin and Dolgintsev (1976) measured the permeability of flake mats for different densities and investigated the effect of further parameters such as moisture content, adhesive content and particle size on permeability.

Wood composites that are produced in a steam injection press typically have a relatively flat density profile. Hata et al. (1993) used samples from such particleboard to measure the permeability for different density levels and investigated the impact of length, width and thickness of the wood particles. They found an almost linear positive correlation between particle thickness and permeability, and negative correlations between particle length and width, respectively, with permeability. Besides, Hata et al.'s measurements confirmed that the in-plane permeability is always larger than the cross-sectional permeability.

Christensen et al. (1987) obtained permeability values for different layers in a particleboard that had a pronounced density profile. By sanding the sample successively from the surface, and comparing the permeability values that were measured before and after sanding, they calculated the permeability value of each layer. However, the variation of permeability across the sample thickness appeared to be larger than the variation of the density, suggesting that it is not possible to achieve a high accuracy by

this method. Similar methods were used before by Sokunbi (1978) and Nketiah (1982). Bolton and Humphrey (1994) questioned the suitability of such methods to measure the density-permeability relationship, as the assumption of uniform sub-layer density may not be justified.

Haselein (1998) developed a technique to determine in-plane and cross-sectional mat permeability simultaneously as a function of compaction. Small circular mats were stepwise compressed to different thicknesses and air was blown through the perforated pressing platens. The airflow was measured at each step for two different boundary conditions. These data were then used to compute the in-plane and cross-sectional permeability values. This technique enables one to determine permeability values for different densities using the same sample. Haselein carried out measurements on un-resinated fiber mats and found good agreement between these results and data obtained from one-dimensional validation experiments.

A comprehensive study of permeability was carried out by von Haas et al. (1998) for different material types. The fiberboards, particleboards and oriented strandboards to be tested were made in a laboratory press under conditions that assured a homogeneous density over the panel thickness. Besides determining the density-permeability relation within a range of  $200 \text{ kg/m}^3$  to  $1200 \text{ kg/m}^3$ , von Haas et al. investigated the effect of adhesive content and moisture content on permeability.

### **2.3.1.4 Gas diffusion**

#### 2.3.1.4.1 General description

While convection is a motion of a gas or a liquid as a whole that is driven by total pressure differences, diffusion is a motion of the molecules of one species relative to the bulk motion. According to Fick's first law, the diffusive flux  $j^d$  is proportional to the concentration gradient  $dc/dl$  in the flow direction such that:

$$j^d = -D \frac{dc}{dl} \quad (2.3)$$

The concentration gradient can be expressed as a gradient of partial pressure, number of moles per unit volume, or moisture content. Commonly used units for the

diffusion coefficient  $D$  are  $\text{cm}^2/\text{s}$  or  $\text{m}^2/\text{h}$ . The obstruction factor for molecular diffusion through a porous material,  $k_d$ , introduced by Krischer (1963) can be obtained by dividing the diffusion coefficient of air by the measured diffusion coefficient of the material. It is a measure for the diffusion resistance the material offers to a diffusive flux and will be discussed in more detail in section 3.3.1.2. Some authors present values for the obstruction factor instead of the diffusion coefficient.

Gas diffusion within the voids of the wood-furnish mat may be of some importance during hot pressing, as considerable partial pressure gradients of air and water vapor develop, at least temporarily, between the surface and the core. Furthermore, gas diffusion may be a significant mechanism during conditioning of the panel after pressing, when convective gas flow ceases to play a major role within the panel.

#### 2.3.1.4.2 Diffusion measurements

While diffusion in solid wood has been investigated extensively in the past, there are few diffusion data for wood-based composites published in the literature. Those studies that have been conducted can be divided into two major groups according to the technique that was used, i.e., steady-state and unsteady-state techniques. The steady-state methods have in common that a defined relative humidity differential is applied to the opposing faces of the test specimen. The flow through the specimen is determined by repeatedly weighing the vapor sink or source. Once the flow has reached a constant level, i.e., the specimen has reached equilibrium conditions, the diffusion coefficient calculation can be executed. In unsteady-state approaches the weight change of the test specimen itself is observed while the specimen is in dis-equilibrium with its surrounding. Both approaches require isobaric conditions at the boundaries.

Comprehensive diffusion measurements through three-layered particleboard under steady-state conditions were carried by Horn (1969). He chose relative humidity values of 60 % and 1.6 %, respectively, for the two surfaces of the sample. The experiments were carried out under an elevated temperature of 40°C in order to reduce the moisture content, and consequently the proportion of moisture that may be transported within the cell wall material. Horn reported a close to linear relationship between density and diffusion resistance; the average obstruction factors for urea-

formaldehyde (UF) bonded panels were 17.5 and 51.8 for densities of 500 and 800 kg/m<sup>3</sup>, respectively. Significantly higher values were found for phenol-formaldehyde (PF) bonded panels. Adhesive content had only a small (for UF) or no (for PF) impact on the obstruction factor. In contrast to most data reported for solid wood, Horn found a slight increase of diffusion resistance with increasing moisture content.

Cammerer (1970) studied water vapor diffusion perpendicular to the panel plane for different types of particleboard over a density range from 250 kg/m<sup>3</sup> to 650 kg/m<sup>3</sup>. Measurements were done under steady-state conditions, applying a vapor pressure differential that corresponded to 35 % and 86 % relative humidity. The results were corrected for flow resistances at the sample surfaces. Cammerer observed a clear relationship between density and diffusion rate. Obstruction factors of 5 to 10 for low densities around 250 kg/m<sup>3</sup> and 40 to 100 for densities between 600 and 700 kg/m<sup>3</sup> were measured.

Lehmann (1972) measured diffusion coefficients for particleboard, hardboard and insulating board perpendicular and parallel to the board plane, using steady-state as well as unsteady-state methods. Results are only summarized for all panels of one type (see Table 2.1), so that more detailed relationships between panel properties and diffusion coefficients cannot be derived from Lehmann's data. The diffusion rates are reported to be primarily controlled by factors which influenced size and quantity of void spaces between particles, such as density or orientation and geometry of the particles, rather than those acting in solid wood, such as lumens, cell walls and pit openings. The diffusion coefficients measured with an unsteady-state method were two to eight times as large as those measured with a steady-state method. For all panel types, the in-plane diffusion rates were significantly higher than the cross-sectional diffusion rates.

Koponen (1984) used an unsteady-state approach to determine moisture diffusion coefficients for medium density fiberboard (MDF) and particleboard in water soaking. Although the results indicate that MDF has a lower diffusion coefficient than particleboard, this may be mainly an effect of the higher density of the MDF samples.

Boehme (1994) reported obstruction factors measured on 5-mm and 38-mm particleboard perpendicular and parallel to the board plane. In addition, samples were divided into surface and core layer prior to repeating the perpendicular measurements.

Density values for the layers as well as average densities for the panels were not specified. All measurements were made using a steady-state method. Boehme found obstruction factors of 30 to 60 for core layers and 90 to 290 for surface layers. However, some data for the overall panel resistance obviously contradict those values measured for each layer, questioning the accuracy of the results.

Cai and Wang (1994) investigated diffusion in particleboards by using steady-state and unsteady-state methods. Relative humidities of 50 % and 100 % were applied for the steady-state measurements. Diffusion coefficients measured under steady-state conditions are up to three times smaller than those measured under unsteady-state conditions. The diffusion rates parallel to the panel plane were found to be 3-5 (unsteady-state) and 10-20 (steady-state) times as large as those perpendicular to the panel plane.

Table 2.1. Diffusion coefficients based upon a bound-water concentration gradient for particleboard perpendicular and parallel to the panel plane. The data were obtained in steady-state experiments.

	Average panel density [kg/m <sup>3</sup> ]	Diffusion coefficient [10 <sup>-6</sup> cm <sup>2</sup> /s]	
		perpendicular	parallel
Lehmann (1972)	620-700	0.04-0.26	0.72-1.15
Cai and Wang (1994)	not specified	0.10-0.49	1.65-5.87

The results of steady-state diffusion experiments obtained by Lehmann (1972) and Cai and Wang (1994) are summarized in Table 2.1. The listed diffusion coefficients are based upon a bound-water concentration gradient. Siau (1984, eq. 6.18) provided an equation to transform such coefficients to coefficients that are based upon the concentration gradient in air. This calculation only provides exact results within an infinitesimally small moisture content range, since the relationship between moisture content and relative humidity is not linear. Such transformation can therefore not be applied here, and this makes a comparison of the listed data with gas diffusion coefficients and diffusion resistant factors difficult.

Most of the studies of moisture transfer under isobaric conditions were carried out on particleboard. The only diffusion rates found in the literature for MDF are those from Koponen's (1984) unsteady-state measurements.

#### 2.3.1.4.3 Critical comments on diffusion measurements

##### *Steady-state versus unsteady-state methods:*

As can be seen from the papers of Lehmann (1972) and Cai and Wang (1994) the data obtained by steady-state methods deviate considerably from those obtained by unsteady-state methods. The diffusion coefficient is a transport coefficient, and values should therefore be independent of the measurement method. This raises the question of which method is appropriate to determine the diffusion coefficient in wood or wood-based composites.

Unsteady-state flow occurs when the flux and gradient are variable in both space and time. For relatively simple situations there are mathematical techniques available to treat flow under unsteady-state conditions (Crank 1975). In wood and wood-based composites, unsteady-state flow is, however, complicated by absorption and desorption processes; these change in space and time and also influence the properties and structure of the cell wall substance. Therefore, steady-state methods seem to provide more accurate results than unsteady-state ones, since the uptake and release of water by the wood is ruled out.

Avramidis and Siau (1987) suggested that for solid wood surface resistance might be a significant part of the total resistance to the transfer of moisture into or out of the tested specimen. Surface resistance is due to the resistance of the air film adjacent to the specimen. It may be expected that the effect of surface resistance is less pronounced under steady-state conditions, since the specimen surfaces are close to equilibrium with the surrounding air. As exact coefficients describing the surface resistance are usually not known, this variable adds another uncertainty to unsteady-state measurements.



*Capillary moisture movement:*

Water vapor diffusion in a hygroscopic porous medium may go along with capillary water movement, which is a consequence of the surface tension of water condensed in fine pores. Krischer (1963) gave a good explanation for this phenomenon. Furthermore, other mechanisms may also contribute to water translation within the cell wall substance. Methods typically used to determine the diffusion coefficient do not separate these different mechanisms. Therefore, diffusion coefficients obtained by such methods possibly deviate from the true molecular gas diffusion coefficients. For a more fundamental treatment of water transport mechanisms within wood-based composites it is desirable to have single transfer coefficients for gas diffusion, capillary water movement, and possibly other transfer mechanisms. None of the researchers referred to above have attempted to provide data that describe each mechanism separately.

Krischer (1963) suggested that capillary water movement explains the observed moisture content dependency of water transfer through hygroscopic materials. Cammerer (1956, in Niemz 1993) reported a twenty-fold increase of the diffusion resistance of solid wood (spruce) when decreasing the moisture content from 20 % to 4 %. Such dependency has yet to be confirmed for wood-based composites. Instead, Horn (1969) reported the opposite tendency for particleboard for the moisture contents ranging between 4 and 8 %. Apparently, theories and findings for solid wood are not directly applicable to wood-based composites as the situation in wood-based composites differs considerably from that in solid wood. To conclude a positive relationship between transfer rate and moisture content from unsteady-state measurements alone, as described by Cai and Wang (1984), is not convincing. This is due to the inaccuracies of the method as stated in the above paragraph. Further investigations under steady state conditions or with inert gases may help to better understand moisture diffusion in wood-based composites.

*Density profile:*

Cammerer (1970) found a clear dependency of diffusion rate on average panel density. Wood-based panels usually show a more or less pronounced density variation across the thickness of the panel. When diffusion measurements are made on samples of

such panels, the obtained diffusion coefficients are only averages over the range of densities in the sample. Boehme (1994) is alone in his attempts to study moisture diffusion in particleboard separately for high-density surface layers and low-density core layers. He confirmed the density dependency of the diffusion rate, but did not report the corresponding density values. All other work described above has been done on samples with a density profile.

### ***2.3.1.5 Hygroscopic relationships***

#### **2.3.1.5.1 Introduction**

Literature concerning the transfer processes within wood-based composite mats during pressing was reviewed in the previous sections. As steady-state conditions within the mat are not reached during hot pressing, the mass and heat fluxes cause changes in the local conditions, i.e., temperature of wood and gas mixture, within-void partial air and vapor pressure, cell wall moisture content, and possibly free water content. Heat is liberated due to vapor condensation and absorption, or is consumed by evaporation of water. Air and vapor pressure depend on the temperature, and the moisture content is related to vapor pressure and temperature. All these dependencies are governed by laws of thermodynamics and by sorption theory.

Basic relationships between temperature, air pressure and vapor pressure are described in many thermodynamic textbooks (e.g., Holman 1980). Only work about the more specific physics of the wood-water system that has been reported in the literature will be summarized here.

#### **2.3.1.5.2 Equilibrium moisture content**

The equilibrium moisture content (EMC) of a hygroscopic material like wood depends on the relative humidity and temperature of the surrounding atmosphere. Besides, it is influenced by the previous exposure history of the wood (hysteresis effect) and varies within and between species.

The relationship between EMC, temperature and relative humidity below 100°C has been investigated by many researchers. Results are typically summarized in tables or

diagrams (e.g., Weichert 1963, Keylwerth 1969). In addition, empirical and theoretical models have been derived which provide equations to describe this relationship. Skaar (1972) gives a good summary of such models. Simpson (1973) compared predictions of theoretical models with data from the literature and concluded that the two-hydrate Hailwood and Horrobin model (1946) gives the most accurate results of the models tested.

Less information is available for temperatures above 100°C. Early measurements were done by Keylwerth (1949), Grumach (1951) and Kollmann and Malmquist (1952) at atmospheric pressure. Noack (1959) compared measurements reported in the literature for temperatures above 100°C at atmospheric pressure and found good agreement between the results.

However, during hot pressing the partial vapor pressure can be expected to exceed one atmosphere at elevated temperatures. For higher vapor pressures only extrapolations were available at the end of the 1950s (e.g., Kauman 1956); extrapolated values varied considerably among authors (Noack 1959). Noack was the first to make some preliminary moisture content measurements at temperatures above 100°C and vapor pressures *exceeding* one atmosphere. Further experiments in such conditions were carried out by Hann (1965), Strickler (1968), Lutz (1974), Engelhardt (1979), and Resch et al. (1988). Among those, Engelhardt's work is the most comprehensive. He determined sorption isotherms of beech within the entire range of relative humidity at four temperatures between 110°C and 170°C.

Some equilibrium moisture content data for 30 % and 80 % relative humidity levels and elevated temperatures reported in the literature are shown in Figure 2.4. For the 30 % relative humidity data, there is relatively good agreement between measurements of different researchers, and also between these measurements and the extrapolations of Kauman (1956). However, the experimental results at 80 % relative humidity suggest that the temperature effect on the equilibrium moisture content is less pronounced than indicated by Kauman's extrapolation.

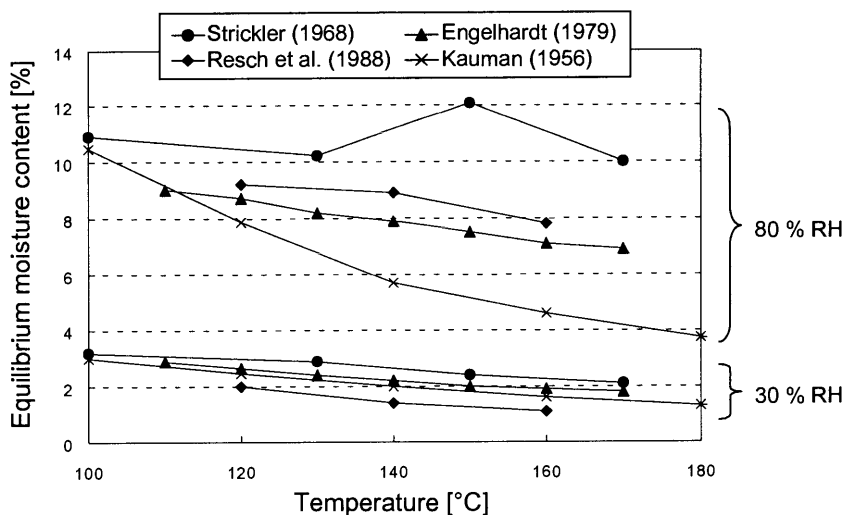


Figure 2.4. Comparison of measurements (solid symbols) and extrapolations (x) of equilibrium moisture content at elevated temperatures for two levels of relative humidity (RH).

Noack (1959) emphasized that, at high temperatures, thermal degradation is of a magnitude that significantly influences the results of sorption tests. Therefore, the measured EMC values have to be reduced by a correction factor. Strickler (1968) did not account for thermal degradation, in contrast to Engelhardt (1979) and Resch et al. (1988), and this may explain the higher EMC values that Strickler found.

Simpson and Rosen (1981) tested the Hailwood and Horrobin model (1946) for temperatures up to 150°C at atmospheric pressure and compared the estimated EMC values with experimental results reported in the literature. Although the estimates deviated by up to 250 % from the measurements around at 150°C, Simpson and Rosen deemed that the agreement was good enough for practical purposes. Our own calculations showed that, for temperatures above 150°C, the model gives somewhat erratic values which deviate considerably from experimental results at all relative humidity levels.

At room temperature, different EMC values are found depending upon whether equilibrium is approached from a higher (desorption) or lower (absorption) moisture content. This hysteresis effect is well described in the literature (see, for example, Kollmann 1959), although there is still some debate about its cause. Kelsey (1957) reported a decline of the hysteresis effect with increasing temperature. According to Weichert (1963) there was no hysteresis effect notable for temperatures above 75°C. He

attributed this to the reduction of internal stresses that occur at these temperatures. Engelhardt (1979), who compared EMC values from absorption and desorption experiments at 110 and 150°C, confirmed Weichert's finding. In contrast to this, Strickler (1968) reported a hysteresis at 130°C.

Most of the experimental work mentioned above has been done for solid wood. For fiber or particle mats the equilibrium moisture content for a given temperature and relative humidity can be expected to be somewhat different. The quantity and accessibility of the hydroxyl groups of the cell wall carbohydrates may be influenced by breakdown and drying of the wood material before the mat is formed, and by the severe conditions within the press. Adhesive and additives may also have an effect on the physical and chemical structure of the wood substance. Some of the investigations about the hygroscopicity of wood composites reported in the literature are qualitative rather than quantitative in nature (May 1985, Sekino and Irle 1996). Roffael and Schneider (1978, 1979, 1980, 1981) published a series of papers about the sorption behavior of particleboard. They investigated the effects of adhesive content and type, wood species and additives on equilibrium moisture content. A comparison of sorption isotherms measured on two different phenol-formaldehyde bonded particleboards and solid wood revealed that EMC values differ little below 10%. Approaching fiber saturation, however, the courses of the sorption isotherms may vary considerably.

#### 2.3.1.5.3 Heat of sorption

As hygroscopic water in the cell wall material has a lower potential energy level than free water, absorption and desorption of water by wood is always accompanied by a corresponding release or consumption of energy. The latent heat of sorption  $H_l$  is the heat generated per unit mass of water absorbed by wood from the liquid state at a given wood moisture content<sup>6</sup>. Its value is (almost) zero at fiber saturation and increases towards lower moisture contents. If water is absorbed from the gaseous state, the latent heat of

---

<sup>6</sup> Note: The term 'latent heat of sorption' is used for consistency; it is synonymous with 'differential heat of sorption from the liquid state'.

evaporation,  $H_{ev}$ , which is the energy that is liberated when water vapor condenses to liquid water, has to be added to the latent heat of sorption,  $H_l$ .

Skaar (1972) described two basic methods for determining the latent heat of sorption,  $H_l$ . The first one is a thermodynamic method that can be applied to derive the values of  $H_l$  from known sorption isotherms. The second method uses direct calorimetric measurements.

Stamm and Loughborough (1935) were the first to employ the thermodynamic method to determine  $H_l$  for wood. They based their computations on sorption isotherms for Sitka spruce and found an almost exponential increase of  $H_l$  for decreasing values of moisture content. Stamm and Loughborough reported that their data were in complete accord with experimental data obtained by Volbehr as early as 1896 (not read) for pine. Kelsey and Clarke (1956) measured the latent heat of sorption,  $H_l$ , for Araucaria. Weichert (1963) used the thermodynamic method to calculate  $H_l$  at a mean temperature of 62.5°C for two different wood species, and validated his results by some calorimetric measurements. His values for spruce agree closely with those data obtained by Kelsey and Clarke and by Stamm and Loughborough.

Engelhardt (1979) derived values for  $H_l$  from sorption isotherms in the temperature range between 110 and 170°C. He found a slight temperature dependence of  $H_l$  for moisture contents above 4 %; values of  $H_l$  decreased with increasing temperature. For moisture contents near zero percent, Engelhard obtained equal values for all temperature levels investigated. The finding that the latent heat of sorption is independent of the temperature at low moisture contents has also been reported by Kelsey and Clarke (1956) and Weichert (1963) for temperatures below 100°C.

## **2.3.2 Mat densification and stress relaxation**

### **2.3.2.1 Introduction**

The loose wood-furnish mat is densified in the hot press close to its final thickness and density level. The response of the mat to compaction pressure has been studied extensively in the past for various reasons. The required pressure during press closure dictates the design of the hydraulic system of the press, optimization of which is

desired for economical reasons. The visco-elastic behavior of the wood-furnish material affects unwanted strain recovery processes (springback) upon press opening. Furthermore, the cross-sectional density profile of the final panel is a consequence of the non-uniformly distributed mechanical mat properties during pressing. As many utility properties of the panel are related to its density profile (see section 2.2 above), the specific control and manipulation of the density profile has been a major concern.

Most of the early work reported in the literature concentrated on the mat's resistance to load during press closure. Experiments were usually carried out by pressing a mat under practice-oriented conditions, so that results were strongly influenced by temperature, moisture and density gradients within the mat, and were therefore rather qualitative in nature. Towards the end of the 1960s investigators started to pay some attention to stress relaxation processes in the mat after the press was closed. Only during recent years have research efforts focused on a more quantitative assessment of the stress-strain relationship by both empirical and fundamental approaches. Such information may be used as input data for models to simulate the hot pressing process.

Until the 1960s the typical technique for industrial composite manufacture was to close single- or multi-opening batch presses (so-called day-light presses) to a fixed position, and to keep this position until venting and press opening. The thickness of the mat was dictated by spacing strips (stops) mounted between the pressing platens. In later years, technology became available to dynamically control the position of the pressing platens, thus providing much greater flexibility throughout the whole pressing cycle. Modern batch presses, as well as continuous working presses, are operated in either load or position control mode, or in a combination of both.

Figure 2.5 shows a typical pressing schedule for particleboard manufactured in a continuous press. The course of the load and thickness curves may vary considerably for different material types, and also depends on the strategy of the respective panel manufacturer.

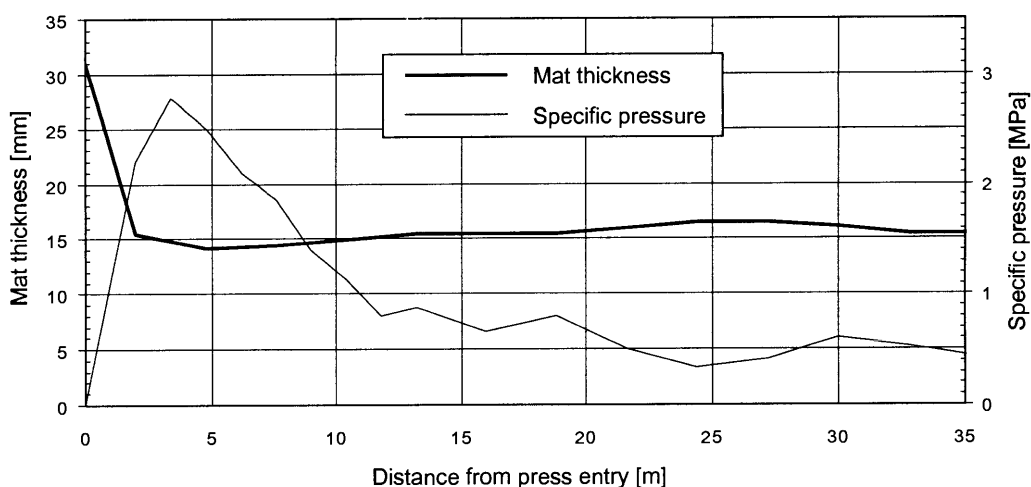


Figure 2.5. A typical pressing schedule in a continuous press for particleboard. (León-Méndez and Thömen 1996)

### 2.3.2.2 Rheological behavior of wood-furnish mats

When a wood-furnish mat is consolidated in a hot press, the material experiences both instantaneous and time-dependent deformation. As will be shown later, time-dependent deformation normally contributes only a small share of the total deformation.

The study of time-dependent stress-strain behavior of materials is called rheology (Bodig and Jayne 1982). Taking the term 'rheology' in its narrower sense, it describes only phenomena such as viscous or delayed-elastic deformation<sup>7</sup>. Stress relaxation and creep processes are consequences of such types of material behavior. However, in this work the term 'rheology' will be used in a broader sense, following the convention facilitated by Ren (1991). According to this definition, the rheological behavior of a material includes time-dependent as well as instantaneous deformation processes. Such usage of the term 'rheology' reflects the fact that both aspects of the material behavior are interactive with each other, and that they are usually described simultaneously by so-called rheological models.

---

<sup>7</sup> The term 'rheology' is derived from the Greek word 'rheo', which means 'flow'.



Kunesch (1961) appears to be the first to emphasize the importance of the visco-elastic behavior of wood-furnish materials for manufacture and usage of particleboard. Relaxation of overall and residual stresses affects the mat behavior at press opening (springback) and the dimensional stability of the panel in use (Plath and Schnitzler 1974). Stress relaxation processes during pressing become evident in typical pressure-versus-time curves recorded under conditions where the mat thickness is held constant after compaction without using stops. Early experiments under such conditions have been reported by May and Mehlhorn (1969) and Liiri (1969). Pressure-versus-time curves displayed by both groups show an immediate pressure drop after the final thickness was reached, before they flattened out. Deppe and Ernst (1964) described stress relaxation after press closing with an exponential function.

The strain developed when stress is applied to visco-elastic materials may be divided into an elastic, a delayed-elastic and a viscous component. Elastic strain occurs instantaneously and is recoverable, delayed-elastic strain is time dependent and recoverable, and viscous strain is time dependent but not recoverable (Kunesh 1961, Kavvouras 1977). The visco-elastic material behavior may be illustrated and arithmetically described by employing rheological models. In such models each strain component is represented by a simple element (e.g., a spring or a dashpot) or by a combination of such elements. The so-called Burger model gives, according to Raczkowski (1969), the best description of a material that simultaneously experiences elastic, delayed-elastic and viscous deformation upon the application of stress. The Burger model is a series connection of a Maxwell model (spring and dashpot in series) and a Kelvin model (spring and dashpot in parallel). Each spring or dashpot may be described by a theoretical property, hereafter referred to as rheological coefficients<sup>8</sup>, and the stress-strain relationship can be calculated once the rheological coefficients are known.

Some researchers suggested that the Burger model may be applicable to wood (for example Kollmann 1961). The first authors who used the Burger model to describe the

---

<sup>8</sup> The values of the rheological coefficients may change with material conditions such as temperature and moisture content. They will therefore not be called rheological constants throughout this work, as it is sometimes found in the literature.

creep behavior of wood-based composites in use were Pierce and Dinwoodie (1977). They derived the rheological coefficients for particleboard from bending tests.

Raczkowski (1969) carried out bending creep experiments on solid pine samples under changing moisture conditions and found that the Burger model does not describe the stress-strain relationship completely if creep processes go along with microscopically small destruction processes within the wood. He therefore suggested to supplement another compound element to the Burger model, which accounts for destruction processes, though he did not give an exact description of the nature of such an element.

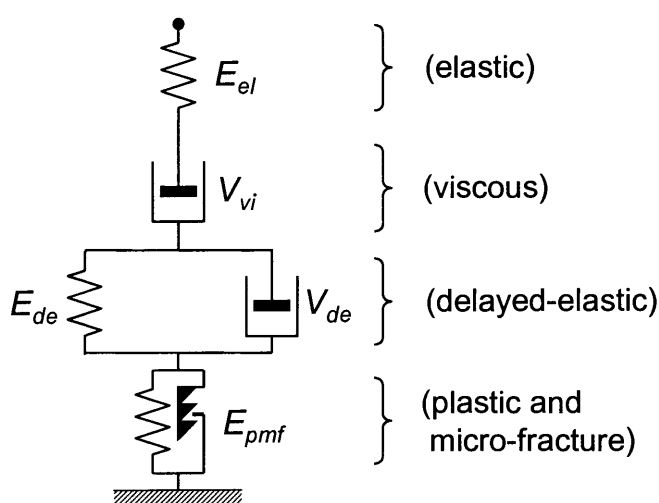


Figure 2.6. Five-element Burger-Humphrey model, representing four strain components.  $E$  = modulus of elasticity,  $V$  = viscosity,  $E_{pmf}$  = coefficient for plastic and micro-fracture element. The non-linear behavior of each element is not symbolized in this schematic. (Refined after Ren 1991)

A similar approach has been applied by Ren (1991) to describe densification and stress relaxation of wood-furnish mats during hot pressing. To account for both, the visco-elastic behavior of the mat as well as irreversible changes of cell wall and mat structure that happen instantaneously upon loading, a plastic and micro-fracture (PMF) element was combined in series with the Burger model (Figure 2.6)<sup>9</sup>. Strain due to PMF effects only occurs if the effective stresses exceed the yield strength of the

<sup>9</sup> The term 'plastic' is sometimes used synonymously with 'viscous'. Throughout this work, plastic deformation is assumed to occur instantaneously upon loading, while viscous deformation is time dependent. Both deformation components are non-recoverable.

microstructures and is not recoverable when the load is removed. Such behavior may be symbolized by a spring that only operates in one direction.

Ren (1991) developed a method to determine the five rheological coefficients of the Burger-Humphrey model by recording and evaluating the strain response to a defined stress course in a miniature sealed press system, and applied this method to un-resinated fiber mats. PMF behavior proved to have the largest effect on overall mat deformation during hot pressing, especially in the initial stages of mat consolidation.

Sitkei (1994) presented expressions which describe the compaction behavior of flakes and sawdust in silos and during the manufacture of briquettes. He suggested to employ an exponential equation for the densification stage and a three-element rheological model to account for the visco-elastic behavior of the material. Such an approach is apparently based on the assumption that both aspects can be exactly distinguished, i.e., that the time dependence of the material behavior during densification is negligible, and that only small changes in deformation occur, once the material has been densified.

Following Sitkei's (1994) approach of subdividing the consolidation process, von Haas (1998) investigated different aspects of mat behavior during hot pressing and described some of these aspects by individual models. Aspects considered include primary and secondary densification, stress relaxation and creep processes. He carried out experiments in a miniature sealed press after the design of Ren (1991) to determine quantitative expressions for the stress-strain relationship in fiber, flake and strand mats.

While von Haas's work may help to improve our understanding about some specific features of rheological mat behavior, his concept of describing individual aspects with different models makes it difficult to use his data, at least directly, to simulate the density profile development during pressing. Processes such as densification, stress relaxation and creep occur simultaneously, and the importance of each individual process changes throughout the pressing cycle and with location. A single model that incorporates the most important aspects of rheological mat behavior is advantageous.

### ***2.3.2.3 Factors influencing rheological behavior***

#### 2.3.2.3.1 Temperature, moisture content and density

Wood-furnish materials behave in a highly non-linear fashion during densification, i.e., the mat's resistance to compression increases greatly with increasing density; this is evident in nearly exponential stress-versus-strain curves (for example May and Mehlhorn 1969). Higher mat densities usually require higher compressive loads throughout the entire pressing time (Strickler 1959, Liiri 1969, May and Mehlhorn 1969, Schweizer 1992).

Before the advent of wood-based composites it was already known that moisture and temperature soften and tend to plasticize solid wood, which makes it more compressible (Thunell 1941, KÜch 1943). The moisture and temperature effect was soon confirmed for particleboard. Kollmann (1957) observed for three-layered particleboard that surface layer densities increased by about 45 % if their moisture content prior to pressing was adjusted to 21 instead of 17.5 %. Kehr and Schölzel (1965) compressed flake mats under constant compaction pressure and found that increasing platen temperature and initial moisture contents reduce the press closing time considerably. Liiri (1969) showed that the maximum compaction pressure required to reach a targeted average panel density drops with higher moisture contents and temperatures. However, for temperatures above 180°C he observed a reversal of the temperature effect and speculated (questionably) that this phenomenon may be due to faster adhesive curing in the surface layers.

Above a critical temperature, known as the glass transition temperature, wood, like many other polymers, experiences a transition that enhances its softening effect. While a pronounced glass transition can be observed for each of the chemical components of wood within a relatively small temperature range, it is more gradual for wood as a whole. Furthermore, moisture reduces the glass transition temperature of wood (Goring 1963, Kavvouras 1977). Kehr and Schölzel (1965) reported a pronounced decrease of press closing time for platen temperatures between 100 and 140°C. The particular softening of the mat in this temperature range may be attributed to the glass transition of wood.

It has already been pointed out that if the mat is held at constant thickness after compaction, stress relaxation processes within the mat become evident. May and Mehlhorn (1969) recorded compaction pressure versus time curves in a series of experiments in which the pressing platen distance was kept constant after press closure without using stops. The absolute value of the measured compaction pressure is then equal to the mat counterpressure. Higher platen temperatures reduced the mat counterpressure during all stages of the pressing cycle. An increase of initial moisture content from 9 to 15 % led to a reduction of the mat counterpressure only during the first half of the pressing cycle, while the opposite effect was observed towards the end. For a correct interpretation of these results it has to be understood that the mat counterpressure is not necessarily equal to those stresses that develop within the wood constituents during compaction. May (1970) sub-divided the mat counterpressure into three components, which he assigned to vapor pressure, compaction of wood constituents and adhesive cure. He attributed the positive correlation between initial moisture content and mat counterpressure at the end of the pressing time reported by May and Mehlhorn to the moisture effect on vapor pressure buildup.

Some studies have been carried out during recent years to investigate temperature, moisture and density effects on the compression behavior of mats under constant temperature and moisture conditions to avoid the development of gradients within the mat. Such homogeneous conditions are necessary to make quantitative statements about the stress strain relationship.

Ren (1991) investigated density, temperature and moisture effects on the densification and stress relaxation behavior of fiber mats and determined the rheological coefficients of the Burger-Humphrey model under constant temperature and moisture conditions. Experiments were conducted within a load range of 1 MPa to 6 MPa, temperature range of 25°C to 150°C and moisture content range of 0 % to 16 %. Ren observed for almost all of the investigated temperature-moisture content combinations that increasing temperature and moisture leads to increased elastic, delayed elastic, viscous and plastic-fractural deformations at given load levels. Haselein (1998) fitted equations to Ren's data to express each of the rheological coefficients as a function of density, temperature and moisture content.

Schweitzer (1992) measured maximum load, i.e., the load immediately after the press is closed, and mat counterpressure 90 seconds after the maximum load was reached in particleboard mats of constant temperature and moisture content. Density, temperature and moisture effects were investigated by defining standard conditions for the mat (target density of  $500 \text{ kg/m}^3$ , temperature of  $20^\circ\text{C}$ , moisture content of 5 %) and individually varying each of these parameters while keeping all other parameter at the standard level. Schweitzer stated that maximum load and mat counterpressure after 90 seconds decreased linearly with increasing temperature and exponentially with increasing moisture content.

Von Haas (1998) studied densification, stress relaxation and creep processes within fiber, flake and strand mats for density, temperature and moisture content ranges that cover almost the entire spectrum prevailing during hot pressing. To avoid possible thermal degradation of the wood material due to long exposure to high temperatures, the mat samples were heated and conditioned by steam injection prior to testing. Von Haas observed for all material types that the moisture effect on mat compressibility increases with increasing temperature. Extraordinary softening of the wood material was reported for certain temperature-moisture combinations, which were:  $110^\circ\text{C}$ , about 14 %;  $140^\circ\text{C}$ , about 10 %;  $190^\circ\text{C}$ , 0-5 %.

#### 2.3.2.3.2 Structure of wood constituents and mats

Experiments made on pulp fiber networks may provide some useful information that can be transferred to fiber mats. Jones (1963) studied the effect of length, diameter and elastic modulus of kraft pulp fibers (and types of synthetic fibers, as well) on the compression behavior of fiber beds at low pressure. He found that compression and recovery were highly dependent on fiber length-to-diameter ratio since it influences the structure of the bed formed, and on fiber modulus of elasticity.

Shape and size distribution of the wood constituents, as well as their arrangement in the fiber or flake network, have an impact on the deformation behavior of the mat. Kehr and Schölzel (1965) observed for particleboard that mats of 0.4 mm thick flakes are less compressible than mats of 0.2 mm flakes, and attributed this difference to the fact that thin wood constituents are easier to bend than thick ones. Similar effects of the

thickness of the wood constituents on mat compressibility have been reported by Schweitzer (1992).

In contrast to this, Kavvouras (1977) observed that flake thickness has very little effect on the maximum mat counterpressure immediately after press closure. When flake thickness increased from 0.2 to 0.6 mm, the maximum counterpressure increased by only 8 %. However, the relaxation of counterpressure appeared to be seriously influenced by flake thickness.

Dai and Steiner (1993) developed a theoretical model that predicts the overall pressure-deformation relationship of random flake mats as a function of both solid flake compression properties and mat structure. The model is based on a modified Hooke's law, combined with probability theory and geometrical considerations first introduced by Suchsland (1959). Pure compression is accounted for, while bending, shear and friction among the wood constituents are neglected. The model was tested experimentally for different mats made of equal-sized veneer flakes. Good agreement was found between predicted and measured compression behavior for all tested flake sizes at 20°C for pressures above 1.5 MPa. The deviation at low pressures was attributed to the fact that during this stage of compression, stress develops from flake bending instead of transverse compression. Apparently, the bending properties of the wood constituents (which include length-to-diameter or length-to-thickness ratios) only influence the mat compression behavior significantly at the early stage of mat densification.

To account for the cumulative effect of strand bending at low pressures, Lang and Wolcott (1996) incorporated an additional simulation routine into the model of Dai and Steiner (1993), which was based on probability distributions and simple beam theory. In that approach, each strand is considered as a small, simply supported beam under distributed load. Geometrical mat and strand characteristics necessary for the bending calculations were determined experimentally. According to Lang and Wolcott, a non-linear strain function describing the transverse strand compression may be derived experimentally, or by using theories of cellular materials.

Lenth and Kamke (1996) suggested combining one cellular material model for the densification of the mat with another for the densification of the individual wood flakes.

They hypothesized that this may be an effective way to model the mechanical behavior of a wood flake mat during consolidation.

#### 2.3.2.3.3 Wood species

Intuition suggests that the stress response of a mat depends on the species of wood used, and early work provided evidence to support this. Rackwitz (1954) found that the pressure required to compress mats to a density of about  $600 \text{ kg/m}^3$  was higher for spruce flakes than for beech flakes (spruce is typically lighter than beech). For increasing densities above this value, the two pressure curves approached each other and finally crossed each other at about  $700 \text{ kg/m}^3$ . Kull (1963) derived similar results, comparing two types of particleboard made from spruce and pine and from beech, and explained this phenomenon as follows: As long as the density of the wood is not reached, mainly the void spaces *between* the particles are reduced. During this period, lighter wood species require higher pressures than do wood species of higher density. Only when higher pressures are applied are the void spaces *within* the particles compressed.

Kehr and Schölzel (1965) measured the compaction pressure that is required to reach the target panel density by pressing particleboard made of different wood species. The densities of the wood species were in the range between  $440$  and  $730 \text{ kg/m}^3$ . Kehr and Schölzel found that the compression behavior of the mat sometimes varies between two species, even though their densities may be similar, and suggested that the different thermoplastic behavior of the cell wall material may be a reason for such differences.

May and Mehlhorn (1969) investigated the rate of stress relaxation after the mat was compressed to its final thickness. They observed that the wood species has an effect on the rate of stress relaxation.

#### 2.3.2.3.4 Adhesive

Once the adhesive starts to cure, inter-particle adhesion forces develop. Part of the compressive deformation of the wood constituents becomes fixed, so that not the entire elastic and delayed-elastic strain components are recoverable any more; residual stresses



build up upon load removal. The not directly measurable inter-particle adhesion forces clearly influence the observable mat counterpressure (May 1970, Kavvouras 1977).

Liiri (1969) found that an increase in adhesive content of the mat reduced the necessary maximum compaction pressure. He suggested that resin has an effect similar to that of water, which promotes the plasticity of wood-furnish materials.

Von Haas (1998) reported experiments in which he resinated particles, and then placed them in a drying-oven for several hours before forming the mat. He compared such mats with resinated mats that were immediately pressed, and with un-resinated mats, and found only small differences in compressibility for different temperature levels.

May and Mehlhorn (1969) observed that the mat counterpressure after press closure declines only slightly faster for resinated particle mats than for un-resinated ones. Von Haas (1998) confirmed this tendency in relaxation experiments.

#### ***2.3.2.4 Factors affecting cross-sectional density profile***

Moisture content and temperature clearly change with location and time during hot pressing. It was early recognized that the variation of these two factors causes a non-uniform densification and is therefore responsible for the development of cross-sectional density profiles (Fahrni 1956, Kollmann 1957). A density profile for particleboard is displayed schematically in Figure 2.7.

Strickler (1959) was one of the first to systematically study the densification process of wood-furnish mats by making particleboard in a laboratory press under varying conditions and measuring the consequent density profiles. Factors varied were density level, overall initial moisture content, initial moisture distribution and pressing cycle. Strickler found that moisture migration towards the central plane of the mat had a strong effect on cross-sectional density variations. Higher overall initial moisture contents caused greater cross-sectional density variations. This effect was accentuated when a non-uniform initial moisture distribution with elevated surface moisture content was employed. Pressing cycles with high initial compaction pressures resulted in high surface densities and correspondingly low core densities; the density profiles tended to become U-shaped instead of M-shaped for high initial compaction pressures.

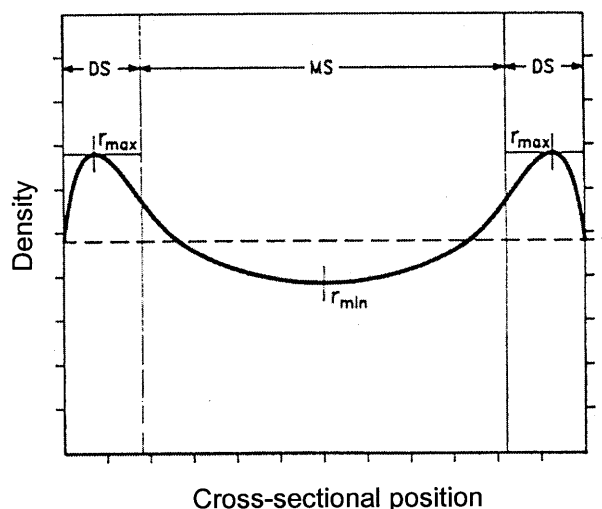


Figure 2.7. Cross-sectional density profile of a particleboard prior to sanding (schematic from Boehme 1992).  $r_{max}$  = density maximum,  $r_{min}$  = density minimum,  $\bar{r}$  = average density, DS = surface layer, MS = core layer.

Similar effects of press closing time and initial pressure on the shape and range of the density profile have been reported by many others, for example Smith (1982) for waferboard and Boehme (1992) for MDF.

Suchsland (1962) suggested that each layer of the mat is compressed according to the lowest compression strength reached during the pressing cycle. As a consequence of the softening effect of temperature and moisture, the individual mat layers will be weakened successively from the faces towards the central plane.

The density profile in multi-layered panels may be manipulated by using different material types in the surface and core layers. To reach high densities near the surface and low densities in the core, surface layer material with low resistance to stress and core layer material with high resistance should be employed. This is usually achieved in three-layered particleboard by using thin flat flakes in the surface layers and short unregularly shaped ones in the core layer (Plath and Schnitzler 1974, Hänsel and Kühne 1988, Boehme 1992).

Hänsel and Kühne (1988) studied the influence of adhesive content on density profile development. They found that varying the adhesive content of the surface layers between 7 and 13 % did not have a statistically significant effect on the density profile.

### ***2.3.2.5 Modeling cross-sectional density profiles***

As the temperature and moisture distribution in the mat dictates the mechanical material behavior, any model that aims to predict the density profile based on fundamental principles clearly has to include heat and mass transfer. An overview of such integrated models will be given in section 2.4 below. In this section, only the specific aspect of modeling the density profile development will be reviewed.

Harless et al. (1987) appear to be the first to describe a heat and mass transfer model for particleboard that includes density profile prediction. Empirically derived data expressing the stress-strain relationship were used to calculate layer densities. Mat deformation was assumed to be instantaneous and irreversible, so that changes in the density profile that may occur due to stress relaxation processes and possible softening of individual layers after press closure could not be accounted for. The stress-strain data used were obtained for four temperature levels between 24°C and 127°C by heating mats throughout in a press and subsequently compacting them. Moisture effects on compressibility of wood-furnish materials, which are known to be considerable, were ignored. It is likely that this deficiency, in combination with obvious weaknesses of the model to predict the mat temperature correctly, are major reasons for overall poor density profile predictions.

Dai and Steiner (1993) suggested that the mat consolidation model described in the section above may be used in combination with a heat and mass transfer model and an expression that accounts for the visco-elastic mat behavior to predict the density profile of flakeboard. Their model, and the models developed by Lang and Wolcott (1996) and by Lenth and Kamke (1996) have in common that the compaction behavior of the mat is assumed to be governed by two independent factors: The geometry of mat and wood constituents, and the properties of solid cell wall substance. If the influence of environmental variables such as temperature and moisture content is restricted to the cell wall substance, as proposed by Wolcott (1989), this approach provides a technique to compute the stress-strain relationship under different environmental conditions relatively easily, once the relevant geometrical parameters are known.

So far, research based on probabilistic and geometrical theory to model mat consolidation has been restricted to mats made of strands or small pieces of veneer. It

seems reasonable to assume that the geometrical characterization of particle or fiber mats is more difficult to achieve. Besides, effects including shear and friction among the wood constituents and fracture due to bending have so far been neglected; these certainly play an important role in particle and fiber mats during consolidation. At this stage, the described approach appears not applicable for modeling the density profile development in fiber or particle mats during hot pressing.

Hubert and Dai (1998) were the first to incorporate probabilistic and geometrical theory in a heat and mass transfer model to predict the density profile development of OSB. However, the visco-elastic behavior of the mat was neglected, leading to inaccuracies in predicting density profile and stress relaxation.

To predict the density profile in fiberboard, Haselein (1998) employed the five-element Burger-Humphrey model described in the previous section (Figure 2.6). The rheological coefficients necessary to characterize the material under changing environmental conditions were derived from empirical data obtained by Ren (1991). Haselein was able to predict important features of the density profile, and to explain effects of press closing time, platen temperature and initial moisture content, among others, on the density profile development. Changes in the cross-sectional density distribution after the press was closed to its target position, which are to be expected due to the visco-elastic mat behavior, could be simulated. Although Haselein reported no comparison of predictions with measurements, his approach seems to be the most promising one among those found in the literature, as it accounts for both irreversible plastic and micro-fracture effects as well as visco-elastic material behavior.

## **2.4 INTEGRATED MODELS**

Two essentially different approaches to model the hot pressing process of wood-based composites can be found in the literature. The first one uses fundamental principles to describe the relevant physical or chemical processes. The second category of models employs statistical methods to link material and process variables to output parameters, which can be, for example, mechanical properties of the final product. The latter type of

models has been described by Lobenhoffer (1990), Ritter et al. (1990) and León-Méndez and Thömen (1996). Only the former approach will be considered here.

It is clear from discussions so far that the different physical processes operative during hot pressing interact with each other in a complex way. Figure 2.8 shows a schematic of the interactions between the most important processes. None of the models described in the literature include all of these mechanisms.

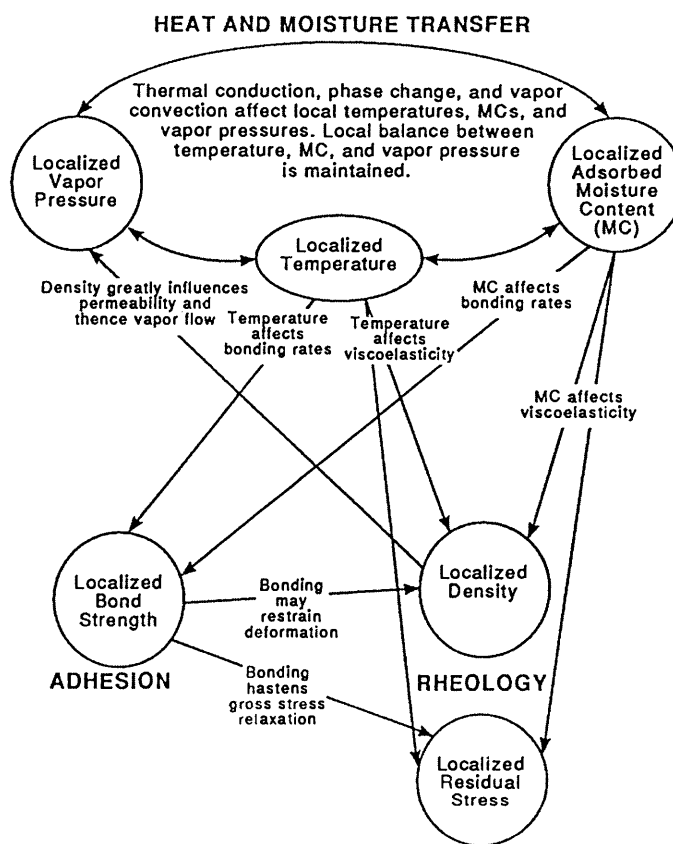


Figure 2.8. Main mechanisms operative within wood-furnish mats during hot pressing. (Humphrey 1994)

Kull (1954) derived an equation to calculate the time required to heat particleboard mats. His one-dimensional model treated conduction as the only heat transfer mechanism, but it did account for heat that is consumed to evaporate water. Kull also developed an approach to calculate the time as a function of temperature that is needed to cure the adhesive.

Some models describe only aspects of heat and mass transfer by physical laws, while empirical measurements are used to determine those variables that cannot be calculated; examples are models reported by Bowen (1970) and Gefahrt (1977). Such models may provide some insight for the specific case, but are not suitable to make predictions under changed conditions or for other panel types.

Apparently, the first heat and mass transfer model based on fundamental physical principles that included vapor convection, heat conduction and convection, and phase change was developed by Humphrey (1982). A good summary of the modeling approach can be found in Humphrey and Bolton (1989a). The model predicted temperature, vapor pressure and moisture content development during hot pressing. A cylindrical coordinate system was employed to model a circular mat, so that cross-sectional as well as radial heat and mass transfer was accounted for. The basis of the model was a modified finite difference approach. Heat and vapor transfer between neighboring grid regions were computed for each time step, and environmental conditions and material properties were updated after each time step. Although the model was thought to be applicable for simulating different material types, it was only applied to particleboard pressing. Comparisons of predicted and measured temperature and vapor pressure curves were reported by Bolton et al. (1989a). The predicted data agreed well in trend with those observed experimentally.

Humphrey and Bolton (1989a) emphasized the need to incorporate a routine to model the density distribution in the mat. However, as a temporary measure they assumed instantaneous closing of the press; the density development throughout the pressing cycle was pre-defined. Humphrey (1994) and Haselein (1998) refined Humphrey's model and added a rheological component to account for mat compression and stress relaxation (see section 2.3.2.5 above).

Humphrey (1991) also developed a method to predict the inter-particle adhesive bond strength development as a function of temperature, moisture content and time. Preliminary simulation results suggested that the lowest bond strength values at press opening might be found in the intermediate layers between surface and central plane.

Although Haselein and Humphrey's model provides predictions that are valuable for scientific and industrial application, it has some important limitations. The round

shape of the modeled mat prevents the simulation of events occurring in the corners of a rectangular panel. Furthermore, differences between material properties in the production direction and that perpendicular to it are disregarded due to the cylindrical coordinate system. Another drawback of the model is the assumption that water vapor is the only gas in the mat. During the initial phase of pressing, air is clearly the prevailing gas component, before it is replaced by vapor later in the cycle.

A one-dimensional heat and mass transfer model has been described by Kayihan and Johnson (1983) that accounts for vapor convection through the void system and moisture flow within the cell wall substance, as well as conductive and convective heat transfer including phase change effects. In-plane vapor and heat loss is governed by a user-defined leak term; this method deviates from the principle that predictions should be dependent only on fundamental physical laws and known properties. Furthermore, densification of the mat was not incorporated in the model. Another weakness of the model is the assumption that transport and material properties are assumed constant throughout the whole pressing cycle. Although convective heat transfer and phase change were reported to be considered, displayed temperature curves do not always show the characteristic plateau, or at least distortion, that must be expected in any transport processes when phase change phenomena are involved.

Harless et al. (1987) developed a one-dimensional model to predict temperature, moisture content and density development in a particleboard mat during pressing. Transfer mechanisms included were heat conduction and vapor and air flow perpendicular to the mat plane. Gas and heat escape through the edges was not accounted for. Evaporation and condensation of water are reported to be considered, but it is not clear how the contribution of phase change to heat transfer was calculated. Bound water is treated as free water, ignoring the hygroscopic character of cell wall material and all related sorptive effects. Deformation of mat layers was computed as a function of load and temperature, assuming instantaneous and irreversible compaction. Moisture effects on mat stiffness were ignored.

Qualitatively correct predictions of the effect of platen temperatures on the cross-sectional density profile could be made, according to Harless et al. (1987), while changes in press closing rates resulted in model-predicted density profiles that contradict the

expected pattern. Temperature and moisture content predictions are not displayed, but it is reported that the core temperature remained near ambient temperature throughout typical simulation runs, indicating unrealistic temperature predictions. Model results were not compared with experimental data.

Hata et al. (1990) described a two-dimensional model to calculate the conductive heat flow in absolutely dry particle mats. Under such conditions, which do not occur in practice, vapor convection and moisture effects can be neglected. Besides, they modeled the temperature development within the mat during steam injection. It is not clear in which way heat convection was accounted for. It is also questionable whether it is appropriate to calculate the convective steam flow in a porous material using a theoretically derived molecular diffusion coefficient.

Suo and Bowyer (1994) attempted to model one-dimensional heat and mass transfer and densification during hot pressing of particleboard. Heat conduction was assumed to be the only heat transfer mechanism. Evaporation and condensation of water, sorptive processes and convective vapor transfer were ignored. The calculation of the moisture flux was based on moisture content gradients, employing transfer coefficients that were derived by Siau (1984) for diffusion through solid wood. The stress-strain relationship of the wood-furnish material during compaction was assumed to be the same as that of solid wood within the elastic range. Due to the lack of the model to account for convective heat transfer, in combination with other apparent oversimplifications, the model is unlikely to predict the hot pressing process correctly.

Hubert and Dai (1998) presented a one-dimensional model for simulating hot pressing of OSB using an implicit finite element modeling approach. Mechanisms included are vapor convection, conductive and convective heat transfer, phase change, adhesive cure and mat densification. Vapor escape through the edges was accounted for by an approximation of the in-plane vapor flow, assuming constant vapor pressure gradients between the horizontal center of the mat and the edges. Adhesive cure is calculated as a function of temperature and time based on empirical data. The visco-elastic behavior of the mat is neglected. Hubert and Dai compared model predictions of various parameters with measured data and reported that typical trends are predicted correctly, but that some magnitude discrepancies exist.



The topic of combined heat and mass transfer with phase change in porous media is quite important in many other engineering areas. Examples include drying processes, geothermal energy production, heat transfer from buried pipelines and electrical cables, and underground nuclear waste disposal. Such processes have therefore been widely studied by agricultural, civil, chemical and petroleum engineers and others. Early fundamental work about transport processes in porous media that is frequently referred to in the literature has been done by Krischer (1963). Classic work published by Luikov (1975) provides mathematical formulations of the transport processes, including phase change, chemical reactions and non-linear transport coefficients. Such formulations have been applied to well defined problems in several engineering fields during recent years, and numerical solutions of the transport equations are reported in the literature. Clearly, these analyses provide valuable information for the specific situations. It is, however, difficult to obtain a general understanding from these works that can be used as a guide for conditions for which no specific solutions are yet available.

Kayihan and Johnson (1983) tried to apply systems of equations derived by Luikov (1975) to model the hot pressing process of wood-based composites. They failed to do so and concluded that this system of equations was not applicable to the problem of hot pressing a wood-furnish mat. So far no comprehensive system of differential equations has been developed for the hot pressing problem that includes three-dimensional mass and heat transfer, sorption processes, phase change, and densification and stress relaxation of the mat.

In light of the preceding review, there remains considerable need to improve existing modeling approaches regarding flexibility of the model and accuracy of its predictions. Furthermore, none of the workers have attempted so far to apply such modeling concepts to continuous pressing technology. The development of an enhanced three-dimensional model that allows one to simulate mass and heat transfer processes and mat densification in both batch and continuous presses is the concern of the chapters to follow.

### 3. MODEL DESCRIPTION

#### 3.1 INTRODUCTION

The model described in this dissertation accounts for combined heat and mass transfer with phase change and mat densification. It draws in part from work of Humphrey and his co-workers (Humphrey 1982, Humphrey and Bolton 1989a, Haselein 1998). The numerical solution of the system of equations has been implemented as a computer program. In its present version the program enables one to simulate the local evolution of temperature, moisture content, vapor and air pressure, density and internal stresses, as well as overall heat and gas flow patterns.

In this work, attention is mainly focused on one wood-furnish material type, which is medium density fiberboard (MDF), although, in principle, most of the mechanisms included are applicable to other materials. However, some of the assumptions made in the model may become unrealistic with increasing size of wood constituents. Relevant aspects of the model should therefore be refined before applying it to particleboard and oriented strandboard (OSB).

The model and associated simulation program have been developed to simulate the pressing process in continuous presses as well as in batch presses. The relevant physical mechanisms apply similarly to both manufacturing processes. For convenience, the model description in this chapter will be based on the batch process unless otherwise stated. The specific aspects of the continuous press model will then be rationalized separately in Chapter 4.

For modeling purposes the wood-furnish mat is considered as a homogeneous mixture of dry wood material, water and air. This is to say that a macroscopic view is used where the size of the representative volume is large with regard to the pores. However, a microscopic view will be used whenever appropriate to illustrate model assumptions or to explain specific features of the modeled system.

The following convention regarding the orientation of the mat within the Cartesian coordinate system will be used throughout this work. The production direction in an industrial manufacturing process is defined as the x-direction. The dimension of the

mat in this direction is called length. Correspondingly, the width and the thickness of the mat are its dimensions in y- and z-directions, respectively.

## **3.2 MODEL DEVELOPMENT**

### **3.2.1 Problem statement and assumptions**

#### ***3.2.1.1 The modeling system***

The wood-furnish mat may be regarded as a capillary-porous material consisting of cell wall substance and inter- and intra-particle voids, which form a system of interlinked cavities. Swelling and shrinking of the hygroscopic cell walls associated with sorbed moisture changes will be neglected in the model. Furthermore, it is assumed that the entire void system is easily accessible; that is to say there are no structures as inclusions or dead ends.

Gas mixtures within the pore spaces of mats consist mainly of air and water vapor. Besides these two main components, Denisov et al. (1975) detected volatile organic compounds of the wood and glue constituents, as well as carbon dioxide. However, the proportion of these components is considered likely to be relatively small and their influence on the gas properties and mass transfer rates is unlikely to be significant. A pure two-component gas mixture is therefore considered here. Other components will, however, be included in future generations of models since they may have environmental significance.

Two moisture phases are recognized, which are bound water in the cell walls and water vapor in the voids. Free water is not considered in the present approach. The exclusion of free water follows from two assumptions: First, that the localized average moisture content is always below fiber saturation, and second, that the moisture is uniformly distributed within single wood particles. The first assumption is well justified by measurements (Maku et al. 1959], Rajman et al. 1992) and simulation results (Bolton et al. 1989b). However, the second assumption is more debatable and will be explored shortly when introducing the assumption of instantaneous sorption equilibrium.

### ***3.2.1.2 Mass transfer***

Water vapor and air are transported both by bulk flow driven by gradients in total gas pressure and by binary diffusion driven by gradients in the partial pressure of each component. These flow mechanisms are treated three-dimensionally in the model. Bulk flow is assumed to be laminar; this assumption can be justified by flow measurements reported by Denisov et al. (1975) and von Haas et al. (1998).

For gas diffusion, two different cases can be considered. If the pore size is in the order of the mean free path of the gas molecules, the diffusion takes place in the Knudsen regime. This is the case if either the pore diameter is very small (micro-pores) or the gas pressure is extremely low. On the other hand, when macro-pores prevail and the gas pressure is not extremely low, the diffusion takes place in the molecular regime.

The mean free path for air at room temperature and pressure is about 60 nm (Cussler 1984). Measurements of the pore distribution in particleboard reported by Schweitzer and Niemz (1991) showed that only 3 % of the pore volume is smaller than 60 nm. The predominance of macro-pores, together with the fact that the total gas pressure will never be below atmospheric pressure during hot pressing, justifies the assumption that only molecular diffusion is significant. Knudsen diffusion has therefore been neglected in the model.

Bound-water diffusion and surface diffusion are not included since the contribution of these mechanisms to overall moisture transfer in wood-furnish mats are likely to be minor in comparison to gas transport mechanisms. Diffusion measurements on particleboard reported by Horn (1969) support the assumption that molecular gas diffusion of vapor through the void system plays the major role in moisture transport under isobaric conditions. Similar conclusions can be drawn from diffusion data published by Siau (1984); a comparison between bound-water and molecular gas diffusion coefficients reveals that diffusion rates within the cell wall substance are two to three orders of magnitude lower than those in air for moisture contents below 20 %. Under non-isobaric conditions, which usually exist during hot pressing, the predominance of convective over diffusive gas flow even more justifies the omission of bound-water and surface diffusion.

Another transport mechanism that may occur in porous media is the translation of liquid condensed in small capillaries. While bound-water diffusion takes place within the cell wall substance, capillary water movement may also arise in small inter-particle pores. Two different driving forces can cause capillary water movement, as described below.

First, the surface tension of the menisci in small pores pulls water from regions of higher to regions of lower moisture content. This phenomenon is sometimes referred to as capillary diffusion and explains the positive correlation between moisture content and diffusion rate reported for some porous materials (Krischer 1963). While such a moisture dependency of the diffusion coefficient has been repeatedly described for solid wood, diffusion measurements on insulating board (Stamm and Wilkonson 1965) and particleboard (Horn 1969) suggest that the situation is different in these types of materials. Apparently, capillary diffusion does not play a major role in moisture transport within wood-based composites. This issue has also been addressed in section 2.3.1.4 of the literature review.

A second possible driving force for capillary water movement is the existence of total gas pressure differentials. However, an order of magnitude calculation presented by Humphrey and Bolton (1989a) shows that liquid water is unlikely to translate through capillaries by this mechanism during hot pressing. Capillary moisture movement is therefore not considered in the present approach. Water is postulated to migrate only in the form of vapor through the voids of the porous material.

### ***3.2.1.3 Supply and transfer of heat***

Heat transfer happens by conduction as well as by convection. Heat radiation is not considered, following the arguments presented by Strickler (1959) and Humphrey and Bolton (1989a). Heat transfer, like mass transfer, is accounted for in three dimensions.

Convective heat transfer is associated with the gas flow (including diffusion) through the mat. In principle, two different mechanisms contribute to convective heat transfer. First, phase change of water always goes along with the release or consumption of latent heat of evaporation and latent heat of sorption. Second, gas that moves from a hot to a cold region releases sensible heat, just as cold gas takes up heat energy when moving into a warmer region. The contribution of the latter mechanism to overall heat

transfer is insignificant as will be shown in section 5.4.1. The transfer of sensible heat is therefore not included in the model.

The platens are assumed to be the only heat sources; no internal sources of heat are included, although electromagnetic heating could, for example, easily be incorporated. Frictional heat generation due to compression of the mat is ignored. A quantitative idea of the effect of compression on the mat temperature can be gained from an experiment reported by Strickler (1959) who pressed mats in a cold press to 10 MPa and observed a temperature increase of 2.8°C. Maximum loads in industrial presses typically do not exceed 5 MPa, so that neglecting the compression effect can be justified. Heating effects of the exothermic curing reaction of the adhesive, adiabatic compaction of the gas, as well as friction due to viscous flow are likely to have only a minor impact on the energy content of the mat.

#### ***3.2.1.4 Equilibrium assumptions***

Two important equilibrium assumptions are made. The first one is the postulation of instantaneous sorption equilibrium while the second one refers to local temperature equilibrium. Both assumptions will be described here in turn.

Heat and moisture transfer are coupled by the requirement that all phases remain in thermodynamic equilibrium with one another. The moisture content of cell wall substance and the vapor pressure within adjacent voids obey a sorption isotherm at the local temperature. It is assumed that there are no cross-sectional moisture gradients within single fibers. Likewise, there are no vapor pressure gradients within the pore spaces between two neighboring fiber surfaces.

Modeling approaches developed by Humphrey (1982) and Kayihan and Johnson (1983) are based on the assumption of such instantaneous sorption equilibrium. In contrast to this, some researchers believe that absorption and desorption occur with a time delay, and that free water on the surfaces of the wood constituents exists at least during some stages of the pressing process (Gefahrt 1977, Kamke and Wolcott 1991). Apparently, sorption experiments on wood fiber and flake materials under realistic pressing conditions, which may provide information about the time dependence of the sorption process, are not reported in the literature. Methods to directly detect free water

during pressing have not been developed so far. Kamke and Wolcott (1991) concluded from model predictions that the moisture content within 0.9 mm thick flakes is not in equilibrium with the internal environment of the mat. The validity of the model results, however, seems to be limited by some of the assumptions that were made.

Christensen and Kelsey (1959) *theoretically* estimated the rate of absorption of water in isolated 3  $\mu\text{m}$  thick cell walls from diffusion coefficients reported in the literature. If the sorptive uptake of water was controlled only by molecular diffusion, 99 % of the moisture change would happen during the first few seconds. A rather low diffusion coefficient of  $10^{-8} \text{ cm}^2/\text{s}$  was used for the calculation. To examine the hypothesis that diffusion is critical for the sorption process, Christensen and Kelsey *experimentally* determined absorption rates for pine on 20  $\mu\text{m}$  thin layers cut with a microtome. As the fibers had a diameter of about 40  $\mu\text{m}$ , such samples contained only one or less double cell walls through the thickness. Applying conditions that correspond to 9.7 % equilibrium moisture content (EMC) to samples of initially 3.7 % moisture content it took 3.5 minutes to absorb 50 % of the total moisture. Changing the conditions from 9.7 % to 14.7 % EMC, the 50 % level was reached after 15 minutes. As a possible explanation for the discrepancy between theoretical and measured sorption rates they suggested that time-dependent mechanical relaxation processes of the cell walls may control the uptake of moisture, and not the diffusive moisture transport.

The measurements of Christensen and Kelsey (1959) suggest that the assumption of instantaneous sorption equilibrium is an over-simplification and does not match the conditions during hot pressing. Yet, this assumption was made in the present model for two reasons. First, reliable data that describe time-dependent absorption and desorption rates for wood-furnish mats under the range of temperatures prevailing during hot pressing are not available. Second, accounting for the generation of free water, which would be a compelling consequence of deviating from the instantaneous sorption equilibrium assumption, introduces a discontinuity into the model. It may therefore require the implementation of a different modeling method than that used in the present approach. Luikov (1975) proposed a two-zone model to describe the drying process within a porous body. This model assumes the existence of a receding evaporation front, which separates the material into a moist zone and an evaporation zone. Lindsay (1989)

applied the concept of moving boundaries to model the progression of a front between liquid water and steam during impulse drying of paper. Our own preliminary work confirmed that the numerical scheme used in the present model might not be suitable to cope with a moving free water front through the mat.

Interestingly, the pronounced temperature plateau around 100°C, which is often regarded as evidence that free water must be present in the mat, is also predicted by the model described here, although the existence of free water is ruled out by definition. Apparently, such phenomena as the temperature constancy near 100°C do not require the consideration of non-equilibrium conditions and free water. However, future models should incorporate these features to further extend the applicability of the models.

The second equilibrium assumption made in this study depends upon the hypothesis that temperatures over the whole cross-section of cell walls and of the gas within nearby voids are constant at any given time. Von Haas (1998) applied a simplistic equation from Kollmann (1955) to estimate the core temperature of long wood particles when surrounding conditions are changed. Assuming an initial wood temperature of 30°C and surface temperature of 100°C, it takes about 0.5 seconds to reach a temperature of 95°C in the middle of a 0.5 mm thick and 2.0 mm wide particle. As the wood constituents in fiber mats are much smaller than that, the time delay between surface and core temperature convergence is believed to be negligible.

### ***3.2.1.5 Rheology***

The heat and mass transfer equations are coupled with a one-dimensional rheological model that accounts for densification of the material as well as build-up and relaxation of stresses within the mat. Only normal compressive stresses acting perpendicular to the mat plane are considered. No shearing stresses are assumed, so that horizontal coupling between regions is not accounted for. Due to the lack of Poisson's ratio values for wood-furnish materials, and to maintain the simplicity of a one-dimensional rheological model, lateral spreading of the mat is ignored. Noticeable lateral spreading can be expected at the early stages of press closure when the mat is relatively loose. Furthermore, lateral spreading may lead to slight density reductions near the edges



of the mat. However, these effects are unlikely to have a significant impact on overall simulation results.

### ***3.2.1.6 Physical properties***

Physical properties of the mat and the gases within vary with respect to both space and time. Most properties are highly dependent on the local conditions within the mat. Furthermore, transport properties (for example, permeability) are allowed to vary in the three orthogonal directions. Differences are sometimes considerable between in-plane and cross-sectional directions. In-plane variations are usually less pronounced, however, and transport property data that distinguish between production direction and its orthogonal in-plane direction are rarely found in the literature. That is not to say that such differences are always unimportant; in-plane orientation of wood constituents is an important means of controlling product properties, and the need for such techniques are anticipated to increase in the future.

### ***3.2.1.7 Summary of important assumptions***

Listed below are assumptions made in the model presented in this thesis:

- The material is macroscopically homogeneous.
- Heat and mass transfer are three-dimensional.
- Water exists in bound water and vapor state; free water is not present.
- Mass transfer of fluids occurs by convection and diffusion of vapor and air; bound water and surface diffusion is neglected.
- Heat is transferred by conduction and convection.
- Local equilibrium between gas phase and cell walls is reached instantaneously.
- Only normal stresses perpendicular to the mat plane are considered.

## 3.2.2 Mathematical formulation

### 3.2.2.1 Mass transfer

#### 3.2.2.1.1 Constitutive equations

The gas in the porous mat is regarded as a pure two-component mixture of air and water vapor. A convective (or viscous) flux  $j^c$  of the gas mixture develops in response to a total pressure gradient. This flux can be calculated by applying Darcy's law. In addition to this convective flux, a diffusive flux  $j^d$  occurs due to partial pressure gradients of each of the components; the steady-state diffusive flux can be described by Fick's first law. As there are both total pressure gradients and partial pressure gradients within the mat during hot pressing, the convective and diffusive fluxes occur simultaneously. The convective flux is superimposed on the diffusive flux and the total flux  $j_i$  of component  $i$ , which can be vapor or air, is given by the following expression:

$$j_i = j_i^d + j_i^c \quad i = v, a \quad (3.1)$$

The diffusive and convective fluxes, respectively, can be calculated as:

$$j_i^d = -D_{eff} \frac{M_i}{RT_{abs}} \nabla p_i \quad i = v, a \quad (3.2)$$

$$j_i^c = -\frac{k_p}{\eta} \frac{M_i}{RT_{abs}} p_i \nabla p \quad i = v, a \quad (3.3)$$

where:

- $v, a$      subscripts to denote vapor or air
- $j_i^{d,c}$     diffusive or convective flux, respectively, of component  $i$  [kg/(m<sup>2</sup>·s)]
- $D_{eff}$      effective diffusion coefficient [m<sup>2</sup>/s]
- $M_i$      molecular mass of component  $i$  [kg/mol]
- $p_i$      partial pressure of component  $i$  [Pa]
- $p$      total gas pressure [Pa]
- $R$      gas constant [J/(mol·K)]
- $T_{abs}$     absolute temperature [K]
- $k_p$      permeability coefficient [m<sup>2</sup>]
- $\eta$      dynamic viscosity of the gas mixture [Pa·s]

The effective diffusion coefficient  $D_{eff}$  depends on the binary diffusion coefficient  $D_{va}$  of the vapor-air gas pair and on the dimensionless obstruction factor  $k_d$ , which is a property of the porous material (Krischer 1963). The physical meaning of the obstruction factor will be described in more detail in section 3.3.1 below.  $D_{eff}$  may be written as:

$$D_{eff} = \frac{D_{va}}{k_d} \quad (3.4)$$

### 3.2.2.1.2 Mass conservation equation

For the multi-dimensional problem, the mass conservation equation for gas component  $i$  (i.e., vapor or air) can be expressed in the following way:

$$-\frac{RT_{abs}}{M_i} \nabla \cdot j_i - p_i \frac{\partial \phi}{\partial t} + \frac{p_i \phi}{T_{abs}} \frac{\partial T}{\partial t} + \frac{RT_{abs}}{M_i} r_i = \phi \frac{\partial p_i}{\partial t}; \quad i = v, a \quad (3.5)$$

(mass flux)    (compression)    (temperature)    (generation)    (pressure)

The various symbols in the equation are defined in the list of nomenclature, and its derivation can be found in Appendix D.

The term on the right hand side of Equation (3.5) describes the change in partial pressure  $p_i$  of gas component  $i$ . The dimensionless variable  $\phi$  denotes the void fraction of the porous material (assuming cell wall material is inaccessible to gas). The change in partial pressure depends on each of the four terms on the left hand side. The first one describes the total mass flux  $j_i$  of gas component  $i$  by convection and diffusion.  $R$ ,  $T_{abs}$  and  $M_i$  denote the gas constant, absolute temperature and molecular mass of component  $i$ , respectively. The second term on the left hand side accounts for the change in void fraction due to compression (or spring-back) of the mat. The effect of temperature on the partial pressure is expressed in the third term on the left hand side. The fourth term accounts for the generation of component  $i$ . The rate of generation,  $r_i$ , is zero in the mass conservation equation for air, as it is assumed that there is no interaction between the air and the cell wall substance or other gas components. In the mass conservation equation for vapor, setting  $r_i$  equal to  $m_{ev}$  accounts for the transformation of vapor into bound-water, or vice versa. The evaporation rate  $m_{ev}$ , which may be expressed in the units of  $\text{kg}/(\text{m}^3 \cdot \text{s})$ , depends on the dependency between temperature, moisture content and vapor

pressure under equilibrium conditions (i.e., on the sorption isotherms). Values for this combination are not known a priori; they have to be approached during an iterative procedure to establish local equilibrium conditions.

It should be noticed that the mass balance is made for water vapor but not for the total amount of water in the system. Instead, the moisture content is linked to the mass conservation equation for water vapor by the evaporation rate  $r_i = m_{ev}$ .

### 3.2.2.2 Heat transfer

#### 3.2.2.2.1 Constitutive equation

The constitutive equation for conductive heat flux is known as Fourier's first law and can be written as:

$$q = -k_t \nabla T \quad (3.6)$$

where the conductive heat flux  $q$  is the quantity of heat [J] translated through the area of one  $m^2$  during one second.  $k_t$  denotes the thermal conductivity of the material in the units of  $W/(m \cdot K)$ , considering the porous medium as a homogeneous continuum, and  $\nabla T$  is the temperature gradient in the flux direction.

#### 3.2.2.2.2 Heat conservation equation

Suppose that the four components dry wood, bound water, water vapor, and dry air are named with the subscripts  $w$ ,  $b$ ,  $v$  and  $a$ , respectively. Further, let us introduce the dimensionless mass content  $u_i = m_i / m_w$ , which gives the local mass ratio of component  $i$  to dry wood. Such a denotation, rather than using the density, is convenient to ensure validity of Equation (3.7) during compression (and spring-back) of the mat, where the volume of the mat, and consequently the density of each component, changes. It should be noticed that, by definition, the mass content of dry wood,  $u_w$ , is always 1 and that the mass content of bound water,  $u_b$ , is the moisture content of wood on a dry weight basis (otherwise symbolized simply as  $u$  throughout this dissertation).

The heat conservation equation for three-dimensional heat flow may be written in a form that follows the formulation of Nasrallah and Perre (1988) for one-dimensional convective drying of porous media:

$$\begin{aligned}
 -\nabla \cdot q & - \underbrace{\nabla \cdot \sum_{i=v,a} (c_i j_i T) - H_v^\circ m_{ev}}_{\text{(convection)}} = \rho_w \frac{\partial}{\partial t} \sum_{i=w,b,v,a} (c_i u_i T) & (3.7) \\
 \text{(conduction)} & & \text{(accumulation)}
 \end{aligned}$$

where  $H_v^\circ$  is defined by  $H_v^\circ = H_v + (c_b - c_v)T$ .

The accumulation term on the right hand side describes energy storage in an infinitesimally small control region, while  $c_i$  denotes the specific heat of component  $i$ ,  $\rho_w$  the density of dry wood and  $T$  the local temperature. The first term on the left hand side describes the conductive heat flow, while the second term expresses the sensible heat transport associated with the mass flow  $j_i$  of vapor or air. The third term on the left hand side describes the generation of heat due to phase change.  $H_v$  denotes the latent heat of sorption from the vapor to the bound water state per unit mass [J/kg] and  $m_{ev}$  the evaporation rate in the units of kg/(m<sup>3</sup>·s); the expression  $(c_b - c_v)T$  accounts for the difference in specific heat between bound water and water vapor.

A simplified form of Equation (3.7) may be derived since the mass of vapor and air within the mat is very small compared to the mass of wood and bound water. Therefore, the transfer of sensible heat associated with the gas flow, as well as heat consumed or liberated when increasing or decreasing the temperature of the gas, may be neglected. The non steady-state heat conservation equation may now be written in the form:

$$\begin{aligned}
 -\nabla \cdot q & - H_v m_{ev} = c_u \rho_u \frac{\partial T}{\partial t} & (3.8) \\
 \text{(conduction)} & \quad \text{(phase change)} \quad \text{(accumulation)}
 \end{aligned}$$

where  $c_u$  and  $\rho_u$ , respectively, denote specific heat and density of the wood-furnish material at current moisture content. This heat conservation equation includes conductive heat transfer as well as that share of convective heat transfer that comes from phase

change. Convective heat transfer resulting from the transport of sensible heat is neglected. The derivation of Equations (3.7) and (3.8) is presented in Appendix D.

### 3.2.2.3 Sorption equilibrium

The relationship between equilibrium moisture content (EMC), temperature, and relative humidity may be expressed by an equation or can be read from a table. The latter approach is used for the present model. A convenient way to present the data in a table is to let EMC and temperature be the independent variables and relative humidity the dependent variable (see Appendix E). Then, for a given EMC-temperature combination, the relative humidity value can be obtained by two-dimensional interpolation. In this work, linear interpolation is used.

The principle of mass conservation requires that the mass change of bound water is equal to the mass of evaporated or absorbed water. The relationship between evaporation rate  $m_{ev}$  and change in moisture content,  $\Delta u$ , during a small time step  $\Delta t$  is described by the equation

$$m_{ev} = -\rho_w \frac{\Delta u}{\Delta t} \quad (3.9)$$

where  $\rho_w$  is the density of dry wood. The moisture content is the mass ratio of bound water to dry wood and may be defined as:

$$u = \frac{m_b}{m_w} \quad (3.10)$$

where  $m_b$  and  $m_w$  denote the masses of bound water and dry wood. This definition of the moisture content  $u$ , given in the units of [%] or [-], will be used throughout this work, unless otherwise stated.

### 3.2.2.4 Thermodynamic relationships

The ratio between actual partial pressure of water vapor,  $p_v$ , and saturated water vapor pressure,  $p_{sat}$ , at a given temperature is described as relative humidity  $\phi$ .

$$\varphi = \frac{p_v}{p_{sat}} \quad (3.11)$$

The relative humidity can be defined in % or as a dimensionless variable. The saturated vapor pressure is influenced by temperature and may be calculated according to an empirical equation (Humphrey and Bolton 1989a):

$$\log_{10} p_{sat} = 10.745 - \frac{2141.0}{T_{abs}} \quad (3.12)$$

Here,  $T_{abs}$  is the absolute temperature in K.

As an approximation, the gaseous mixture is supposed to be an ideal mixture of perfect gases. Then, the equation of state of an ideal gas describes the relationships between the thermodynamic properties for each of the gas components  $i$ :

$$p_i V_{eff} = \frac{m_i}{M_i} RT_{abs}; \quad i = v, a \quad (3.13)$$

where:

$p_i$	partial pressure of component $i$ [Pa]
$V_{eff}$	volume occupied by gas mixture [m <sup>3</sup> ]
$m_i$	mass of component $i$ [kg]
$M_i$	molecular mass of component $i$ [kg/mol]
$R$	gas constant [J/(mol·K)]
$T_{abs}$	absolute temperature [K]

According to Dalton's law, the total gas pressure  $p$  of a mixture of ideal gases is equal to the sum of its partial pressures  $p_i$ :

$$p = \sum_{i=v,a} p_i \quad (3.14)$$

In the present approach, vapor ( $v$ ) and air ( $a$ ) are assumed to be the only gas components.

To increase the temperature of a solid, liquid or gas, a certain amount of energy,  $\Delta Q$ , has to be transferred or generated. This amount in Joules is proportional to the mass  $m$  of the body in kg and to its temperature change  $\Delta T$ . The heat energy necessary to

increase the temperature of a mixture can be calculated by adding the required energy for all components  $i$ :

$$\Delta Q = \sum_i (c_i m_i) \Delta T \quad (3.15)$$

The proportionality factor  $c_i$  is called the specific heat of the component  $i$ , given in the units of J/(kg·K).

Phase change of water is always associated with consumption or release of heat energy. The relationships between latent heat of evaporation and temperature, and between latent heat of sorption and moisture content may be expressed by equations (see section 3.3.1 below).

### 3.2.2.5 *Mat densification and stress relaxation*

In the present work the rheological behavior of the wood-furnish mat is described by the Burger-Humphrey model (Figure 2.6) introduced in section 2.3.2.2. This model uses a system of linked springs and dashpots as an analogy to calculate the stress-strain relationship of the mat (Ren 1991).

Strain, which is a dimensionless quantity, may be defined as the ratio of the change of length of a member,  $\Delta l$ , to its original length  $l$ :

$$\varepsilon = \frac{l - l_{new}}{l} = -\frac{\Delta l}{l} \quad (3.16)$$

This definition is based on the assumption that the deformation is distributed uniformly over the length  $l$ . For convenience, the sign convention is chosen so that compressing the member yields a positive strain.

The Burger-Humphrey model accounts for four different sources of deformation. These are elastic ( $el$ ), viscous ( $vi$ ), delayed-elastic ( $de$ ), and plastic and micro-fracture ( $pmf$ ) strain. The total strain  $\varepsilon$  is the sum of these four strain components:

$$\varepsilon = \varepsilon_{el} + \varepsilon_{vi} + \varepsilon_{de} + \varepsilon_{pmf} \quad (3.17)$$

Figure 3.1 shows the response of each of the strain components when applying a sudden stress at time  $t_0$ , then keeping the stress constant for a certain period until  $t_1$ , and



eventually dropping the stress to zero again. As can be seen from this figure, elastic as well as plastic and micro-fracture deformation occurs instantaneously upon the application of stress, whereas viscous and delayed-elastic deformation are time-dependent. Further, it should be noticed that only elastic and delayed-elastic deformation are recoverable after the stress is removed at  $t_1$ , but not the other two strain components.

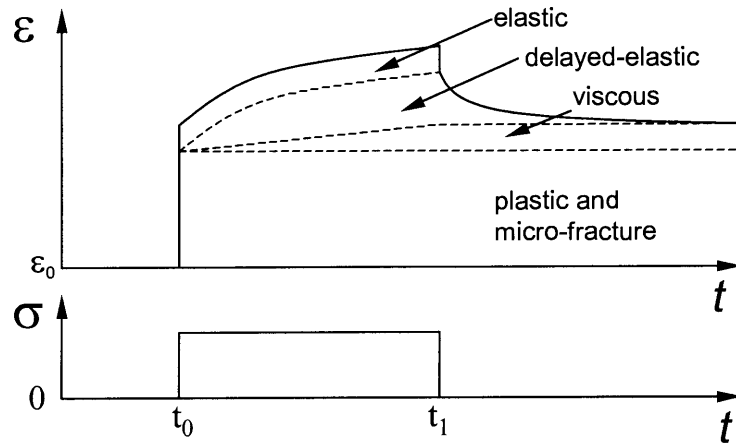


Figure 3.1. The four strain components described by the Burger-Humphrey model as a function of stress and time.

Ren (1991) presented the following expression to describe the relationship between stress and total strain under conditions of compression:

$$\epsilon = \frac{\sigma}{E_{el}} + \frac{\sigma t}{V_{vi}} + \frac{\sigma}{E_{de}} \left( 1 - e^{-\frac{E_{de} t}{V_{de}}} \right) + \frac{\sigma}{E_{pmf}} \quad (3.18)$$

where:

$\epsilon$	total strain [-]
$\sigma$	stress [Pa]
$t$	time [s]
$E_{el}$	modulus of elasticity (MOE) of elastic strain component [Pa]
$V_{vi}$	viscosity of viscous strain component [Pa·s]
$E_{de}$	MOE of delayed-elastic strain component [Pa]
$V_{de}$	viscosity of delayed elastic strain component [Pa·s]
$E_{pmf}$	coefficient of plastic and micro-fracture strain component [Pa]

Equation (3.18) gives the strain as a function of stress for the linear case, provided that  $\varepsilon = 0$  at  $t = 0$ , and that the stress is constant. For mat densification during hot pressing it is known that the wood-furnish material behaves in a highly non-linear fashion; each of the rheological coefficients change with progressing consolidation, and also depend, to some degree, on temperature and moisture content (Ren 1991, von Haas 1998).

To apply the Burger-Humphrey model to the hot pressing process, a mathematical formulation is needed that accounts for the non-linear character of the rheological coefficients, as well as for the non-constant stress course. Expressions appropriate to compute the stress-strain relationship under such conditions will be derived here in turn for each of the four strain components.

#### 3.2.2.5.1 Spring (elastic strain component)

The elastic strain component is represented by a single spring that obeys Hook's law. For a small deformation, and if  $\sigma = 0$  when  $\varepsilon = 0$ , a general expression can be written as:

$$\varepsilon = \frac{\sigma}{E} \quad (3.19)$$

In order to derive a mathematical expression for the spring behavior, it is important to acknowledge that instantaneous deformations are caused not only by a change of stress, but also by a change of the modulus of elasticity (MOE). Therefore,  $\varepsilon$  has to be differentiated partially with respect to both  $\sigma$  and  $E$ :

$$d\varepsilon = \frac{\partial \varepsilon}{\partial \sigma} d\sigma + \frac{\partial \varepsilon}{\partial E} dE \quad (3.20)$$

Equation (3.20) together with Equation (3.19) gives:

$$d\varepsilon = \frac{1}{E} d\sigma - \frac{\sigma}{E^2} dE \quad (3.21)$$

Integrating Equation (3.21) over the time interval  $\Delta t$  yields:

$$\Delta \varepsilon = \frac{1}{E} \Delta \sigma - \frac{\sigma}{E^2} \Delta E \quad (3.22)$$

The physical meaning of the second term on the right hand side can be understood when imagining a spring under constant load that is heated. Due to the softening of the spring it will change its length. Applying this analogy to wood-furnish materials, it seems reasonable to expect further deformation resulting from the elastic strain component when heating or wetting a mat under constant pressure. However, it is not so clear whether the mat will expand when it cools or dries, again neglecting all other strain components in this train of thought. This shows that the assumption made above, namely that deformation is caused by any change in MOE, may not always be true.

#### 3.2.2.5.2 Dashpot (viscous strain component)

A dashpot behaves as a Newtonian fluid and is used here to explain the viscous component of the material behavior. The rate of strain  $d\varepsilon/dt$  in a perfectly viscous fluid is connected with the stress  $\sigma$  by:

$$\sigma = V \frac{d\varepsilon}{dt} \quad (3.23)$$

where  $V$  denotes the viscosity of the liquid. This equation may also be written as:

$$d\varepsilon = \frac{\sigma}{V} dt \quad (3.24)$$

which can be integrated over the time interval  $\Delta t$  to obtain:

$$\Delta \varepsilon = \frac{\sigma}{V} \Delta t \quad (3.25)$$

It is clear from these equations that a sudden change of  $\sigma$  or  $V$  does not lead to an instantaneous deformation of the viscous element.

### 3.2.2.5.3 Kelvin model (delayed-elastic strain component)

The delayed-elastic component of the material behavior is symbolized by the Kelvin model (sometimes called Voigt model), which is a parallel arrangement of a spring and a dashpot (Figure 3.2). Immediately after a sudden stress is applied in such a system, the entire stress acts on the dashpot, while the spring is still relaxed. As time elapses and the piston in the dashpot changes its position, the stress acting on the spring gradually increases, while the stress acting on the dashpot decreases and eventually approaches zero.

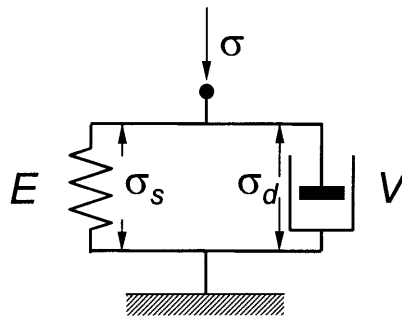


Figure 3.2. Kelvin model.  $E$  = modulus of elasticity,  $V$  = viscosity,  $\sigma$  = effective stress,  $\sigma_s$  = stress acting on spring,  $\sigma_d$  = stress acting on dashpot. The non-linear behavior of both elements is not symbolized in this schematic.

An expression commonly stated in the literature to describe the time-dependent stress-strain relationship in a Kelvin model is:

$$\varepsilon = \frac{\sigma}{E} \left( 1 - e^{-\frac{E}{V}t} \right) \quad (3.26)$$

which is the third term on the left hand side of Equation (3.18). This expression has been derived for the case of constant stress and coefficients. For varying stress and coefficients, an appropriate formulation of the Kelvin model has not been found in the literature and will therefore be derived here.

The two elements, spring and dashpot, are described by Equations (3.21) and (3.24), respectively. These equations are connected by two conditions. First, the deformation of the spring is always equal to the deformation of the dashpot. Second, the

total stress  $\sigma$  is the sum of the partial stresses acting on spring and dashpot. These constraints can be expressed as:

$$d\varepsilon = d\varepsilon_s = d\varepsilon_d \quad (3.27)$$

$$\sigma = \sigma_s + \sigma_d \quad (3.28)$$

where the subscripts  $s$  and  $d$  stand for spring and dashpot.

In consideration of Equations (3.27) and (3.28), Equation (3.24), which describes the dashpot, can be used to calculate the effective strain change  $d\varepsilon$  of the Kelvin model:

$$d\varepsilon = \frac{(\sigma - \sigma_s)}{V} dt \quad (3.29)$$

In order to determine  $\sigma_s$ , which denotes the stress acting on the spring at time  $t$ , Equation (3.21) for the spring and Equation (3.29) for the dashpot can be substituted into Equation (3.27):

$$\frac{1}{E} d\sigma_s - \frac{\sigma_s}{E^2} dE = \frac{(\sigma - \sigma_s)}{V} dt \quad (3.30)$$

Rearranging this expression gives:

$$d\sigma_s = \frac{E(\sigma - \sigma_s)}{V} dt + \frac{\sigma_s}{E} dE \quad (3.31)$$

$\sigma_s$  can be obtained by adding up all stress changes  $d\sigma_s$  since time  $t = 0$ .

$$\sigma_s = \sum_0^t d\sigma_s \quad (3.32)$$

Equations (3.29), (3.31) and (3.32) represent the final set of equations needed to calculate the strain change  $d\varepsilon$  at time  $t$  for the Kelvin model. The stress of the spring,  $\sigma_s$ , contains information about the history of the material. Unlike the single spring and dashpot, the strain represented by a Kelvin model does not only depend on the prevailing values of the effective stress and rheological coefficients, but also on the stress distribution between spring and dashpot, which itself is a consequence of the previous course of deformation.

Integrating Equations (3.29) and (3.31) over the time interval  $\Delta t$  and summarizing Equations (3.31) and (3.32) leads to:

$$\Delta \varepsilon = \frac{(\sigma - \sigma_s)}{V} \Delta t \quad (3.33)$$

$$\sigma_s = \sum_0^t \left( \frac{E(\sigma - \sigma_s)}{V} \Delta t + \frac{\sigma_s}{E} \Delta E \right) \quad (3.34)$$

#### 3.2.2.5.4 Hindered spring (plastic and micro-fracture strain component)

Strain as a consequence of plastic and micro-fracture (PMF) effects is represented by a spring that can be compressed but not expanded. The spring experiences compression upon application of load, but when the load is partially or fully removed the spring stays in its position of maximum compression. To further compress the spring, the load has to go beyond a critical value.

According to Ren's (1991) definition of PMF strain in wood-furnish materials, strains due to PMF effects only occur if the effective stresses exceed the yield strength of the microstructures. Haselein's (1998) interpretation of this definition was to assume that fracture would occur only if the stress exceeds the previous stress maximum. A somewhat different interpretation will be adopted here.

Suppose that a mat is compressed to its final thickness by two distinct densification steps, where the main densification happens at the beginning and the second densification step towards the end of the pressing cycle. Such cycles are typical for pressing MDF; the second densification step may reduce the mat thickness by as much as 15 % or more (see Figure C.1 in Appendix C). An order of magnitude calculation showed that unrealistically high pressing forces would be required if only elastic, viscous and delayed-elastic strain contributed to densification at this late stage of the pressing cycle. However, the actual compaction pressure during the second densification step does not usually reach the maximum pressure applied during the earlier main densification stage. Apparently, further densification due to PMF effects happens without requiring the effective stress to exceed the previous stress maximum. Softening of the mat, due to temperature and moisture content changes, seems to reduce the yield strength of the

microstructures, which is, according to Ren (1991), the critical stress value to be exceeded in order to let further compression occur.

Let us define  $c_{crit}$  as a constant that includes information about the conditions from the last time the effective stress  $\sigma$  exceeded the yield strength  $\sigma_{yield}$ . The following set of equations provides a mathematical formulation of the PMF element:

$$\sigma_{yield} = c_{crit} \cdot E_{pmf} \quad (3.35)$$

$$\text{if } \sigma > \sigma_{yield} : \quad d\varepsilon = \frac{1}{E_{pmf}} d\sigma - \frac{\sigma}{E_{pmf}^2} dE_{pmf} \quad (3.36)$$

$$c_{crit} = \frac{\sigma}{E_{pmf}} \quad (3.37)$$

$$\text{if } \sigma \leq \sigma_{yield} : \quad d\varepsilon = 0 \quad (3.38)$$

$$c_{crit} = \text{const.} \quad (3.39)$$

where  $E_{pmf}$  denotes the coefficient of plastic and micro-fracture strain component. Further deformation may only happen if the effective stress surpasses the yield strength of the material. In this case, the constant  $c_{crit}$  has to be updated to store the new criterion for the yield strength. As can be seen from Equation (3.35), the yield strength decreases when the material is softened by heat and/or by moisture. Equation (3.36) constitutes the formulation derived above for a simple elastic spring.

Integrating Equation (3.36) over  $\Delta t$  yields

$$\Delta\varepsilon = \frac{1}{E_{pmf}} \Delta\sigma - \frac{\sigma}{E_{pmf}^2} \Delta E_{pmf} \quad (3.40)$$

### 3.2.3 Initial and boundary conditions

#### 3.2.3.1 Initial conditions

In the current version of the simulation program, the wood-furnish mat is allowed to consist of either one or three layers. For the latter case, the arrangement of the layers is symmetrical around the central plane. However, the program could be altered easily to account for mats with two, four or more layers and asymmetrical structures. Initially,

each layer has a constant thickness over the x-y plane and a uniform distribution of its conditions and properties. The pressing pressure is zero at the onset of press closure. For the one-layered mat, the initial conditions may be represented in the following way:

$$\begin{aligned}
 T|_{x,y,z,t=0} &= T_0; & u|_{x,y,z,t=0} &= u_0; & \rho|_{x,y,z,t=0} &= \rho_0; & (3.41) \\
 p|_{x,y,z,t=0} &= p_{amb}; & p_v|_{x,y,z,t=0} &= f(T_0, u_0); \\
 d|_{x,y,t=0} &= d_0; & \sigma_{press}|_{x,y,t=0} &= 0;
 \end{aligned}$$

where:

$T$	mat temperature
$u$	moisture content
$\rho$	mat density
$p$	total gas pressure
$p_{amb}$	ambient total gas pressure
$p_v$	partial vapor pressure
$d$	thickness of mat
$\sigma_{press}$	pressing pressure
$0$	subscript for time $t = 0$

### 3.2.3.2 Boundary conditions

Three types of spatial boundaries have to be considered: First the interface between the composite material and the hot platen, second the interface between composite material and ambient air, and third those at the symmetry planes.

While the mat is always regarded as being symmetrical across its width (y-direction), symmetries in x- and z-direction are optional. Clearly, when simulating a continuous press, a symmetrical treatment of the mat in production (x) direction is not appropriate. The option of allowing an asymmetrical structure of the mat in the z-direction may be helpful in the future to account for slight vertical deviations from symmetry, that are commonly observed in the industrial process, or to simulate asymmetric scenarios that may be desired.

For the purpose of presenting a mathematical formulation of the boundary conditions, it is assumed here that the rectangular mat is symmetrical in all directions. The boundary conditions are presented here for a batch press.



### 3.2.3.2.1 Mass transfer

The interface between mat and pressing platen is assumed to be impermeable. However, when extending the model to describe a steam injection press, gas movement through this boundary has to be taken into account. Assuming impermeable pressing platens for the time being, the boundary condition can be written as:

$$\left. \frac{\partial p_i}{\partial z} \right|_{z=0} = 0; \quad i = v, a \quad (3.42)$$

where:

$p_i$  partial pressure of component  $i$   
 $v, a$  subscripts to denote vapor or air

The edges of the mat are open for vapor and air flow. Due to gas turbulences and the irregular shape of the press components close to the edges of the mat, the temperature and vapor pressure distribution in the air is relatively complex. An exact arithmetical consideration of this interface seems to be rather complicated. Therefore, a homogenous temperature and vapor pressure distribution in the ambient surrounding air is assumed in the present approach. A more elaborate treatment of this interface may be necessary in the future. However, external gradients are unlikely to be significant compared to those within the mat. The boundary conditions at the mat edges are:

$$p_i \Big|_{x=0} = p_i \Big|_{y=0} = p_{i,amb}; \quad i = v, a \quad (3.43)$$

where  $p_{i,amb}$  denotes the partial vapor and air pressures, respectively, prevailing in the ambient air.

By definition, no mass transfer occurs across symmetry planes.

$$\left. \frac{\partial p_i}{\partial x} \right|_{x=\frac{l}{2}} = \left. \frac{\partial p_i}{\partial y} \right|_{y=\frac{w}{2}} = \left. \frac{\partial p_i}{\partial z} \right|_{z=\frac{d}{2}} = 0; \quad i = v, a \quad (3.44)$$

Here,  $l$ ,  $w$  and  $d$  symbolize the length, width and thickness, in that order, of the mat.

### 3.2.3.2.2 Heat transfer

The temperature of the mat at the mat-platen interface is equal to the platen temperature  $T_{press}(t)$ , which may vary with time according to a specified temperature course. The temperature of the heat source is assumed to be unaffected by conductive heat loss towards the wood material. Such addition would require the incorporation of a heat transfer analysis for the platen heat sources. Furthermore, screens, that are sometimes placed between pressing platens and mat, are disregarded.

$$T|_{z=0} = T_{press}(t) \quad (3.45)$$

When considering conductive energy transfer through the interface between mat and ambient air, compared with the energy loss through this interface by convection, the conductive heat transfer is assumed to be rather small. For that reason, heat conduction at the edges is not accounted for.

$$q_x|_{x=0} = q_y|_{y=0} = 0 \quad (3.46)$$

where  $q_{x,y}$  are the conductive heat fluxes in x- and y-directions.

No conductive heat transfer happens through the symmetry planes

$$\frac{\partial T}{\partial x} \Big|_{x=\frac{l}{2}} = \frac{\partial T}{\partial y} \Big|_{y=\frac{w}{2}} = \frac{\partial T}{\partial z} \Big|_{z=\frac{d}{2}} = 0 \quad (3.47)$$

### 3.2.3.2.3 Mat densification

The model presented here accounts for two different press control modes, which are termed *position control* and *load control*. The final thickness of the mat is assumed to not be dictated by spacing strips mounted on the pressing platens, or by similar devices.

In the case of position control, the target thickness of the mat is specified for distinct times, and the thickness values for any intermediate time can be obtained by linear interpolation between the two adjacent thickness values specified. The pressing platens are assumed to be rigid, forcing the mat to have a constant thickness  $d$  across its x-y plane.

$$d|_{x,y} = d(t) \quad (3.48)$$

When the press is assumed to be operated in load control mode, the pressing pressure is specified in a similar way to that for thickness. It is assumed that the applied stress is the same all over the x-y plane. Consequently, the thickness response may alter with position in the x-y plane due to different temperature and moisture conditions, implying that the pressing platens are not rigid but are allowed to bend.

$$\sigma_{press}|_{x,y} = \sigma_{press}(t) \quad (3.49)$$

A refined approach that treats the pressing platens as rigid bodies may consider the specified target pressing pressure as the average pressure over the total platen area, assuming constant thickness but varying stress response for different horizontal positions. However, preliminary simulation runs showed that the assumption of uniform stress (and not uniform thickness) leads to thickness deviations between center and edge of less than 5 %. Inaccuracies due to such small platen deflections can be expected to have only minor effects on heat and mass transfer and density profile predictions. Furthermore, the assumption of totally rigid pressing platens does not necessarily reflect reality in large-sized industrial presses (Heller 1995). Incorporating bending effects of the platens into the model would require a structural analysis of the pressing platens itself, which is beyond the scope of this work.

### 3.3 PHYSICAL PROPERTIES

#### 3.3.1 Material properties

In order to make predictions with a simulation model, information about the material properties has to be available and provided as model input data. Some properties of a given wood-furnish material are highly dependent on the physical conditions of the material, such as temperature, moisture content and density. Analytical descriptions of these relationships are in general difficult to derive. Therefore, empirically derived data have to be used.

Material property data are specific to the wood-furnish material type to be used. As differences in anatomical cell wall structure or material treatment prior to pressing may influence the properties of the mat material considerably, care has to be taken when using data from a different material type. Sensitivity studies by means of simulation may provide valuable information to assess the robustness of the model towards changes in material properties. Such studies have been reported by Haselein (1998) for thermal conductivity and permeability. Haselein showed that relatively small changes in these two properties could have a significant impact on several internal mat conditions.

Referring to the importance of using appropriate data for the material type of interest, Humphrey (1991) suggested to develop and improve automated techniques to evaluate material characteristics. The possibility of applying such techniques on a routine basis would be desirable, particularly when employing simulation models in the industrial setting.

### 3.3.1.1 Permeability

Two alternative sets of permeability data are provided as input data for the simulation program. Those data reported by Haselein (1998) were measured on unresinated fiber discs, applying a technique that simultaneously determines in-plane and cross-sectional permeability from airflow measurements. Von Haas et al. (1998) measured in-plane and cross-sectional permeability on samples prepared from consolidated panels. Only data for MDF are presented here. The adhesive content of these samples was 11 %.

Both sets of data give the permeability as a function of density and can be expressed by an exponential equation of the form:

$$k_p = e^{\frac{1}{a + b\rho + c/\ln\rho}} \quad (3.50)$$

where permeability  $k_p$  and density  $\rho$  have the units of  $\text{m}^2$  and  $\text{kg}/\text{m}^3$ , respectively. The coefficients  $a$ ,  $b$  and  $c$  are specified in Table 3.1.

Table 3.1. Coefficients for Equation (3.50) to determine in-plane and cross-sectional permeability.

	Flow direction	$a$	$b$	$c$
Haselein (1998)	in-plane	-0.006	2.95E-06	-0.199
	cross-sectional	-0.026	4.98E-06	-0.074
von Haas et al. (1998)	in-plane	-0.041	9.51E-06	-0.015
	cross-sectional	-0.037	1.10E-05	-0.037

### 3.3.1.2 Obstruction factor for molecular diffusion

The resistance that a porous medium offers to a diffusive flux may be expressed by the obstruction factor  $k_d$ . This quantity is, like the permeability  $k_p$ , a material property that depends upon the pore structure of the medium; it is independent of the gas properties. However, pore size and shape influence diffusive and viscous fluxes in different ways (Cunningham and Williams 1980). While viscous flux rates are strongly related to the diameters of the capillaries, diffusive flux is independent of this characteristic unless the diameter is in the order of the mean molecular free path and Knudsen diffusion is relevant. It follows from this difference that there is no simple way to relate permeability values to the obstruction factor.<sup>10</sup>

The obstruction factor of a porous medium is usually obtained from diffusion experiments. Suppose that  $D_{eff}$  is the measured diffusion coefficient and  $D_{va}$  the binary diffusion coefficient for the vapor-air gas pair at the same temperature and pressure conditions. The obstruction factor  $k_d$  can then be calculated from Equation (3.4). It follows from this definition of  $k_d$  that this quantity describes how many times the diffusion resistance of the material exceeds that of an open space devoid of walls.

---

<sup>10</sup> Cunningham and Williams (1980) pointed out that it would be more consistent to refer to  $k_d$  as permeability for molecular diffusion, and continue to call  $k_p$  the permeability for laminar flow, or instead refer to  $k_p$  as the obstruction factor for laminar flow, and continue to call  $k_d$  the obstruction factor for molecular diffusion.

Diffusion rates within a porous medium are decreased by both the reduced cross-section available for flow and the lengthening of the flow paths around the obstacles. The reduction of the cross-section depends directly on the void fraction  $\phi$  of the material. The obstruction factor  $k_d$  combines both material characteristics into one quantity and may be expressed as  $k_d = \tau / \phi$ , where  $\tau$  is the tortuosity factor of capillary pathways (Krischer 1963)<sup>11</sup>. The irregular shape of single pores makes it impossible to measure or theoretically derive exact values for the tortuosity factor, but it may be calculated if  $k_d$  and  $\phi$  are known. For most purposes, however, it is not necessary to know the actual value of the tortuosity factor.

An equation has been derived from data measured at the Ordinariat für Holztechnologie (Universität Hamburg, Germany) to relate the obstruction factor of MDF to material density:

$$k_d = 0.334e^{5.08 \cdot 10^{-3} \rho} \quad (3.51)$$

where  $k_d$  and  $\rho$  denote the dimensionless obstruction factor and the material density (in the units of  $\text{kg/m}^3$ ), respectively. A summary of the diffusion experiment is given in Appendix A.

### 3.3.1.3 Thermal conductivity

For MDF, von Haas (1998) described the relation between thermal conductivity perpendicular to the panel plane and density by:

$$k_t^{0,30} = 4.86 \cdot 10^{-8} \rho^2 + 4.63 \cdot 10^{-5} \rho + 4.38 \cdot 10^{-2} \quad (3.52)$$

with density  $\rho$  in the units of  $\text{kg/m}^3$ .  $k_t^{0,30}$  denotes the thermal conductivity in the units of  $\text{W}/(\text{m}\cdot\text{K})$ , measured at 0 % moisture content and 30°C. Equation (3.52) will be used in the present work for the reason that the thermal conductivity measurements reported by

---

<sup>11</sup> Confusion exists about the term 'tortuosity' as some authors use it synonymously with the term 'obstruction factor' (for example, Cussler 1984). Considering a material with only straight pores in flow direction, 'tortuosity' appears to be an unfortunate wording to describe the reduction of the diffusive flux.

von Haas were done on fiber material from the same manufacturer as the mats for the validation experiments described in section 5.2.3.

A comparison of thermal conductivity versus density curves for different temperatures (von Haas 1998) and different moisture contents (Haselein 1998) reveals that the curves approximately follow similar courses, which differ only by a constant quantity  $\Delta k_t$  from each other. Therefore, the assumption appears to be justified that, within limits,  $\Delta k_t$  is independent of density and may be added to the values obtained by Equation (3.52) to account for moisture and temperature effects. Haselein (1998) evaluated data presented by Shao (1989) and Kühlmann (1962) to derive such a correction term. The expression to account for moisture and temperature effects may be written as:

$$\Delta k_t = 4.9 \cdot 10^{-3} u + (1.1 \cdot 10^{-4} + 4.3 \cdot 10^{-5} u)(T - T_{exp}) \quad (3.53)$$

where moisture content  $u$  and temperature  $T$  are in the units of % and °C, respectively.  $T_{exp}$  is the average experimental temperature used when measuring the thermal conductivity (here 30°C). The thermal conductivity as a function of density, temperature and moisture content,  $k_t$ , can then be calculated by combining Equations (3.52) and (3.53) to yield:

$$k_t = k_t^{0,30} + \Delta k_t \quad (3.54)$$

An estimation of the effect of heat flux direction relative to the mat's structure on thermal conductivity has been reported by Humphrey and Bolton (1989a). They suggested to calculate the thermal conductivity parallel to the mat plane,  $k_{t,x-y}$ , as:

$$k_{t,x-y} = 1.5 k_t \quad (3.55)$$

#### 3.3.1.4 Specific heat

The specific heat of dry wood, as for many organic materials, has been reported to increase with increasing temperature. Skaar (1972) presented equations from six authors that all reported a nearly linear relationship between specific heat and temperature, two of

them for temperatures up to 140°C. In contrast to wood, the specific heat of water in its liquid phase is almost independent of temperature (VDI 1988).

In order to calculate the compound specific heat of wood, which contains sorbed water, several researchers have based their calculations on the assumption that wood and water contribute to the heat capacity in proportion to their masses (e.g., Kollmann 1951). By using this method of simple mixtures, and averaging the intercepts and slopes of the six equations given by Skaar (1972) to account for the temperature effect, Haselein (1998) derived the following equation:

$$c = \frac{1131 + 4.19T + 4190u}{1 + u} \quad (3.56)$$

where:

$c$	specific heat of wood at current moisture content [J/(kg·K)]
$T$	temperature [°C]
$u$	moisture content [-]

This expression will be used in the present work to relate the specific heat of wood to moisture content and temperature. However, as Kelsey and Clarke (1956) pointed out, the actual specific heat of wood is higher than the value calculated by treating water and dry wood as a simple mixture. They showed arithmetically that this deviation is a consequence of the temperature dependence of the heat of sorption. Kühlmann (1962) gave a similar explanation for the elevated specific heat of moist wood. It is interesting to note that the effect of temperature on the heat of sorption is only significant for moisture contents above 5 %. Consequently, at low moisture contents, where water molecules are strongly bound to the cellulose, the apparent specific heat of the bound water has about the same values as for liquid water. Only for less strongly bound water, the apparent specific heat deviates from that one of liquid water. Kelsey and Clarke did not rationalize this phenomenon.

Kühlmann (1962) measured the specific heat for particleboard and found no significant difference, compared to solid wood. The same can be expected for fiberboard, since the specific heat depends on the chemical structure of a material rather than on its physic or geometric structure.



### 3.3.1.5 Hygroscopicity

Engelhardt (1979) presented sorption isopsychrens (i.e., lines of equal relative humidity) that are based on measurements reported by Weichert (1963) for temperatures below 100°C, and on his own measurements in the temperature range between 110°C and 170°C (Figure 3.3). Both researchers used beech samples for their experiments.

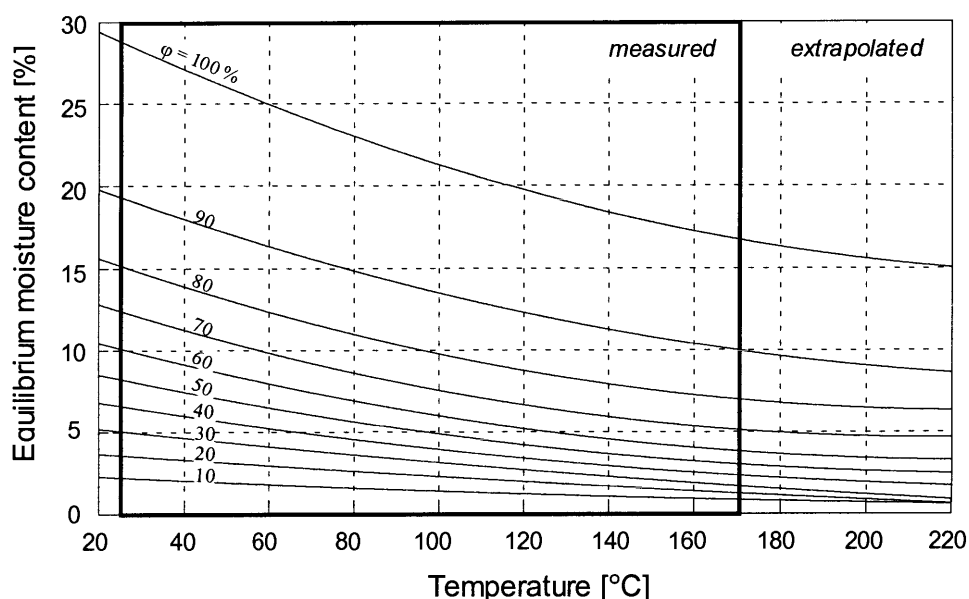


Figure 3.3. Measured and extrapolated sorption isopsychrens for beech presented by Engelhardt (1979).

During panel pressing, temperatures in those layers of the wood-furnish mat close to the surfaces often exceed 170°C. However, it appears that experimental data for such high temperatures are not available. Therefore, the curves presented by Engelhardt (1979) were extrapolated by fitting a second order polynomial to the measured data, and then calculating equilibrium moisture content values for the temperature ranges of 20 to 25°C and 170 to 220°C. The extrapolated curve segments are included in Figure 3.3.

In order to represent the data in a table with the relative humidity as dependent variable, sorption isotherms were plotted, and the relative humidity values were determined graphically. The table is displayed in Appendix E.

### 3.3.1.6 Heat of sorption and heat of evaporation

The heat energy,  $H_v$ , required to evaporate a unit of water bound in the wood cell wall consists of both the latent heat of sorption,  $H_l$ , and the latent heat of evaporation from a free liquid surface,  $H_{ev}$ .

$$H_v = H_{ev} + H_l \quad (3.57)$$

$H_v$  is sometimes also called the heat of sorption from the vapor state. The units of  $H_v$ ,  $H_{ev}$  and  $H_l$  are J/kg.

Flowers and Mendoza (1970, in Humphrey and Bolton 1989a) presented the Clausius Clapeyron equation in the following form to relate the latent heat of evaporation of free water to temperature  $T$ , given in °C:

$$H_{ev} = 2.511 \cdot 10^6 - 2.48 \cdot 10^3 T \quad (3.58)$$

Bramhall (1979) derived an equation that gives the latent heat of sorption as a function of moisture content. The equation is based on measurements made by Weichert (1963) for solid wood.

$$H_l = 1.172 \cdot 10^6 e^{-0.15u} \quad (3.59)$$

Here,  $u$  denotes the moisture content in %.

Several authors (e.g., Kelsey and Clarke 1956, Engelhardt 1979) have reported a temperature effect on the heat of sorption. This effect is, however, rather small compared to the summated latent heats of evaporation and sorption, and neglecting temperature dependencies therefore appears to be justified. The heat of sorption measured for solid wood may also differ from values for wood-furnish mats. Yet, Equation (3.59) will be used in the present work since no latent heat of sorption data are reported in the literature for composite mats or panels.

### 3.3.1.7 Rheological data

In the model presented here, densification and internal stresses are calculated by means of the Burger-Humphrey model (Figure 2.6) described above. For that, rheological

coefficients of the five elements are needed as model input data. These coefficients are functions of temperature, moisture content and density.

Two different sets of data are available so far, either of which may be used for the simulation model. The first one was measured by Ren (1991) and fitted to equations by Haselein (1998). The second set of data was obtained by von Haas (1998) for fiber, particle and strand materials. Von Haas's data for fiber will be used for simulation runs throughout this work.

Von Haas (1998) described the mat behavior separately for different phases and aspects of the pressing process. He did not use the Burger-Humphrey model, which integrates the most important aspects of the material behavior into one approach. The five rheological coefficients for the Burger-Humphrey model can, however, be derived from the results of two different experiments reported by von Haas.

In creep experiments, von Haas (1998) compressed fiber disks in a miniature press, following a pressing program that allowed him to compute the rheological coefficients for the four-element Burger model from the defined stress and measured thickness course. This procedure was repeated for different temperature, moisture content and density levels. For each of the four rheological coefficients the results were fitted to an equation of the form:

$$\ln C_0 = a_1 u + b_1 T + c_1 + \rho e^{(a_2 u + b_2 T + c_2)} \quad (3.60)$$

where:

$C_0$	rheological coefficient $E_{el}$ , $V_{vi}$ , $E_{de}$ or $V_{de}$
$T$	temperature [°C]
$u$	moisture content [%]
$\rho$	material density [kg/m <sup>3</sup> ]

The constants  $a$ ,  $b$  and  $c$  are presented in Table 3.2.

Table 3.2. Constants presented by von Haas (1998) for Equation (3.60) to calculate the rheological coefficients of the four-element Burger model for fiber mats.

	$a_1$	$b_1$	$c_1$	$a_2$	$b_2$	$c_2$
$E_{el}$ [MPa]	4.22E-02	-2.74E-02	3.25E+00	-1.86E-02	3.24E-03	-5.10E+00
$V_{vi}$ [MPa·s]	-3.87E-02	-2.09E-02	9.71E+00	-2.45E-02	2.22E-03	-5.32E+00
$E_{de}$ [MPa]	-1.57E-02	-2.37E-02	3.70E+00	-2.17E-02	3.11E-03	-5.33E+00
$V_{de}$ [MPa·s]	-1.24E-01	1.30E-03	5.29E+00	2.45E-02	-2.23E-03	-5.34E+00

The strain definition as it is used in the present work is  $\varepsilon = \Delta l/l$ , while the coefficients calculated using Equation (3.60) are based on the strain definition  $\varepsilon = (l_2 - l_1)/l_0$ . Therefore, these coefficients have to be converted as follows:

$$C = C_0 \cdot \frac{\rho_0}{\rho} \quad (3.61)$$

where:

- $C$  rheological coefficient based on strain definition  $\varepsilon = \Delta l/l$
- $C_0$  rheological coefficient based on strain definition  $\varepsilon = (l_2 - l_1)/l_0$
- $\rho_0$  reference density (given as 198.3 kg/m<sup>3</sup> by von Haas)
- $\rho$  material density [kg/m<sup>3</sup>]

Equation (3.60) in combination with Equation (3.61) gives the four rheological coefficients  $E_{el}$ ,  $V_{vi}$ ,  $E_{de}$  and  $V_{de}$  as they are needed for the Burger-Humphrey model.

The remaining coefficient,  $E_{pmf}$ , can be derived from data presented by von Haas (1998) for the stress-density relationship during the period of primary mat densification. Von Haas expressed this relationship by the following equation:

$$\sigma = a\rho^b \quad (3.62)$$

where  $\sigma$  and  $\rho$  denote stress and density respectively, and  $a$  and  $b$  are constants that were provided in a table for 22 different temperature-moisture content combinations. The constants for fiber mats are listed in Appendix F. Figure 3.4 gives an example of the stress-density relationship for fiber mats of different moisture content.

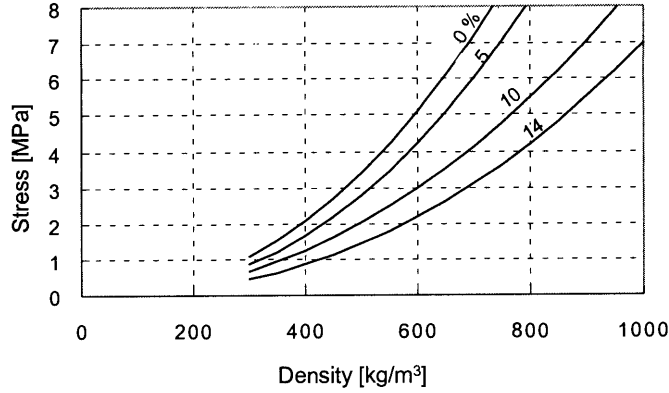


Figure 3.4. Stress-density relationship during densification of a fiber mat at 80°C for four different moisture levels, calculated from Equation (3.62).

Von Haas also showed that the speed with which the mat samples were compressed only had a minor effect on the stress-density curves, indicating that creep processes are relatively unimportant in comparison with instantaneous mat deformation. Assuming that all deformation is instantaneous, the total strain  $\varepsilon_{inst}$  may be divided into its plastic and micro-fracture (PMF) strain component and its elastic strain component:

$$\varepsilon_{inst} = \varepsilon_{el} + \varepsilon_{pmf} \quad (3.63)$$

If  $\varepsilon_{inst}$  is described by a non-linear spring model, in accordance with the formulation of  $\varepsilon_{pmf}$  (see section 3.2.2.5 above), and using the strain definition given by Equation (3.16), the spring coefficient  $E_{inst}$  may be defined as:

$$E_{inst} = \frac{d\sigma}{dl} l \quad (3.64)$$

Differentiating Equation (3.62) with respect to  $l$  and substituting the result in Equation (3.64) yields (after some algebraic transformations):

$$E_{inst} = ab\rho^b \quad (3.65)$$

with  $\rho$  denoting density [ $\text{kg/m}^3$ ] and  $a$  and  $b$  being the same constants as in Equation (3.62). Equation (3.65) is the basic equation that relates the material density to the spring coefficient  $E_{inst}$  for discrete combinations of temperature and moisture content.

Finally, knowing  $E_{el}$  from von Haas's (1998) creep experiments described above, the coefficient of the PMF element,  $E_{pmf}$ , can be calculated by using the relationship described in Equation (3.63):

$$E_{pmf} = \frac{1}{\frac{1}{E_{inst}} - \frac{1}{E_{el}}} \quad (3.66)$$

$E_{pmf}$  has the units of MPa. Two-dimensional interpolation is necessary to obtain  $E_{pmf}$  for any temperature and moisture content.

The experiments of von Haas (1998) were carried out at four moisture content values ranging between 0 % and 14 %, six temperatures ranging between 20°C and 190°C, and within the density range of 300 kg/m<sup>3</sup> to 1050 kg/m<sup>3</sup>. This array can be expected to cover most of the conditions that occur within mats during hot pressing. However, to avoid failure of the simulation program when exceeding the range of measured data, some extrapolations may be necessary.

Equations (3.65) and (3.66) provide values for the rheological coefficient  $E_{pmf}$  as a function of density for discrete temperature-moisture content combinations. In order to derive a single equation that relates  $E_{pmf}$  to temperature, moisture content and density, a linear multiple regression analysis was carried out. Values for  $E_{pmf}$  were generated from Equations (3.65) and (3.66) for the validity range, and a regression equation was then fitted to these values:

$$\ln E_{pmf} = 17.10 - \frac{88.44}{\ln \rho} - 7.57 \cdot 10^{-2} u - 8.53 \cdot 10^{-3} T ; \quad R^2 = 0.92 \quad (3.67)$$

where  $E_{pmf}$  has the units of MPa. The other variables have the same units as those in Equation (3.60). Equation (3.67) is more convenient but gives less accurate results than interpolating values from Equation (3.65) in combination with Equation (3.66). Both approaches have been implemented in the simulation model.

### 3.3.2 Properties of vapor-air mixtures

#### 3.3.2.1 Viscosity

For ideal gases, the dynamic viscosity  $\eta$ , hereafter referred to simply as viscosity, is independent of pressure. This independence applies to water vapor and air as a good approximation for pressure levels that occur within a wood-furnish mat during pressing. The viscosity of gases rises with increasing temperature as described by the Sutherland equation:

$$\eta = \frac{aT_{abs}^{1.5}}{T_{abs} + b} \quad (3.68)$$

where  $T_{abs}$  is the absolute temperature in K, and  $a$  and  $b$  are constants to be determined by fitting the equation to experimental data. Following this method, Humphrey and Bolton (1989a) derived the following expression for the viscosity of water vapor:

$$\eta_v = \frac{1.12 \cdot 10^{-5} (T + 273.15)^{1.5}}{T + 3211.0} \quad (3.69)$$

with  $\eta$  and  $T$  in the units of Pa·s and °C, respectively.

In the present work Equation (3.68) was fitted to experimental data for air from Munson et al. (1990). The viscosity of air,  $\eta_a$ , is related to temperature by:

$$\eta_a = \frac{1.37 \cdot 10^{-6} (T + 273.15)^{1.5}}{T + 358.9} \quad (3.70)$$

Besides temperature, the viscosity of a gas mixture depends on its composition. However, procedures for theoretically calculating the viscosity of a mixture are relatively complex. In the model presented here, the viscosity of the vapor-air mixture is obtained from a linear combination of the component viscosities weighted by the mole fractions in the mixture. This is only a first order estimate and should be refined in future work to account for the non-linear effect of composition on viscosity.

### 3.3.2.2 Molecular diffusion coefficient

In two-component mixtures, the diffusion coefficient of component 1 in component 2 is equal to the diffusion coefficient of component 2 in component 1. Thus, diffusion in a two-component mixture (also called a binary mixture) is described by a single diffusion coefficient.

Temperature and pressure dependencies of the diffusion coefficient have been investigated extensively in the past on theoretical as well as empirical bases for many different gas pairs. The empirical correlation most frequently found in the literature for gaseous diffusion suggests that the diffusion coefficient is inversely proportional to the total gas pressure and directly proportional to  $T^{1.75}$  (e.g., Fuller et al. 1966). From this relationship, the diffusion coefficient  $D$  at temperature  $T$  and pressure  $p$  can be calculated as:

$$D = D_1 \left( \frac{p_1}{p} \right) \left( \frac{T}{T_1} \right)^{1.75} \quad (3.71)$$

where  $D_1$  is any known diffusion coefficient measured at temperature  $T_1$  and pressure  $p_1$ . To derive such an expression for the binary diffusion coefficient  $D_{va}$  of the vapor-air gas pair, experimental data reported by Cussler (1984) were substituted into Equation (3.71). The resulting equation is:

$$D_{va} = 2.60 \cdot 10^{-5} \left( \frac{101325}{p} \right) \left( \frac{T_{abs}}{298.2} \right)^{1.75} \quad (3.72)$$

where:

$D_{va}$	binary diffusion coefficient of the vapor-air gas pair [ $\text{m}^2/\text{s}$ ]
$p$	total gas pressure [Pa]
$T_{abs}$	absolute temperature [K]

Marrero and Mason (1972) evaluated binary diffusion coefficients for 74 gas pairs, including water vapor-air systems. They reported that the magnitude of the composition dependence was never more than 5 %. Neglecting composition effects on the diffusion coefficient therefore appears to be justified.



### 3.4 NUMERICAL PROCEDURE

#### 3.4.1 Classification of the employed numerical method

The starting point for the type of numerical methods most frequently used when modeling complex physical systems is a mathematical model that consists of a set of differential equations. The governing differential equations are then replaced with simple algebraic equations (so-called discretization equations), which are subsequently solved. Two common alternative approaches to discretization are the finite-difference method and the finite-element method.

A different solution scheme will be employed in this work that has been conceived of by Humphrey (1982) to model heat and vapor flow during hot pressing of wood-furnish mats. Algebraic equations rather than differential equations are used as a starting point<sup>12</sup>. Computations for each time step include two distinct consecutive procedures; these are calculation of heat and mass fluxes through the faces of all the control regions, and subsequent determination of the new conditions within each control domain.

An important characteristic of the method described by Humphrey is that it is strongly based on physical considerations, not just on mathematical manipulations. This approach facilitates overall heat and mass balances; it has the advantage of assuring the conservation of the fluxes and thus avoiding the generation of parasitical sources. Although this method utilizes many ideas that are typical of the finite-difference methodology, it appears to be misleading to call it a finite-difference method in its narrower sense.

Main reasons for using this method in the work presented here are:

- It emphasizes physical considerations.
- Changes and additions are relatively simple to implement in the program code.

---

<sup>12</sup> The differential Equations (3.5), (3.7) and (3.8) in section 3.2.2 were developed and presented for the sake of completeness, though they are not used here for the numerical solution.

- Deviation from a rectangular grid, necessary for modeling the continuous press, does not require sophisticated grid generation methods.

Humphrey (1982) gave a comprehensive description of the numerical solution scheme used. It will be summarized here; only those aspects that had to be refined or added for the present study will be explained in more detail.

### 3.4.2 Underlying concept for heat and mass transfer

The body to be modeled is sub-divided into finite control regions, and the pressing time is sub-divided into small time steps. An important assumption is that local conditions and properties stay constant during one time step. This assumption is only justified if the duration of each time step is small enough that the change in gradient between any pair of adjacent control regions will be small compared to the gradient itself. Computations for each time step include two distinct consecutive procedures:

1. Fluxes between the mid-points of adjacent control regions are calculated under steady-state conditions. This is to determine the diffusant quantities (e.g., energy) flowing across the interfaces between neighboring regions (Figure 3.5a).
2. Knowing gains and losses of the diffusant within each control region, new values for the state variables (e.g., temperature) are calculated.

In general form, and including a generation term, the balance for the diffusant in a control region may be written as:

$$\left( \begin{array}{c} \text{diffusant transfer} \\ \text{into the region} \end{array} \right) - \left( \begin{array}{c} \text{diffusant transfer} \\ \text{out of the region} \end{array} \right) + \left( \begin{array}{c} \text{diffusant} \\ \text{generation} \end{array} \right) = \left( \begin{array}{c} \text{diffusant} \\ \text{accumulation} \end{array} \right) \quad (3.73)$$

Assumptions that specify the gradients within and between control regions are essential for any numerical solution scheme. Two simple profile assumptions are sketched in Figure 3.5b. The piecewise-linear profile describes a physical quantity as following constant gradients between adjacent grid points. Using the stepwise profile

assumption, it is presumed that a physical quantity is uniformly distributed within each control region. Both profile assumptions are employed in the approach described here<sup>13</sup>.

For procedure 1 the state variables are assumed to follow a piecewise-linear profile, while the physical properties are described by a stepwise profile. For flow calculations the latter are averaged over two neighboring regions. For procedure 2 all variables, including the state variables, are assumed to follow a stepwise profile. Clearly, a number of alternative approaches are possible, including piecewise-linear profiles for all variables in procedure 1, or the use of non-linear profiles.

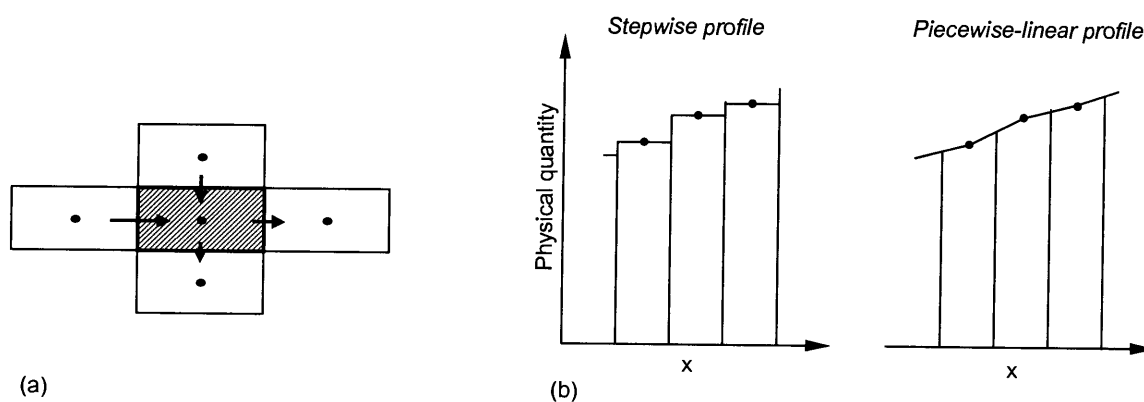


Figure 3.5. (a) Two-dimensional schematic of flow through a control region. Note: the model does operate in three dimensions. (b) Two simple profile assumptions.

### 3.4.3 Grid and time steps

A three-dimensional grid in the Cartesian coordinate system is used. Each control region is a hexahedral with a rectangular base area, but with the possibility of trapezoid shapes in the  $x$ - $z$  and  $y$ - $z$  plane (Figure 3.6a). The deviation from a simple cuboid shape (all sides orthogonal to the axes) may be negligible for modeling a batch press, since platen bending effects and differences in cross-sectional density profiles within the  $x$ - $y$  plane are relatively small. The trapezoid shape of the control region does, however, become evident in the in-feed section of a continuous press.

<sup>13</sup> It should be noticed that it is not a contradiction to use two different profile assumptions simultaneously. A good contribution about this topic can be found in Patankar (1980).

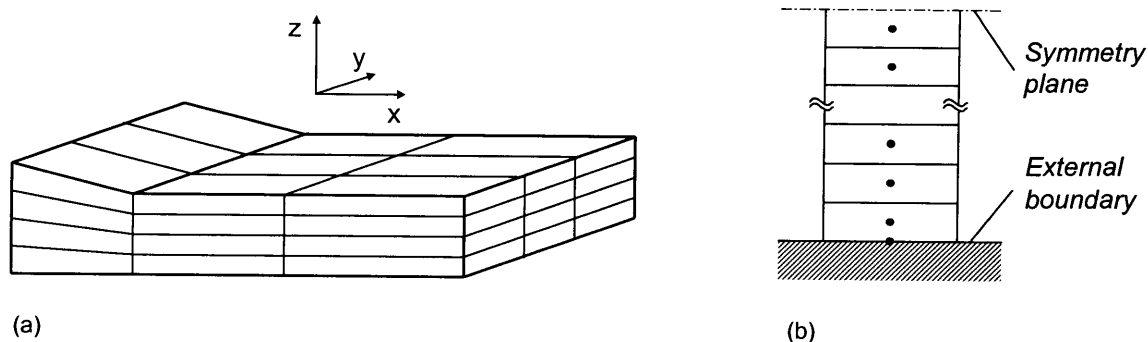


Figure 3.6. (a) Three-dimensional segment of model grid. (b) Locations of control regions and grid points.

An important feature of the numerical scheme described here is that control regions are of constant mass; the thickness of regions, and consequently their volume, therefore change throughout simulation. Initially, all control regions have the same thickness. The dimensions of the regions in x- and y-directions do not change with time. They are uniformly distributed in the y-direction, but may vary in the x-direction (production direction).

The grid points are located mid-way between the faces of the regions. Additional boundary grid points are placed on the faces of the control regions next to the external boundaries (Figure 3.6b).

While the total time to be simulated is divided into small time steps of duration  $\Delta t_p$ , each of these primary time steps may be sub-divided to  $\Delta t_i$  (Figure 3.7). This approach of embedding an inner time loop into a primary time loop has been implemented to improve the overall efficiency of the computations. Only vapor and air flow are calculated in the inner time loop, as the stiffness of the governing Equation (3.5) requires extremely short time steps when using an explicit solution scheme (see section 3.4.4 below). All other calculations are done in the primary time loop with a lower frequency.

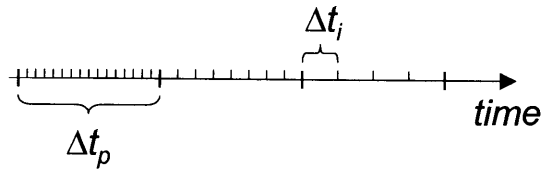


Figure 3.7. Diagram of adaptive time step scheme.  $\Delta t_p$  = duration of primary time step,  $\Delta t_i$  = duration of inner time step.

The primary time step duration  $\Delta t_p$  is held constant throughout the entire simulation, while an adaptive approach is used to adjust  $\Delta t_i$  to the current conditions. The value of  $\Delta t_i$  necessary to obtain stability is calculated before entering the inner time loop; it then stays constant for the period of one primary time step.

### 3.4.4 Stability

An important requirement of a numerical solution is that it retains stability. Instabilities occur when the cumulative effect of all rounding errors is not negligible but increases exponentially with the number of time steps. The limit where a numerical solution becomes unstable depends in part on grid size and time step length. These stability conditions can be estimated.

Gas convection is clearly the most critical physical mechanism concerning numerical stability. Therefore, the estimation of the numerical stability conditions will be based on this mechanism. For one-dimensional convection through a porous medium, and assuming uniform material and gas properties, the governing differential equation may be written as:

$$\frac{\partial p}{\partial t} = \frac{k_p}{\eta \phi} \frac{\partial}{\partial l} \left( p \frac{\partial p}{\partial l} \right) \quad (3.74)$$

where:

$p$	total gas pressure [Pa]
$k_p$	permeability coefficient [ $\text{m}^2$ ]
$\eta$	dynamic viscosity of the gas [ $\text{Pa}\cdot\text{s}$ ]
$\phi$	void fraction of porous material [-]
$t$	time [s]
$l$	spatial variable [m]

The discretization equation is derived by integrating Equation (3.74) over the control region of length  $\Delta l$  and over the time interval from  $t$  to  $t+\Delta t$ . For the explicit scheme, the discretization equation can be written as:

$$\Delta l(p_{j,t+\Delta t} - p_j) = \frac{k_p}{\eta\phi} \frac{\Delta t}{\Delta l} [p_{j-0.5}(p_{j-1} - p_j) - p_{j+0.5}(p_j - p_{j+1})] \quad (3.75)$$

The subscripts  $j-1, j$  and  $j+1$  denote three adjacent control regions of equal length  $\Delta l$ , and  $p_{j-0.5}$  and  $p_{j+0.5}$  are the gas pressures at the two faces between the regions. Furthermore,  $p_{j,t+\Delta t}$  is the gas pressure at time  $t+\Delta t$ , whereas all other pressures refer to time  $t$ . After some algebraic rearrangement, Equation (3.75) becomes:

$$K \cdot p_{j,t+\Delta t} = p_{j-0.5}p_{j-1} + p_{j+0.5}p_{j+1} + (K - p_{j-0.5} - p_{j+0.5})p_j \quad (3.76)$$

$$\text{with } K = \frac{\eta\phi}{k_p} \frac{(\Delta l)^2}{\Delta t}$$

Patankar (1980) showed that the term in brackets has to be positive to maintain stability. Knowing this, a stability criterion can be established that gives the maximum time step length for given conditions:

$$\Delta t < 2 \frac{\eta\phi}{k_p(p_{j-1} + 2p_j + p_{j+1})} (\Delta l)^2 \quad (3.77)$$

This equation may be simplified to become:

$$\Delta t < 0.5 \frac{\eta\phi}{k_p p} (\Delta l)^2 \quad (3.78)$$

which is the typical form of the stability criterion for unsteady-state diffusion processes given in many text books (e.g., Crank 1975). From Equation (3.78) it becomes clear that the smallest dimension of the control region has a quadratic effect on the maximum time step length. That is to say, doubling the number of control regions in order to improve the spatial accuracy leads to an eightfold computation time. The material density, however, has an even stronger effect on time step lengths, as the density is exponentially related to the permeability  $k_p$ . For example, at room temperature and atmospheric pressure Equation (3.78) gives a critical time step length of  $3.3 \cdot 10^{-4}$  seconds for air convection through a

wood fiber mat of  $800 \text{ kg/m}^3$  density (for  $\Delta l = 1 \text{ mm}$ ). Under the same conditions, but considering a density of  $300 \text{ kg/m}^3$ , the critical time step length becomes as small as  $4.5 \cdot 10^{-6}$  seconds.

Although the mass transfer mechanisms operative during hot pressing are much more complex than the assumptions that were made when establishing the stability criterion, test runs of the simulation program confirmed that this criterion serves as a good tool to estimate the critical time step length necessary to avoid instabilities.

### 3.4.5 Sequence of computation

A primary time step covers the period from  $t$  to  $t + \Delta t_p$ . An explicit scheme is employed for the primary time loop; that is to say that all calculations are evaluated at time  $t$ . Computations are done in the following sequence:

1. Determine boundary conditions
2. Update material and gas properties
3. Calculate conductive heat flow
4. Calculate new vapor and air pressure in an inner time loop (compression of the control region is temporarily neglected)
5. Calculate new thickness of control regions
6. Update variables of state

Points 3 to 6 will be described in turn.

#### 3.4.5.1 *Conductive heat flow*

Equation (3.6) is the constitutive flux equation for conductive heat transfer and provides the quantity of energy flowing during the period  $\Delta t_p$  through the interface between two adjacent regions. The length of the flow path is taken as the sum of both region's dimensions, divided by two (distance between A'' and B' in Figure 3.8). This is not quite exact if the shapes of the control regions deviate from a simple cuboid. However, the aberration from the true distance between the two grid points A and B in Figure 3.8 is negligible and does not exceed 0.3 % in the in-feed section of a continuous

press. The area of the region's interface is calculated as the average of the cross-sectional areas at the mid-points.

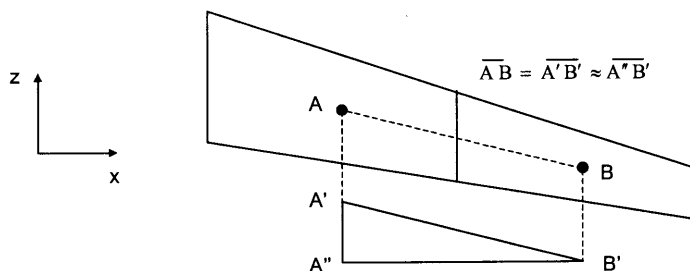


Figure 3.8. Exaggerated sketch of two adjacent control regions in the in-feed section of a continuous press.

### 3.4.5.2 Inner time loop

Two different approaches to the gas flow computations have been implemented in the simulation program and may be used alternatively. The first one is a fully explicit scheme and requires extremely short time steps to maintain stability. The second approach may be described as a combination of an explicit and implicit method. This scheme typically allows inner time step durations,  $\Delta t_i$ , similar to those of the primary time steps,  $\Delta t_p$ . For both approaches material and gas properties, as well as temperature and material density, are taken as constant for the entire period of the primary time step  $\Delta t_p$ . This assumption can be justified since typical values of  $\Delta t_p$  are still in the order of  $5 \cdot 10^{-3}$  seconds.

#### 3.4.5.2.1 Explicit approach

The vapor and air pressure at the end of a time step is calculated by following the scheme described in section 3.4.2 above. The quantities of vapor and air flowing through the faces of the control regions during the time interval from  $t$  to  $t + \Delta t_i$  are determined by the constitutive flux Equations (3.2) and (3.3). Applying Equation (3.73) for mass balance (the generation term is zero), and using the ideal gas law as given in Equation (3.13), new values for vapor and air pressure are computed for each control region at the end of each time step  $\Delta t_i$ .



For calculating the length of the flow path and the area of the interfaces between two adjacent control regions, the same assumptions apply as those stated in section 3.4.5.1 for conductive heat flow. The criterion that provides an estimate of the time step length  $\Delta t_i$  necessary to maintain numerical stability has been described in section 3.4.4 above; the value of  $\Delta t_i$  is given by Equation (3.78), multiplied by a safety factor.

#### 3.4.5.2.2 Implicit approach

Convective gas flow, caused by total pressure gradients, is the mechanism that dictates the frequency with which calculations in the inner time loop are done. Being more specific, from Equation (3.78) it becomes clear that it is the convective flow through the cross-section of the mat (flow in the z-direction) that requires extremely short time steps  $\Delta t_i$ . This is because the dimensions of the control regions in the z-direction are usually more than 100 times smaller than in the other directions.

The physical interpretation of the stiffness of Equations (3.5) and (3.74), and hence of the extremely short time steps required, is that any total pressure gradients in the z-direction dissipate very rapidly. Trial runs of the simulation program, using the fully explicit approach, confirmed that the predicted total pressure drop in the z-direction is always very small (unlike the partial pressure differences). A simple calculation of the gas pressure distribution in a 20 mm thick porous material leads to the same conclusion. It showed that, for measured permeability values of a wood fiber mat, any cross-sectional gas pressure drop dissipates almost instantaneously. This topic will be discussed in more detail in section 5.4.3.

It should be noticed that the calculations referred to above were made for fiber mats. Furthermore, it should be clear that the assumptions stated in this context were made for conventional batch or continuous presses. The situation may be different for other material types and for steam injection presses.

Since in-plane gas convection and diffusion, as well as cross-sectional gas diffusion, are not critical for numerical stability, these mechanisms are computed using the explicit scheme as described in the previous section. Only for cross-sectional gas convection a mechanistic approach is employed, which is based on the assumption of an instantaneous cross-sectional equalization of the total gas pressure. Calculations are done

in turn for all x-y-positions. As pressure builds up, both air and vapor are pushed towards the low-pressure zone. The new vapor and air pressure distribution for two neighboring regions is calculated so that the total pressure in both regions becomes the same. This is done for all pairs of adjacent regions through the mat thickness (Figure 3.9a), and the full sequence is repeated several times. By this iterative procedure the total gas pressure within one stack of control regions approaches a uniform distribution (Figure 3.9b).

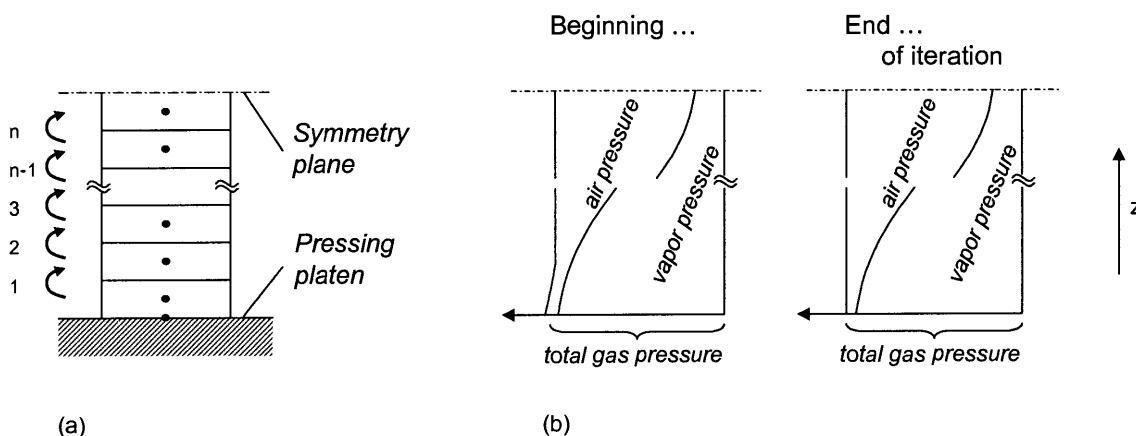


Figure 3.9. (a) Illustration of the procedure used for equalization of total gas pressure through a cross-section of the mat. (b) Schematic showing gas pressure distributions before and after the iterative relaxation procedure.

The procedure described above may be categorized as an implicit scheme since the gas pressure at time  $t+\Delta t$  is not only affected by the gas pressures at time  $t$ , but is also linked to the unknown gas pressures of the adjacent regions at time  $t+\Delta t$ . Comparative model runs with both approaches for the cross-sectional gas flow (Darcian flow and the assumption of instantaneous pressure equalization) showed no discernable differences, except immediately after press opening. The assumption of instantaneous pressure equalization therefore appears warranted. Yet, a more sophisticated implicit approach may be used in the future.

### 3.4.5.3 Rheology

External stresses acting on the wood-furnish mat in the z-direction are counteracted by internal stresses of the material as well as by the internal gas pressure.

Neglecting cross-sectional total gas pressure gradients, a uniform stress distribution prevails throughout one stack of control regions. The stress  $\sigma_z$  acting in the z-direction on any of the control regions may be written as:

$$\sigma_z = \sigma_{press} - p \quad (3.79)$$

where  $\sigma_{press}$  denotes the stress transferred from the pressing platens to the stack of control regions, and  $p$  is the total gas pressure prevailing at the corresponding x-y-position.

When simulating a press operated in load control mode, the pressing pressure  $\sigma_{press}$ , and consequently the stress  $\sigma_z$  acting on the control regions, are known. The strain of any control region can be calculated directly by using the algebraic equations presented in section 3.2.2.5. Knowing the strain of a region, the new thickness of the region is obtained from Equation (3.16).

An iterative procedure is employed when simulating a press in position control mode. A convergence criterion terminates the iteration loop as the mat thickness approaches the specified value. Calculations are done successively for all stacks of control regions in the x-y plane.

#### ***3.4.5.4 Update variables of state***

The variables of state are updated at the end of a primary time step  $\Delta t_p$  for each of the control regions. The amount of vapor transferred into the region by convection and diffusion can be calculated by comparing the vapor pressure at time  $t$  with the new vapor pressure obtained in the inner time loop. Knowing the amount of vapor transferred into the region, and the quantity of energy, which entered the region by conduction, local equilibrium between moisture content, vapor pressure and temperature has to be re-established. A protocol established by Humphrey (1982) is used for this purpose.

As a first approximation, the total amount of water gained or lost by the region is added to or deducted from bound water. The new equilibrium conditions are then approached through an iterative procedure. Water is redistributed between the bound water phase and the vapor phase. The new temperature depends on the quantity of heat the region gained or lost by conduction, as well as on the quantity of heat liberated or

consumed due to phase change of the water. All equations necessary are summarized in sections 3.2.2.3 and 3.2.2.4 above.

In addition to determining moisture content, vapor pressure and temperature in an iterative procedure, the new air pressure obtained in the inner time loop has to be corrected for compression of the control region.

### **3.5 MODEL IMPLEMENTATION**

The program code is written in the programming language ANSI C, using a 32-bit C++ compiler (Visual C++, Version 4.0). Reflecting the complexity of the problem, a modular programming style was chosen. The features listed in section 3.4.5 are implemented in separate routines, which are executed consecutively during each time step. The modular approach ensures the flexibility necessary for incorporation of changes and expansions in the future. The program is structured such that executions of model runs for the batch and continuous presses are identical, except that different boundary conditions are applied.

Input data to specify a model run and material property data are read from ASCII files. Input specifications include raw material and surrounding conditions, pressing conditions, model definitions and output organization. The input data can be changed in a text editor before starting a model run. Files with material property data for four different material types (including particleboard and oriented strandboard) are on hand. Two alternative output formats are available, so that the generated output files may be read directly into standard spreadsheet programs or into the graphics program Techplot<sup>®</sup>, respectively, for visualizing the simulation results. The output files would be extremely large if data were stored for all grid points over the entire time that is simulated. Therefore, a selective approach was chosen that allows one to specify grid positions and times for which the output data are to be recorded. Additional output files to save pressing schedule and statistics of the model run are generated by default for each run.

## 4. THE CONTINUOUS PRESS

### 4.1 INTRODUCTION

The model presented in this work has been outlined so that it can be applied to both the batch as well as the continuous pressing process. The basics of the model and the numerical procedure employed have been described in detail in the previous chapter. Only those aspects that are specific to the modeling of the continuous press will be rationalized in this chapter.

The earliest continuously working hot presses for particleboard were developed at the end of the 1950s by the German machine-building company Bison. This first generation of continuous presses, however, was not very successful (Deppe and Ernst 1996). Only new technological concepts developed in the 1970s and 1980s provided the basis for the breakthrough in this press type. Since then, the quantitative and economical importance of the continuous pressing process has increased steadily. Not only does the productivity of this technology exceed that of the batch process, but it also has opened new opportunities to better manipulate panel properties in desirable ways. Modern continuous presses for medium density fiberboard (MDF) typically have a production width of 2.10 to 3.15 meters, press lengths up to 50 meters and production capacities as great as 280,000 m<sup>3</sup> per year (from data published by Sunds Defibrator 1997).

The press design varies between different press manufacturers. In order to provide a model that does not describe only one specific type of continuous presses, a rather general formulation of the boundary conditions has been chosen. This approach enables one to simulate a wide range of different press designs and methods of operation.

### 4.2 CHARACTERISTICS OF THE PROCESS

The adhesive-treated wood-furnish mat is conveyed through the press between two endless steel belts. For mat densification and adhesive cure, heat and pressure have to be transferred from the press into the moving mat. A simplified representation of the cross-sectional structure of the press is given in Figure 4.1. The pressing force is exerted from closed frames onto the press beams and heating platens. Important components for

the heat and pressure transfer into the mat are the rolling elements (usually steel rods) that are located between the heating platens and the steel belts. The steel rods allow almost frictionless movement of the mat through the press. Isobaric approaches where heat and pressure is transferred via a thin oil film, as used in coating presses, have proven, to date, inappropriate for wood-based composite production.

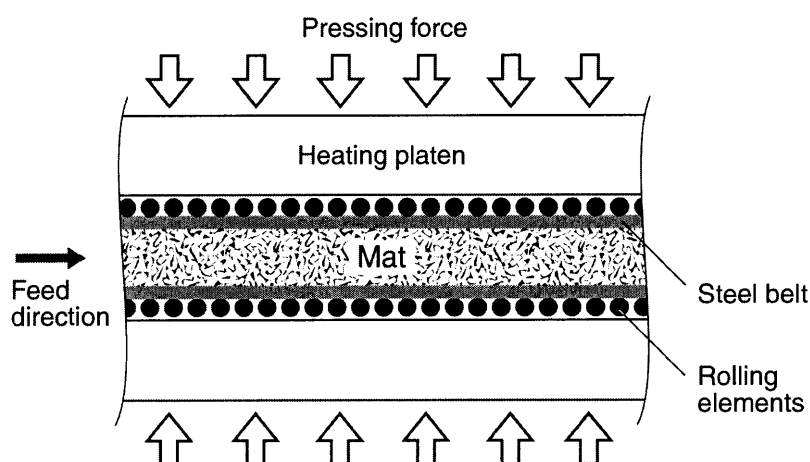


Figure 4.1. A cross-section of the center zone of a typical continuous press.

Figure 4.2 shows a typical arrangement of the pressing frames over the length of the press. For each frame, the vertical position (i.e., distance between steel belts) or the pressing pressure is controllable within limits that are dictated by the vertical position in the two neighboring frames. Hence, a thickness or pressure profile over the length of the press can be established. In addition, for some of the frames it is possible to vary the mat thickness over the width of the press.

The platens are divided longitudinally into heating zones. Usually, the temperatures in these zones decrease towards the press outlet. Since the steel rods and the steel belts move through the press together with the mat, heat is conveyed horizontally in the feed direction as well as migrating vertically into the mat. This horizontal 'dragging' of heat makes it difficult to accurately infer steel belt temperatures from known platen temperatures.

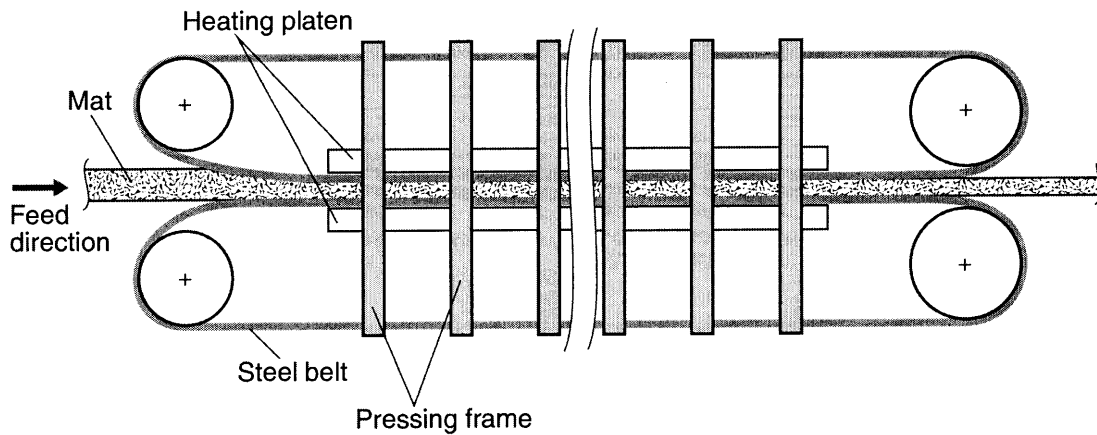


Figure 4.2. Schematic of a typical continuous press.

The possibility of varying temperature, position, and pressing pressure in the feed direction of a continuous press is an important distinction from a batch press, both technologically and from the modeling point of view.

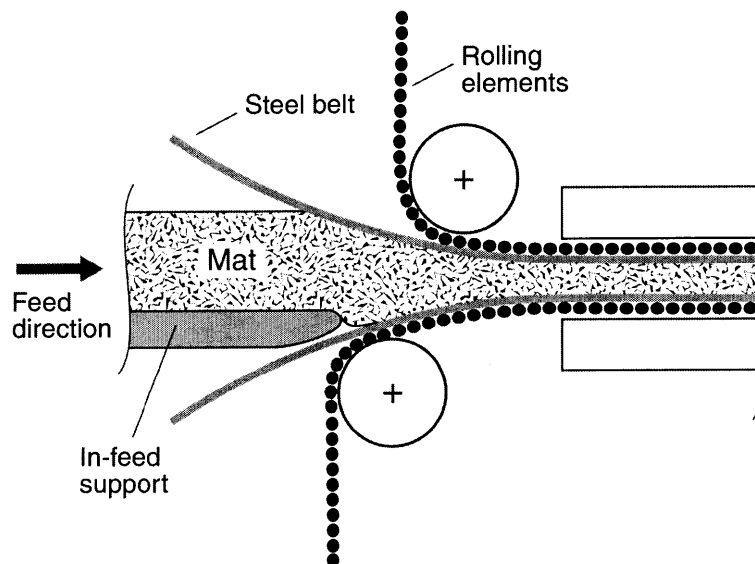


Figure 4.3. Example of an in-feed section.

The geometry, technical details, and controlling strategies of the in-feed section, where the mat enters the press, depend on the press manufacturer. A typical in-feed section is given in Figure 4.3. A large proportion of the total mat densification is affected

in this part of the press, and this creates a significant back-flow of the vapor-air mixture out of the press counter to the feed direction. The shape of the in-feed section is adjustable up to a certain degree for many presses. By changing this shape, the gas back-flow, as well as the density profile as a consequence of the densification sequence, may be manipulated.

### 4.3 SPECIFIC ASPECTS OF CONTINUOUS PRESS MODELING

While hot pressing in a batch press represents an unsteady-state type of problem, continuous pressing can be described as a steady-state process when using the press as the reference system. For any spatial position, the conditions stay constant over time unless the material properties or pressing conditions are changed. However, if the moving wood-furnish mat is used as the reference system, instead of the press, then the process must again be treated as an unsteady-state type of problem. After careful consideration, the latter approach was selected for use here.

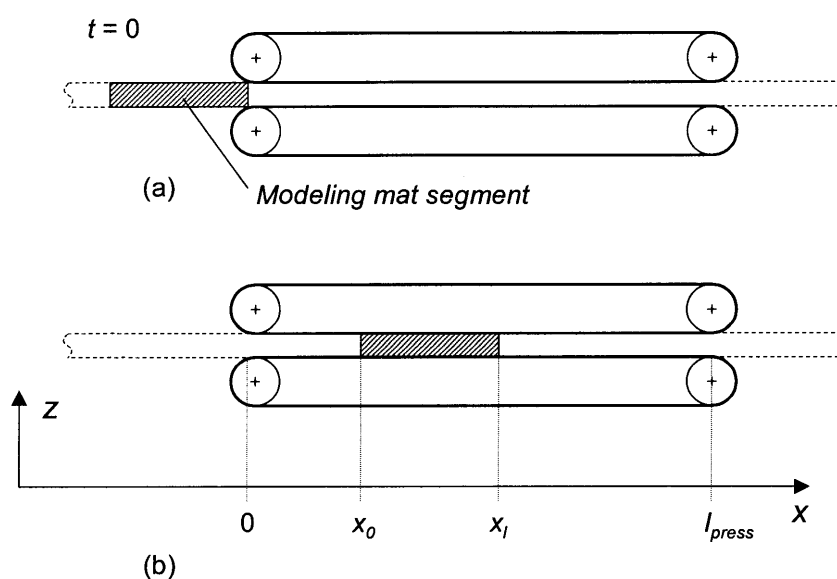


Figure 4.4. Schematic of the modeling mat segment passing through the continuous press: (a) beginning of simulation; (b) mat segment within press.  $x_0$  = position of left boundary,  $x_l$  = position of right boundary,  $l_{press}$  position of last mat-steel belt contact.



In order to model the endless mat moving through the press, only a segment of finite length in the  $x$ -direction will be considered (Figure 4.4). The simulation starts before the mat segment enters the press, and ends after the segment has left the press. During each time step  $\Delta t$  the segment moves forward by the small distance  $\Delta x = v \cdot \Delta t$ , where  $v$  is the feed speed. Heat and mass transfer and rheology are computed for the modeling mat segment as described in Chapter 3. The basic idea of this approach is that only the boundary conditions differ from those of a batch press, while the body to be modeled and the description of the physical mechanisms are the same for both continuous and batch presses.

Some attention has to be paid to the two boundaries in the  $y$ - $z$  plane (perpendicular to the feed direction). Such boundaries can be treated either as open or as closed to gaseous flow. Both choices are extreme situations and do not reflect reality; inaccuracies are inevitable. Towards the central  $y$ - $z$  plane (i.e., half way between these two boundaries), the inaccuracies decline. Therefore, the ratio of length to width of the modeling mat segment has to be chosen to be big enough so that the inaccuracies at the boundaries do not affect the central  $y$ - $z$  plane. Trial runs showed that the effect of the boundaries in the  $y$ - $z$  plane is negligible for length-to-width ratios larger than five. The control regions in the central  $y$ - $z$  plane are named 'reference regions' (Figure 4.5). These regions are monitored while the mat moves through the press, and results for these regions are recorded.

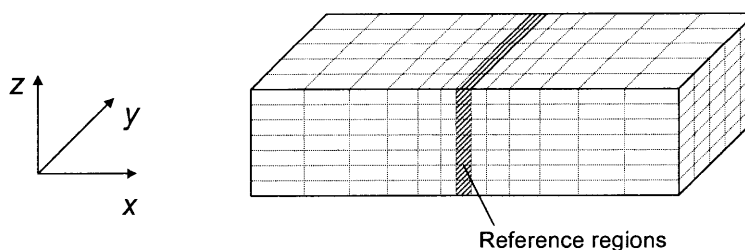


Figure 4.5. Modeling mat segment with grid clustered around reference regions.

Another source of inaccuracy that has to be considered is the discontinuity in the boundary conditions at the contact points where the steel belt touches the mat (press entry) and leaves the mat (outlet). A control region adjacent to the horizontal boundary is

treated as open to the ambient atmosphere as long as the center of the region is outside the press. Once the center of the region has passed the mat-steel belt contact point it is assumed that the surface of the control region is entirely covered by the steel belt. The resolution, and therefore the accuracy, becomes better the narrower the grid is in the  $x$ -direction at these particular positions. On the other hand, to avoid unacceptably long execution times, the number of grid cells cannot be infinitely high. In order to minimize the error caused by the discontinuity in the boundary condition while keeping the number of control regions reasonably small, the regions may be clustered in the  $x$ -direction around the reference regions as demonstrated in Figure 4.5. This approach was justified by test runs with different grid schemes. Other grid schemes may also be specified for simulation runs.

#### 4.4 BOUNDARY CONDITIONS

Assumptions and simplifications are necessary to describe the model boundaries in terms of straightforward geometries. The scheme of the mat within a continuous press as it is used in the present model is shown in Figure 4.6. The surfaces of the mat are the upper and lower model boundaries. The lower surface follows a flat plane, while the shape of the upper steel belt can be specified (position control). Alternatively, data from any given pressure profile may be used as input data for the model (load control). The upper and lower steel belts contact (at the press entry) or leave (at the outlet) the mat at the same horizontal positions. The shape of the upper steel belt in the in-feed section is specified by the in-feed radius  $R$ . Consequently only position control is possible in the in-feed section.

Both mat surfaces are sealed against gas escape when within the press and are assumed to be open to the ambient atmosphere in front of and behind the press. Although the mat may lie on an impermeable conveyer belt before entering the press, the gap between conveyer belt and steel belt at the press entry justifies the assumption of gas escape through the lower surface. The sides of the mat are open to the ambient atmosphere.

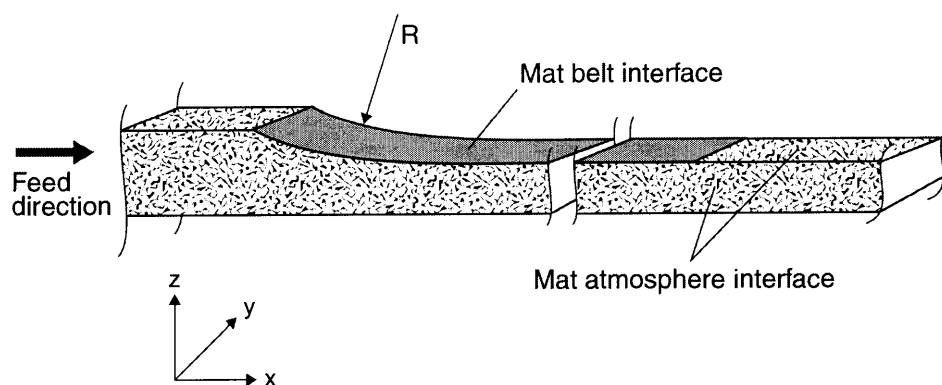


Figure 4.6. Schematic of the model boundaries.

The difficulty of inferring steel belt temperature from heating platen temperature has already been mentioned. The belt temperature versus position in the feed direction is therefore directly defined as a boundary condition. Future refinements of the model might include an interfacial heat transfer term. However, it is assumed in the present approach that the mat surface temperature is equal to that of the steel belt.

At the mat surfaces in front of and behind the press, and at the edges of the mat, almost all heat transfer is due to escape of vapor and air. The importance of conductive heat transfer at these boundaries is believed to be minor and therefore is not considered.

## **5. PREDICTIONS OF THE MODEL**

### **5.1 INTRODUCTION**

This chapter's objectives are to present simulation results, to use the model predictions in discussion of the physics governing the hot pressing process, and to compare predictions with experimental and industrial measurements.

Measurements in industrial and laboratory pilot trials are usually restricted to only a few positions within the mat. The limited number of measuring points provides information only for specific positions, while a coherent picture of the physical conditions inside the mat may be difficult to derive from the discrete data. Furthermore, some variables, such as moisture content or material properties, are difficult or impossible, so far, to measure during the process. These limitations do not hold for theoretical simulation models. In principle, all variables included in the model may be output and displayed for any location and for the entire time period that is simulated. Clearly, only a small fraction of the range of possibilities can and need to be presented. In practical use of the simulation program, the output range has to be chosen according to the specific questions to be addressed.

In sections 5.2 and 5.3 of this chapter, model predictions for batch and continuous presses, respectively, will be presented and compared with measurements. The comparison will be qualitative as well as quantitative in nature for the batch press, whereas a rather qualitative comparison will be carried out for the continuous press. Finally, in section 5.4, a small selection of specific aspects of the physics, which are relevant to both press types, will be discussed.

### **5.2 EVALUATION OF BATCH PRESS MODEL PREDICTIONS**

In order to validate the simulation model presented in this work, measurements of temperature and internal gas pressure were made in medium density fiberboard (MDF) mats during pressing in a large-size (4 x 8 ft.) laboratory hot press. A summary of the methods used to collect these data and of the derived results is given in Appendix B. A total of four trials were carried out. The pressing and initial material conditions were

almost identical for the four trials; only the pressing schedule was varied significantly. In trial 1 the press was closed to final thickness in only one densification step, whereas a second densification step at a later stage of the pressing cycle was included in the other three trials.

As the most straightforward pressing schedule was applied in trial 1, a simulation of this trial will be used here to illustrate the basic physical mechanisms that are important during hot pressing. Afterwards, the simulation results will be compared with measurement data. Since the four trials only varied in the pressing schedules, while important parameters such as moisture content and platen temperature were the same, the curves of some variables such as core temperature look relatively similar for all four trials. A detailed comparison between model predictions and experimental data for all four trials would be repetitive without providing additional information. Therefore, the comparison for trial 1 will be complemented by the other trials only where appropriate. The limited number of mats available and technological constraints prohibited a more extensive test series with parameters other than the pressing schedule varied.

Time dependent changes in internal mat conditions are highly dependent on the wood-furnish material properties. Therefore, a *quantitative* comparison between simulation and measurement requires exact knowledge of the material used for the measurements. Such a quantitative comparison is possible here only because the wood-furnish mats that were consolidated in the laboratory press were from the same manufacturer as the material that was tested by von Haas (1998) and von Haas et al. (1998) to provide material properties input data for the simulation model. The material property input data can be expected to closely reflect the true properties of the material used for the four trials, although seasonal and raw material variations are still possible and have to be considered when comparing predictions and measurements.

### **5.2.1 Specification of input conditions**

The input conditions specified here correspond to the pressing conditions of trial 1. Table 5.1 summarizes the main input specifications. A one-layered 2.30 m x 1.33 m MDF mat was modeled, with homogeneous initial mat conditions throughout the entire mat. Target thickness and target density, both prior to press opening, were 39 mm

and  $697 \text{ kg/m}^3$ , respectively. The press was operated in position control mode following the pressing schedule displayed in Figure 5.1. The idealized case of first platen-mat contact at  $t = 0$  (beginning of the simulation) was assumed for both upper and lower pressing platens. The mat was compressed in four stages of decreasing press-closing rates. During the real experiment the platen positions at the two pressing pistons sometimes deviated from one another. For these periods the average positions at the two pistons were chosen as input data for the simulation. The final thickness of 39 mm was reached after 110 seconds and was held constant until the end of simulation at  $t = 630 \text{ s}$ . Upper and lower pressing platens had a temperature of  $190^\circ\text{C}$ .

Table 5.1. Input conditions for simulation of batch press trial 1.

<u>Panel specifications</u>	
Material:	One-layered MDF mat
Size:	$2.30 \times 1.33 \text{ m}^2$
Target thickness:	39 mm
Target density (dry wood basis):	$697 \text{ kg/m}^3$
<u>Initial mat conditions</u>	
Bulk height:	295 mm
Temperature:	$26^\circ\text{C}$
Moisture content:	9.9 %
<u>Pressing parameters</u>	
Control mode:	Position control
Platen temperature:	$190^\circ\text{C}$
<u>Model definitions</u>	
Grid (x, y, z):	6 x 6 x 20
Symmetries:	x-, y- and z-direction
Time steps per second:	500 for primary and inner time loops

All material property data were used for the simulation as specified in section 3.3.1. If alternative sets of data were available, as was the case for mat permeability and rheological coefficients, those data provided by von Haas (1998) and von Haas et al. (1998) were chosen. The model can, however, also be executed using permeability data collected by Haselein (1998) and rheological data measured by Ren (1991) and calculated by Haselein (1998). The interpolation approach described in section 3.3.1.7 was applied to determine the rheological coefficients.

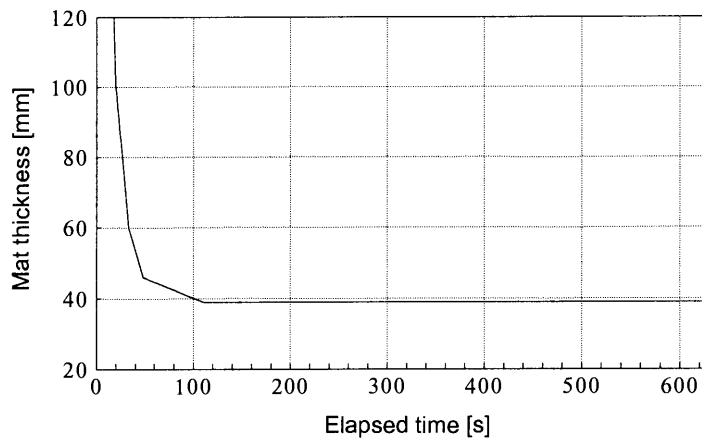


Figure 5.1. Specified pressing schedule for simulation of batch press trial 1. The initial mat thickness at  $t = 0$  is 295 mm.

Symmetry of the mat in x-, y- and z-direction was assumed, so that computations had to be done for only one eighth of the mat volume. A modeling grid of 6 x 6 x 20 control regions (x, y, z) was used. Test runs showed that a higher resolution in the horizontal plain would not significantly increase the accuracy of the predictions, whereas steep cross-sectional gradients required a high resolution in the z-direction. The control regions were uniformly distributed in x-, y- and z-directions. The implicit approach, based on the assumption of instantaneous gas pressure equalization, was employed to compute the cross-sectional gas flow. Both primary and inner time loops were executed with 500 time steps per second. The total execution time for the simulation run on a personal computer with a Celeron<sup>TM</sup> processor and 400 MHz frequency was about 6 hours.

### 5.2.2 Presentation and discussion of model predictions

Figure 5.2 to Figure 5.5 display the time dependent changes of temperature, moisture content, internal gas pressure<sup>14</sup> and density in the horizontal center of the mat for ten cross-sectional positions. While the half-mat thickness was divided into 20 layers for the purpose of simulation, the curves for only every other cross-sectional position are shown in the figures.  $z = 1$  represents the layer adjacent to the pressing platen,  $z = 2$  the third layer,  $z = 3$  the fifth layer and so on. Only  $z = 10$  corresponds to the innermost layer, which is layer 20 instead of layer 19.

The model predictions for the three variables of temperature, moisture content and gas pressure will be discussed concurrently using the curves for three cross-sectional positions: the surface layer ( $z = 1$ ), one intermediate layer ( $z = 4$ ) and the central plane ( $z = 10$ ). Such an approach appears appropriate to illustrate the physical mechanisms operative during pressing and to demonstrate the capability of the model to account for these features. Predictions for the density development will then be rationalized with respect to the dynamic changes of temperature and moisture content.

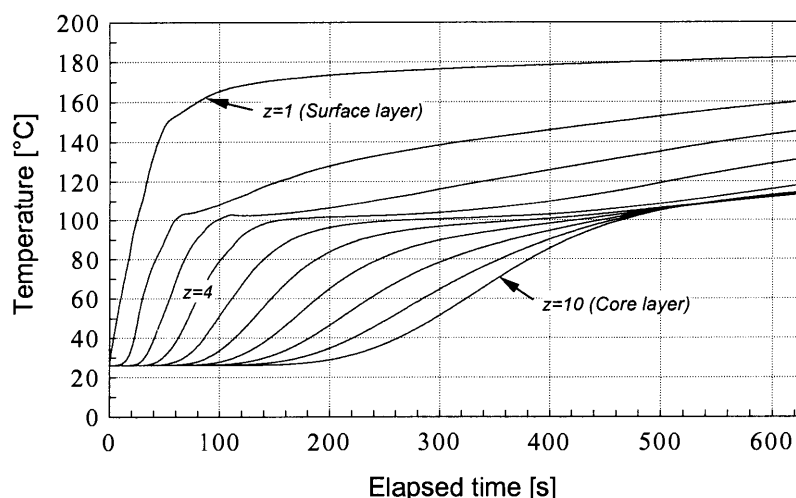


Figure 5.2. Predicted temperature development within the mat at ten cross-sectional positions in the horizontal center. (Batch press trial 1)

---

<sup>14</sup> Vapor, air and total gas pressure are referred to as absolute pressures throughout this dissertation unless otherwise stated.



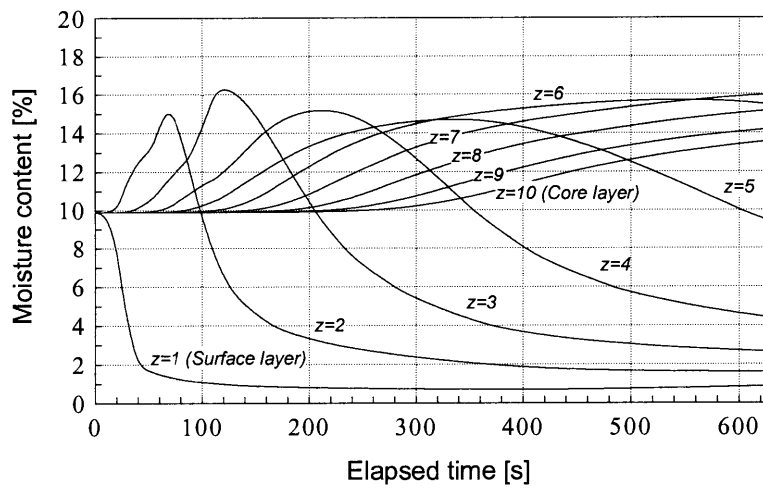


Figure 5.3. Predicted moisture content development within the mat at ten cross-sectional positions in the horizontal center. (Batch press trial 1)

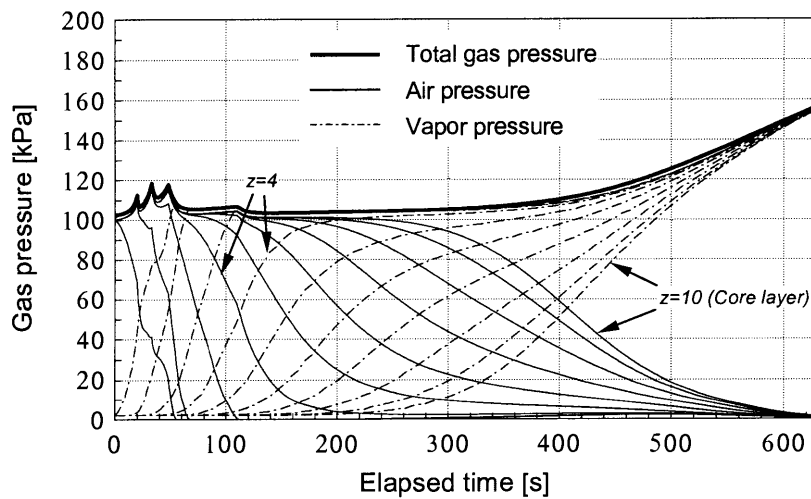


Figure 5.4. Predicted gas pressure development within the mat at ten cross-sectional positions in the horizontal center. (Batch press trial 1)

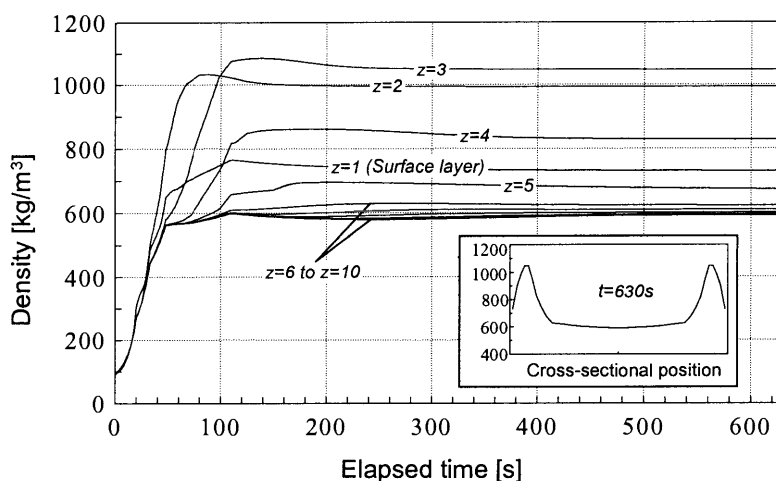


Figure 5.5. Predicted density development within the mat at ten cross-sectional positions in the horizontal center. Inset: Density profile after 630 seconds. (Batch press trial 1)

### 5.2.2.1 Surface layer ( $z = 1$ ) behavior

The curves for the surface layer actually represent the quantities at the center of the outermost modeling region, i.e., about 1.25 % (with respect to the total mat thickness) below the platen-mat interface. Heat energy is translated by thermal conduction from the hot pressing platen into the surface layer. The temperature increases rapidly during the first stage of the pressing cycle (Figure 5.2). This temperature rise would be even steeper if part of the energy was not required to evaporate bound water. An order of magnitude calculation showed that between 50 and 60 % of the energy consumed in the surface layer during the first 40 seconds accounts for heat of sorption and evaporation. During this period the wood-furnish material dries rapidly and the moisture content drops to about 2 % (Figure 5.3).

Several workers have assumed in the past that considerable evaporation only happens once the material reached the boiling temperature of free water at the prevailing pressure. Humphrey and Bolton (1989a) pointed out that such an assumption is incorrect. Any change in temperature will affect the equilibrium moisture content, and vapor is therefore generated as soon as the temperature of the wood particles increases.

Due to evaporation of bound water in the surface layer, the total gas pressure in this layer increases slightly, causing an immediate flow of the vapor-air mixture towards the central plane of the mat. It should be noted that it was assumed for this simulation run that any total gas pressure gradient in the cross-sectional direction dissipates instantaneously. Thus, there is no difference between the total gas pressure curves for different layers visible in Figure 5.4. However, model predictions that were made by using the fully explicit approach (Darcy's law for cross-sectional gas flow computations) instead of applying the assumption of instantaneous dissipation of cross-sectional pressure gradients, showed no discernable differences in total gas pressure between the different layers (see Figure 5.26). It is therefore reasonable to assume that the total gas pressure curves in Figure 5.4 would have the same appearance if the fully explicit approach were to be used.

As only vapor is generated, but not air, the proportion of air in the surface layer decreases steadily. Figure 5.4 suggests that all air is replaced in this layer by vapor during the first minute of the pressing cycle. According to the simulation results, considerable partial pressure gradients are established between surface and inner mat layers during this stage. The air has effectively been 'pushed' towards the central plane.

After the rapid temperature increase during the first stage of the pressing cycle, the temperature curve flattens out and slowly approaches the platen temperature of 190°C. The moisture content stays at a relatively low level until the end of the simulation. The predictions suggest that some air may diffuse back into the surface layer at a later stage (see Figure 5.4 after 350 seconds), due to steep cross-sectional partial pressure gradients.

Simultaneously with mass and heat transfer from the surfaces towards the central plane of the mat, in-plane total gas pressure gradients develop between the center and the edges. Such gradients develop not only in those layers where vapor is generated, but are of (almost) the same extent in all layers. The flow of the vapor-air mixture along these in-plane pressure gradients slows down the gas pressure rise within the mat that is due to vapor generation.

### 5.2.2.2 *Intermediate layer ( $z = 4$ ) behavior*

The theory of a vapor front progressing from the surface towards the central plane of the mat (see Figure 2.1) is generally accepted among researchers, although not all details are clear yet. The progressing vapor front can be satisfactorily explained by following the time curves at the cross-sectional position  $z = 4$ .

Vapor generated in the outer mat layers is driven towards the central plane. The requirement of local thermodynamic equilibrium between temperature and vapor pressure causes condensation of vapor when the vapor reaches relatively cool regions. As already stated, the term 'condensation' is used here in a sense that includes sorptive processes.

During the first 40 seconds of the pressing cycle no significant temperature, moisture content or vapor pressure increases are detectable in this layer. The increase of total gas pressure during this first period is solely due to compression of air within the mat when the press is closed (this holds for all other layers as well).

Once a considerable quantity of vapor condenses in the layer, the local moisture content increases (Figure 5.3). The release of latent heat inherent in the condensing vapor, together with conductive heat flow from the warm surface regions, causes a relatively steep temperature rise, which then flattens out after about 140 seconds (Figure 5.2). Most of the air in the layer is replaced by vapor during this stage of the pressing cycle (Figure 5.4).

The subsequent time period shows a temperature plateau near 100°C; between 150 and 300 seconds the temperature increases only slightly from 100 to 104°C. The moisture content reaches its maximum in the middle of this period at approximately  $t = 220$  s. Until then, vapor still condenses within the layer, so that the moisture content continues to rise and latent heat inherent in the vapor is liberated. Once the moisture maximum has been reached, this process is reversed and energy is then spent to evaporate water. Apparently, the contribution of conductive heat transfer to the overall energy input into this layer increases and becomes dominant over convective heat transfer.

Temperature gradients towards neighboring layers are smallest during this period. Once a steeper gradient towards the adjacent outer layer builds up, conductive heat flow into the layer  $z = 4$  improves, and the slope of the temperature curve increases again. This second temperature rise starts well before the rate of evaporation (i.e., the slope of the

moisture content versus time curve) has reached its maximum. That is to say, although the quantity of heat required to evaporate water continues to increase, enough energy is transferred into the layer to increase the temperature at the same time.

A simplified explanation of the progressing vapor front and the temperature plateau near 100°C has been reported by some workers (e.g., Gefahrt 1977). This explanation emphasizes abrupt condensation and evaporation fronts, with a zone of constant conditions between these two fronts. However, the simulation results presented here show that condensation and evaporation may happen even *within* the zone of nearly constant temperature. Thus, the assumption of constant conditions between distinct condensation and evaporation fronts is not mandatory to explain the progressing vapor front and the temperature plateau. Furthermore, it is irrelevant for explaining these phenomena whether vapor condenses to free liquid water or is absorbed immediately by the cell wall substance, as assumed in the present model.

### **5.2.2.3 Core layer ( $z = 10$ ) behavior**

During the first three minutes or so temperature, moisture content and vapor pressure in the core layer do not notably deviate from their initial values. The subsequent rise of these variables is less steep than predicted for the intermediate layers. The onset of the vapor pressure rise occurs considerably earlier than the onset of the major rise in total gas pressure (Figure 5.4). Evidently, gas escape through the edges of the mat still compensates for most of the vapor generated. The vapor pressure continues to rise faster than the total gas pressure until almost all air is replaced by vapor by the end of the pressing cycle. The course of the total gas pressure curve is a consequence of the interaction between the rise in vapor pressure and the decline in air pressure. Such pressures are highly affected by the material's in-plane permeability and by the length and width of the mat.

Some workers have stated that the onset of the total gas pressure rise should coincide with the moment when the core temperature reaches the boiling temperature of liquid water (e.g., Rauch 1984). Such an assertion is only likely to be true if a surplus of free water exists in the mat, and if the size of the mat is relatively small. The predictions

presented here show that the total gas pressure may start to rise substantially before 100°C is reached in the core layer.

The core temperature  $T$  reaches 115°C and the within-void relative humidity  $\varphi$  exceeds 90 % towards the end of the pressing cycle. Under such conditions ( $\varphi > 90\%$  and  $T < 120^\circ\text{C}$ ) it can be shown by thermodynamic reasoning that the temperature is closely linked to the prevailing vapor pressure; the actual temperature cannot exceed the saturation temperature corresponding to the prevailing vapor pressure by more than 3°C. Thus, the temperature is dictated, within tight limits, by the vapor pressure. On the other hand, the vapor pressure that builds up in the horizontal center of a mat depends, among other things, upon the size of the mat. In a small mat where gas can escape easily, vapor pressures usually exceed atmospheric pressure only modestly (see for example Rauch 1984). The saturation temperature at atmospheric pressure is 100°C, and that is why the core temperature measured in small-size laboratory presses typically has a plateau near 100°C. The temperature only further increases once the moisture content, and consequently the relative humidity, drops down.

In industrial or large-size laboratory presses, as simulated here, greater vapor pressures build up in the mat. The core temperatures, therefore, exceed 100°C and continue to rise together with the vapor pressure as shown by the simulation results. The close link between core temperature and mat size has been observed by several researchers in laboratory and industrial experiments (e.g., Humphrey and Bolton, 1989b).

#### ***5.2.2.4 Time dependent changes in layer density***

Due to the significant influence that cross-sectional density profiles have on many panel properties, its formation throughout the pressing cycle has been of considerable interest in the past. While the density profile of the final panel can be measured, little is known about time dependent changes in layer density during pressing. Most of the discussion has been rather speculative in nature so far, as there were no reliable data available.

Haselein (1998) was apparently the first to display the simulated formation of the density profile. Only recently Winistorfer and co-workers developed an in-situ density

monitoring system that, for the first time, allows one to measure changes in layer density during pressing (Winistorfer et al. 1998, Wang et al. 2000). The laboratory-based system uses radiation from caesium<sup>137</sup> sources to beam-through the mat at three cross-sectional positions while the mat is consolidated in the press. Reported measurements recorded for OSB indicate that the cross-sectional density profile is formed from a combination of actions that occur both during consolidation and also after the press has reached final position (Wang et al. 2000). In other words, the density profile continues to change after press closure.

Similar conclusions can be drawn from the simulation results displayed in Figure 5.5. During the early stages of press closure, that is before major temperature and moisture changes take place in the mat, an almost uniform densification of the entire mat is evident. Between about 50 and 110 seconds the pressing pressure persists at a high level (see Figure 5.11) while the mat is compressed to its final thickness. A more or less rapid density rise in the outer mat layers is visible during this period. The inner layers, which experience almost no temperature and moisture content changes at the early stages of pressing, show only a small increase in density; this is mainly caused by the viscous and delayed-elastic material behavior.

Once the final thickness has been reached at  $t = 110$  s, further cross-sectional redistribution of the wood-furnish material takes place, due to proceeding changes of the rheological material properties as well as visco-elastic effects. The density in some layers continues to rise while it decreases in other layers. Most of these changes happen within the next 90 seconds, and only minor changes in layer density are predicted for the rest of the pressing cycle after  $t = 200$  s. It should be noted that the density curves displayed in Figure 5.5 denote the density values on a dry wood basis. Thus, the average density of the entire mat stays constant after press closure, regardless of changes in moisture content.

The cross-sectional density profile develops as a consequence of the unequal density progressions in the different mat layers. The profile predicted here shows the typical M-shape with density maxima somewhat away from the surfaces. The pronounced density drop from the maxima towards the surfaces has been subject to some discussion in the past. An explanation proposed by some researchers (e.g., Plath 1971, Boehme 1992) may be summarized as follows: The adhesive in the surface layers cures before the

maximum pressing pressure has been reached, causing poor bonds between the wood constituents. After press opening the surface layers experience a significant spring-back so that the density profile shows considerably lower densities at the surfaces than in subsequent layers. This theory is shown to be faulty by the present model results.

The pronounced density drop at the immediate surfaces can be explained conclusively by the simulation results, even though adhesive cure is not accounted for in the model. The stiffening effect of drying counteracts the softening effect of heating in the surface layers, so that the resulting compressibility is lower than in intermediate layers. This explanation, however, does not exclude the possibility of adhesive cure having some additional impact on the density profile development.

Temperature, moisture content, and consequently also rheological material properties develop somewhat differently throughout the horizontal plane of the mat. Thus, final cross-sectional density profiles vary slightly with horizontal position. An example of such differences will be given when discussing the predictions for the continuous press in section 5.3.2.

### **5.2.3 Comparison of model predictions with measurements**

Unless otherwise stated, all experimental results presented in this section refer to trial 1 of the measurements described in Appendix B, and all predictions are from the simulation run specified and discussed in the previous section (see Table 5.1 and Figure 5.1). As the model does not account for venting effects before press opening, the simulation for trial 1 was stopped after 630 seconds. Similarly, measured curves are only displayed for the first 630 seconds before venting of the mat was started.

Overall, simulated and experimental results match well, qualitatively as well as quantitatively. However, for a complex system as it is modeled here exact agreement between predictions and measurements cannot be expected. Reasons for disagreements may be:

- The material property input data used for the simulation do not necessarily characterize exactly the wood-furnish material used in the validation experiments.



- Inhomogeneties in the mat prior to pressing are not accounted for in the simulation.
- Experimental errors are unavoidable when determining the material properties as well as carrying out the validation experiments.
- Deficiencies in the model itself may also account for part of the deviations.

All dependent variables interact with one another in the process. This interaction makes it difficult, or sometimes even impossible, to infer the exact reasons for deviations between prediction and measurement. A detailed treatment of all results was beyond the scope of this dissertation. Instead, only some of the more significant aspects will be discussed here.

### 5.2.3.1 *Temperature and gas pressure*

In Figure 5.7 temperature and gas pressure measured at different spatial positions in the mat are compared with model predictions. The temperature measurements were made with thermocouples. To monitor the internal gas pressure, thin steel tubes connected to pressure transducers were inserted into the mat. A schematic of the mat that shows the positions of the measuring points is displayed in Figure 5.6. After pressing, the exact positions of the probes were determined by dissecting the panel; for trial 1 they are stated in Table 5.2. All probes were placed close to the central y-z plane.

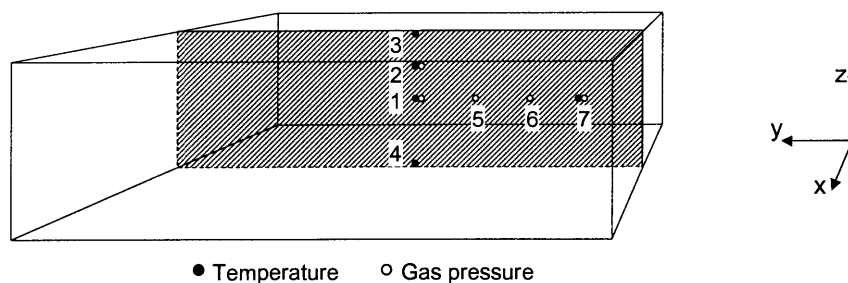


Figure 5.6. Schematic of mat with positions of temperature and gas pressure probes.

Table 5.2. Positions of temperature and gas pressure probes in percent of mat dimensions for batch press trial 1. Coordinates and numbering are used as specified in Figure 5.6.

	Temperature sensors					Gas pressure sensors				
	T1	T2	T3	T4	T7	P1	P2	P5	P6	P7
x	49 %	50 %	48 %	50 %	45 %	51 %	50 %	55 %	defective	45 %
y	50 %	50 %	53 %	50 %	13 %	50 %	50 %	38 %		13 %
z	50 %	85 %	upper surface	lower surface	50 %	50 %	85 %	58 %		50 %

Temperature measurements were recorded at the upper and lower surfaces and at three intermediate positions within the mat. Gas pressures were measured at three points in the central plane; a fourth sensor (number 6) proved defective during trial 1. One additional gas pressure probe was placed at the horizontal center of the mat between the surface and the central plane. In Figure 5.7, simulated temperature and gas pressure curves are displayed for those grid points whose coordinates were closest to the positions of the measuring points.

Temperatures measured at the upper (*T3*) and lower (*T4*) surfaces deviate from each other. This asymmetry may result from the screen being placed between the lower platen and the mat or from inhomogeneties within the mat prior to pressing. As only one half of the mat thickness was modeled, such asymmetries are not accounted for.

The gas pressure measured at the intermediate position between central plane and surface (*P2*) is a little higher than that measured at the core (*P1*). However, for two of the four trials, somewhat lower gas pressures were recorded at *P2*, compared to *P1* (see Appendix B). Hence, it is reasonable to assume that these differences are artifacts. The gas pressure at *P1* and *P2* are identical in the simulation, and *P2* is therefore not displayed.

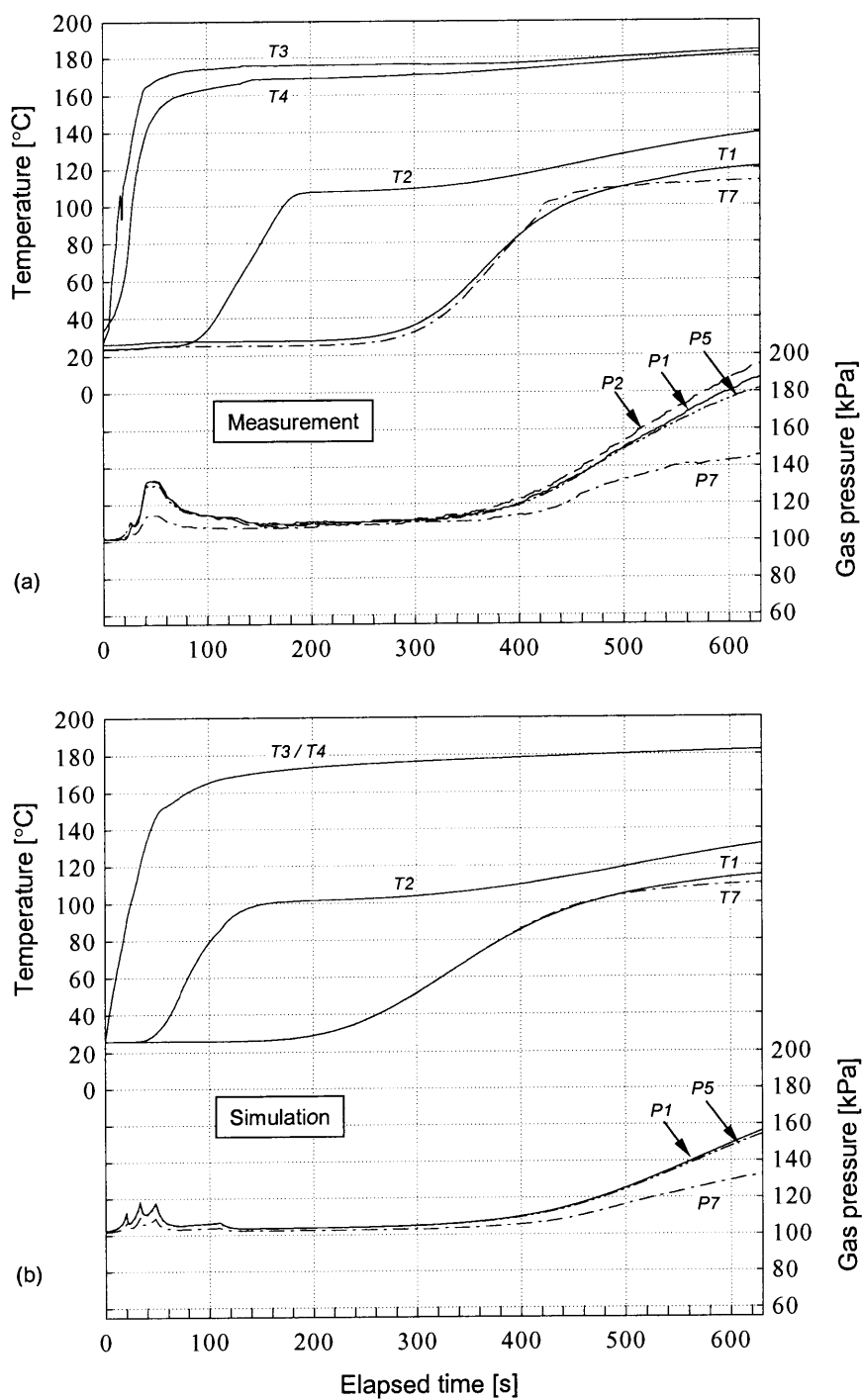


Figure 5.7. Comparison of measured (a) and predicted (b) temperature and total gas pressure development within the mat. Positions of sensors are specified in Figure 5.6 and Table 5.2. (Batch press trial 1)

The measured gas pressure curves displayed in Figure 5.7 are more or less smooth during press closure, while predictions show pronounced peaks that coincide with respective changes of the consolidation rate. The explanation for the smooth courses of the measured gas pressures is that the pressing pressure reached its allowed maximum (limited by the press hydraulics) between 50 and 100 seconds in trial 1 (Figure 5.11). During this period the pressing pressure dictated the platen position and caused a gliding transition from one to another consolidation rate. In trials 2 and 3 the allowed pressure maximum was not reached; thus the measured gas pressure curves show pronounced peaks, which agree well with those predicted (Figure 5.8).

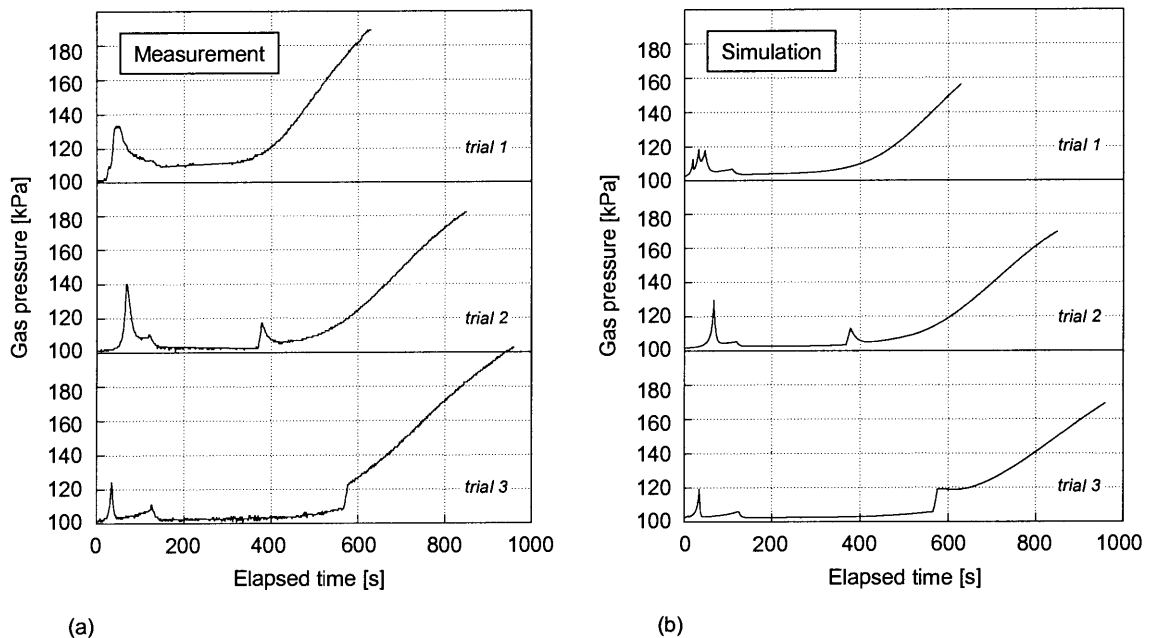


Figure 5.8. Comparison of measured (a) and predicted (b) total gas pressure in the center of the mat ( $P1$  position in Figure 5.6). Displayed are curves for batch press trials 1 to 3.

The actual average surface density was higher than the simulated one (Figure 5.9). This explains part of the differences between predicted and measured temperature and gas pressure curves in Figure 5.7; as the thermal conductivity is positively related to density, higher densities near the surfaces enhance the conductive heat transfer from the pressing platens to the progressing condensation front. A routine has been implemented within the simulation program that allows model runs with pre-defined density profiles.

An identical simulation of trial 1, but assuming a density profile that reflects the measured one, resulted in significantly higher temperatures and internal gas pressures as those predictions presented in Figure 5.7.

### 5.2.3.2 Cross-sectional density profile

A comparison of simulated and measured final density profile is presented in Figure 5.9. In both cases the profile has its maxima about 3 mm inside from the surfaces, with a steep density drop towards both the surfaces and the core. The maxima of the measured density profile are abnormally high, reaching  $1240 \text{ kg/m}^3$ , while the core density drops down to almost  $400 \text{ kg/m}^3$ . Such extreme profiles are usually not produced in industrial processes. It should be noted that even the predicted profile with maxima around  $1040 \text{ kg/m}^3$  has to be considered as extreme, although to a less pronounced extent. Several explanations are possible for the differences in predicted and measured density profile.

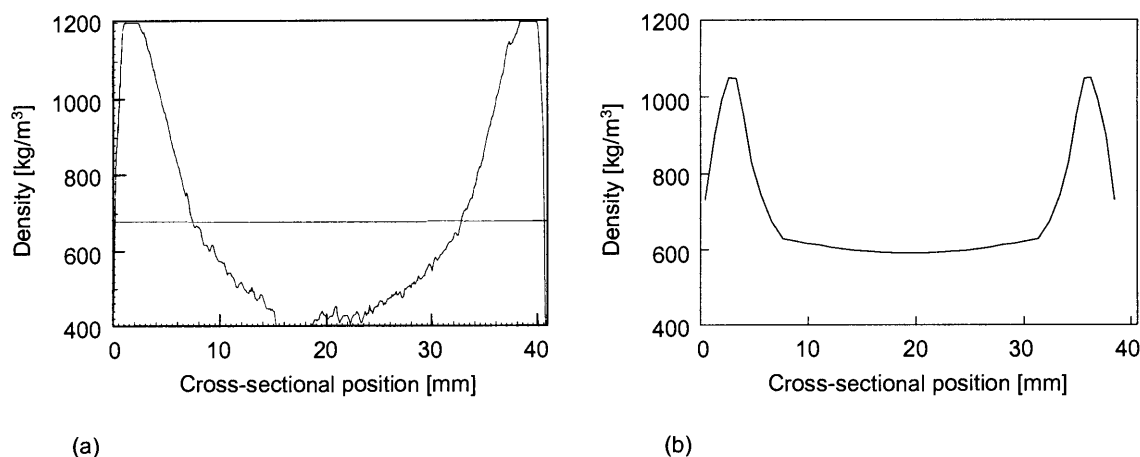


Figure 5.9. Comparison of cross-sectional density profile in the horizontal center of the panel: (a) measured, (b) predicted after 630 seconds of pressing, but before press opening. (Batch press trial 1)

The formation of the cross-sectional density profile is a consequence of the migration of heat and moisture within the mat throughout the pressing process and the resulting rheological behavior in different mat layers. Consequently, incorrect predictions

of the temperature and moisture content development lead directly to an inaccurate simulation of the density profile. These effects are likely to account for part of the differences, but not for all of them. This conclusion comes from the following reasoning.

The simulation results show that temperature and moisture content in the inner layers begin to rise only after the final thickness has been reached. This prediction is likely to correspond with the real conditions that occur during pressing. That is to say that the core has a temperature of 26°C and a moisture content of 9.9 % when the maximum pressing pressure of 4 MPa is reached. Under these conditions, a core density of 605 kg/m<sup>3</sup> has to be expected from von Haas's (1998) densification experiments. This value is considerably higher than the core density of somewhat above 400 kg/m<sup>3</sup> measured for the final panel after pressing. Further, rheological data from different sources suggest that it is unlikely that the material in the core expands during the later stages of the pressing cycle or upon press opening by such a great amount after being compressed to about 600 kg/m<sup>3</sup> during press closure.

Apparently, the core material is stiffer during press closure than assumed in the simulation. Differences between the material property input data used for the simulation and the material characteristics of those mats used in the validation experiments may be one reason for this discrepancy. Another possible explanation is that the known initial moisture content is only an average value over the cross-section of the single wood fibers, while defacto a more complex moisture distribution exists microscopically. If most of the moisture were concentrated near the fiber surfaces or even in the adhesive, the inside of the fibers would be dryer than assumed. Such moisture distribution may affect the rheological behavior of the material.

One of the simplifications made in the model is that effects of adhesive cure are not accounted for. The density redistribution after press closure noticeable in Figure 5.5 may be hindered by the formation of inter-fiber adhesive bonds. However, as can be seen from the density versus time curves in Figure 5.5, only a minor proportion of the difference between predicted and measured density profile can be explained by the omission of adhesive cure.

### 5.2.3.3 Cross-sectional moisture profile

A pronounced cross-sectional moisture profile develops during the pressing process, with relatively dry surface layers and core moisture contents that, at least temporarily, exceed the initial moisture content. To determine the moisture profile through the cross-section of the final panel, a 50 x 50 mm<sup>2</sup> sample was sliced into five layers about 5 minutes after press opening, and each layer was sealed immediately in a plastic bag to avoid further moisture changes prior to testing. Measured and simulated moisture profiles are presented in Figure 5.10. The asymmetry of the curve in Figure 5.10a was mainly caused by differences in thickness of the five layers. The displayed moisture profile for the experiment must therefore be regarded only as an approximation of the exact moisture profile.

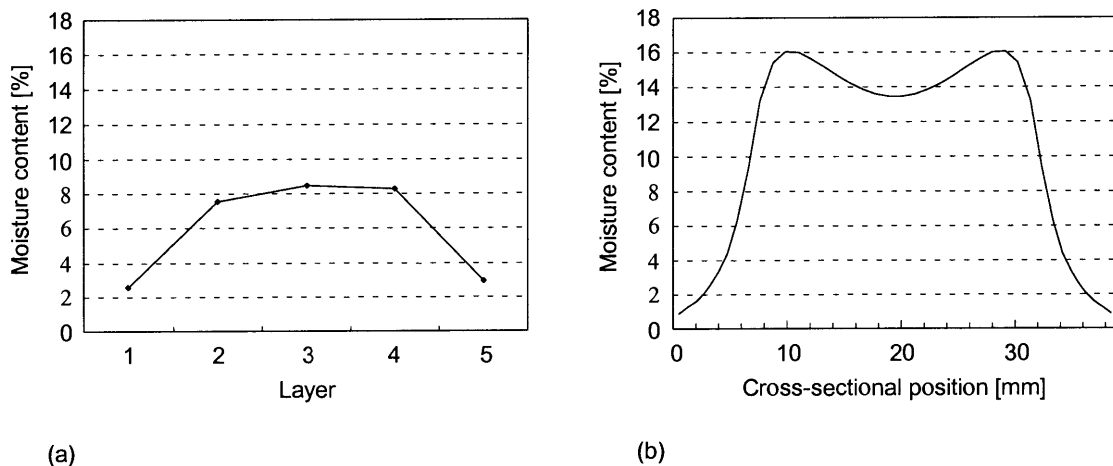


Figure 5.10. Comparison of cross-sectional moisture profile in the horizontal center of the panel. (a) Measurement for 730 seconds pressing time after press opening. (b) Prediction at 630 seconds before press opening. (Batch press trial 1)

Measured and predicted cross-sectional moisture profiles show similar qualitative trends. Moreover, the M-shape of the predicted profile (Figure 5.10b) agrees well with measurements reported by Rackwitz (1954) and Maku et al. (1959). Quantitative accord of the two curves could not be expected for two reasons. First, the simulation was stopped after 630 seconds, while the mat actually stayed in the press for 100 further seconds. Second, vapor escapes from the mat when venting and opening the press, and

this may lead to a drop in core moisture content. Such moisture drop after the panel left the press can be recognized in Figure 5.17 showing continuous press predictions.

However, it is likely that these two explanations do not account for the total difference between measured and simulated moisture profile. As mentioned above, the predicted gas pressure lags behind the measured gas pressure. Higher internal gas pressures enhance the vapor escape through the edges, and therefore the overall moisture loss. It is also possible that shortcomings in the model itself are responsible for underestimating the moisture decline in the mat.

#### ***5.2.3.4 Pressing pressure***

A comparison of recorded and simulated pressing pressure courses for trial 1 is shown in Figure 5.11. The displayed curves agree very well for the entire period of press closure. The decline of the mat counterpressure is correctly predicted in trend, but stress relaxation processes are apparently underestimated by the simulation. The same tendencies, namely correct predictions of press closure and underestimating subsequent stress relaxation, are also evident for trials 2 and 3. Pressing pressures predicted for the second densification step of trials 2 and 3 are somewhat high.



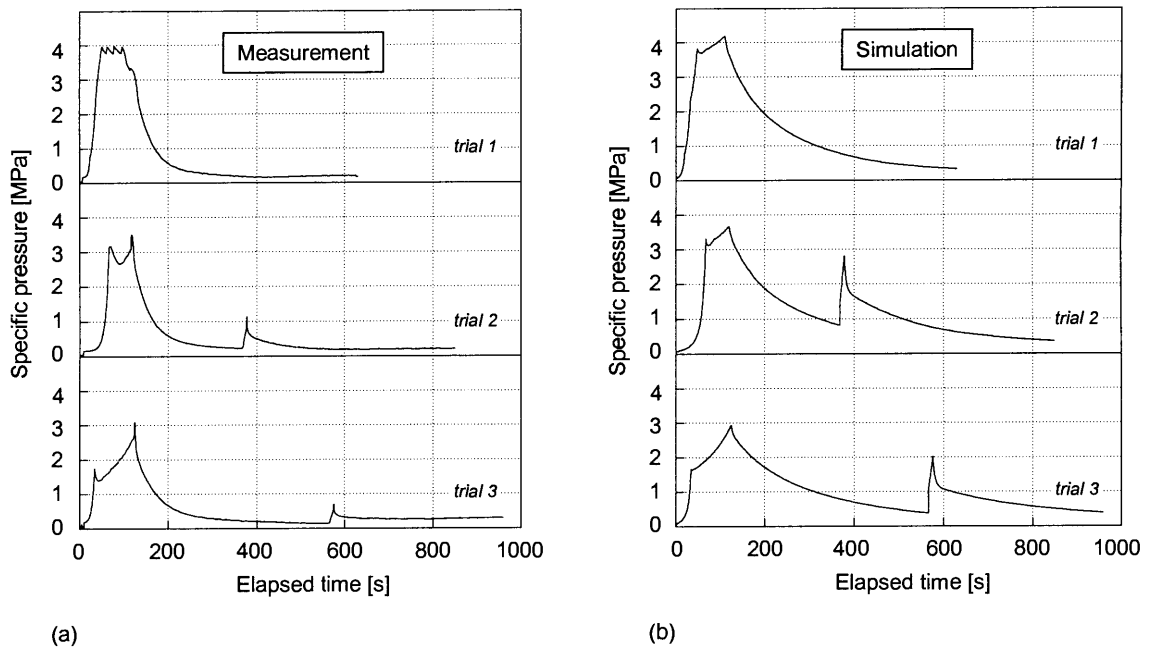


Figure 5.11. Comparison of recorded (a) and predicted (b) pressing pressure. Displayed are curves for batch press trials 1 to 3.

The following factors may contribute to inaccurate predictions of the pressing pressure course during the latter stage of the pressing cycle:

- Imprecise predictions of temperature and moisture content directly affect the rheological mat behavior.
- It may be necessary to revise how the rheological coefficients used as model input data were derived from the experimental data.
- By applying the Burger-Humphrey model, the entire spectrum of interacting rheological processes occurring during hot pressing is described by only five elements. Such a relatively simple model clearly has the advantage of being well comprehensible. However, the establishment of alternative rheological model techniques may be required to improve the accuracy of the simulation.

### 5.3 EVALUATION OF CONTINUOUS PRESS MODEL PREDICTIONS

Temperature and gas pressure measurements were made in an industrial continuous press (28 m press length, 2.3 m mat width) for MDF production. A summary of the methods used to make the measurements is given in Appendix C. The objective of the experiment was to test a new apparatus that was developed for such measurements, and to investigate internal mat conditions during continuous hot pressing. Gas pressure measurements in continuous presses for wood-based composites have not been reported before.

A *quantitative* comparison between measurement and prediction as it was made in the previous section for a laboratory batch press was not intended for the continuous press data. The main reasons are:

- The exact material properties of the consolidated mats were not known.
- Perhaps even more important are uncertainties in pressing parameters recorded in the industrial continuous process. Sensors are usually not calibrated to a degree of accuracy required for exact measurements. Furthermore, variations in steel belt temperature, mat thickness, and pressing pressure across the width of the press are not known, although they may be considerable in a continuous press.

A general discussion of a typical simulation of the continuous press is therefore presented here, followed by a *qualitative* comparison of predicted gas pressure curves and density profiles with results of the industrial measurements. Basic features of the predictions that have been already discussed in the previous section for the batch press will be repeated only when appropriate.

While the representation of predictions by XY-plots is advantageous for a quantitative evaluation of simulation results, 3D-plots may help one to appreciate the dynamic changes of a variable throughout pressing. Such 3D-plots are introduced here to supplement the information given by the more exact XY-plots used for the simulation results for the batch press.

### 5.3.1 Specification of input conditions

The input specifications for the simulation run discussed here were chosen to reflect the conditions of the continuous press for which the temperature and gas pressure measurements were made. Trial 3 out of the four trial measurements was the basis of the simulation.

Table 5.3. Input conditions specified for the continuous press standard simulation run.

<u>Panel specifications</u>	
Material:	One-layered MDF mat
Width:	2.30 m
[Target thickness:	≈ 20 mm]
[Target density (dry wood basis):	≈ 800 kg/m <sup>3</sup> ]
<u>Initial mat conditions</u>	
Bulk height:	160 mm
Bulk density (dry wood):	100 kg/m <sup>3</sup>
Temperature:	40°C
Moisture content:	9.6 %
<u>Pressing parameters</u>	
Control mode:	Load control
Press length:	27.85 m (first to last mat-steel belt contact)
In-feed radius:	30 m
Feed speed:	129 mm/s
<u>Model definitions</u>	
Length of modeled mat segment:	10 m
Grid (x, y, z):	15 x 5 x 10
Grid scheme:	Clustered around reference regions
Symmetries:	y- and z-direction
Time steps per second:	500 for primary and inner time loops

Input specifications are listed in Table 5.3. A one-layered MDF mat with homogeneous initial conditions was modeled. Target thickness and density were about 20 mm and  $800 \text{ kg/m}^3$ , respectively. However, as load control was assumed, the actual final panel thickness and density is a consequence of bulk height, bulk density, and the course of the specified pressing pressure. The total length of the press, measured from first to last mat-steel belt contact, is 27.85 meters. This value is composed of the length of the in-feed section and the distance between the end of the in-feed section and the press outlet. The latter was specified here as 25 meters, while the length of the in-feed section is dictated by the in-feed radius. The specified course of the pressing pressure is displayed in Figure 5.12. Within the in-feed section the pressing pressure cannot be stated directly, but is dictated by the in-feed radius and the absolute level of the upper steel belt.

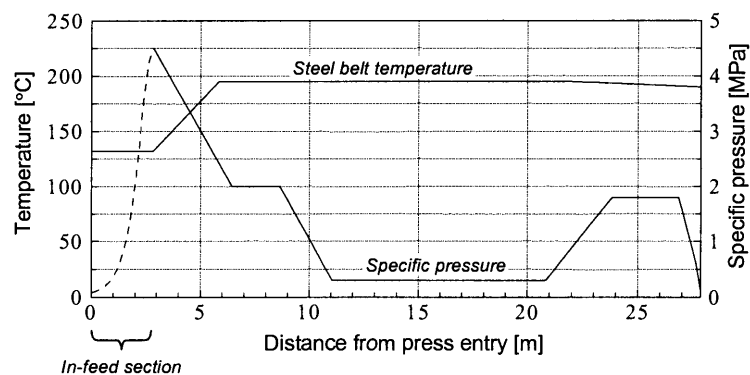


Figure 5.12. Specified pressing pressure and steel belt temperature for the continuous press standard simulation run. In the in-feed section the pressing pressure cannot be defined directly, but is dictated by the radius and absolute level of the upper steel belt.

The steel belt temperature was needed as a boundary condition. Neither the temperatures recorded for the heating platens nor the temperature measured near the surface of the mat represent the exact steel belt temperature. In the absence of reliable industrial data, an estimate of the longitudinal temperature profile was made (Figure 5.12). This estimate is based on the steel belt temperature measured right in front of the press entry and the temperature measured near the surface of the mat.

A 10 meter long mat segment was considered for modeling purposes. The mat was assumed to be symmetrical along the width and the thickness, so that calculations

were done for only one fourth of the mat. A modeling grid of 15 x 5 x 10 control regions (x, y, z) was used, and the control regions were clustered in the feed direction (x-direction) around the reference cells, with a size ratio of outermost to innermost regions of 7. All results are plotted for the reference cells, i.e., half way between the two boundaries perpendicular to the feed direction. The implicit approach was employed to compute the cross-sectional gas flow. The same material property data were used as for the simulation of the batch press (see section 5.2.1). Total execution time on a personal computer with a Celeron<sup>TM</sup> processor and 400 MHz frequency was about 3 hours.

All predictions for the continuous press presented in this dissertation refer to the simulation run specified in Table 5.3 and Figure 5.12.

## **5.3.2 Presentation and discussion of model predictions**

### ***5.3.2.1 Gas pressure predictions***

The gas pressure predictions will be discussed first this time for conceptual reasons.

Before the uncompressed mat enters the press, about 96 % of the total gas pressure can be attributed to air in the vapor-air mixture. The fast compression of this air as the mat enters the press leads to a total gas pressure maximum about 0.75 bar above atmospheric pressure early in the pressing cycle (Figure 5.13). Towards the end of the press, the vapor pressure increases considerably within the mat. This generation of vapor, together with the compression of the gas during the second densification step near the end of the press, causes the final gas pressure maximum of almost 1.5 bar above atmospheric pressure right before the panel leaves the press. Across the width of the mat, a near-parabolic gas pressure distribution is generated with, as expected, a maximum along the axial centerline of the press. The contact points of the mesh lines in Figure 5.13 represent the centers of the grid regions. Hence, the first and last plotted values over the width represent the total gas pressure 5 % inside from the actual mat edge.

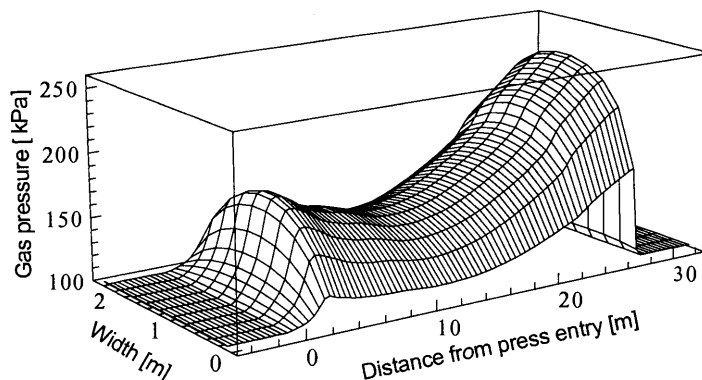


Figure 5.13. Predicted total gas pressure distribution within the central layer of the mat. (Continuous press standard run)

Figure 5.14 shows the core layer distribution of total gas pressure for the first six meters of the press. The arrows represent the horizontal gas velocity in the central layer, defined as the volumetric gas flow per second per unit cross-sectional area of the porous material. The gas pressure maximum is reached three meters into the press in the middle of the mat. Most of the air-vapor mixture escapes through the edges in the in-feed section, and through the surfaces right before the mat enters the press. The magnitude of such gas counter-flow may be of practical importance since it can lead to disruption of the loosely packed mat. The highest gas velocity is reached at the edges about half way between the press entry and the region of the gas pressure maximum. Once the mat is densified, the flow resistance within the mat is on the order of 500 times greater than at the press entry. Although greater gas pressure gradients prevail in the compressed mat, the gas velocity is considerably reduced.

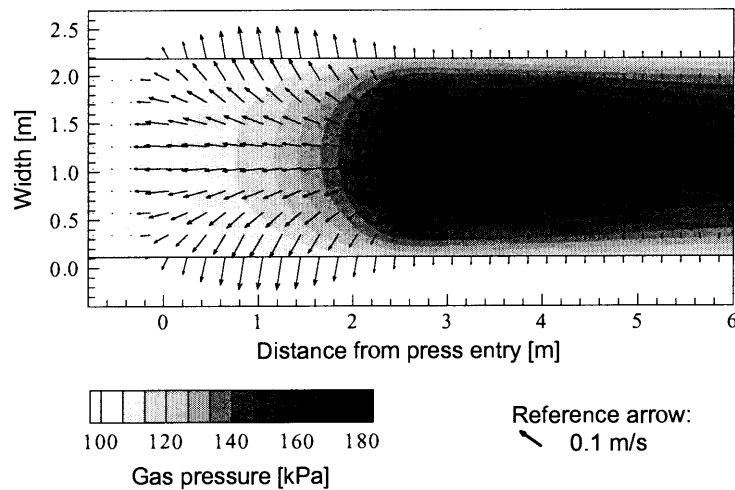


Figure 5.14. Predicted total gas pressure distribution and gas velocities (arrows) for the first 6 meters within the central layer of the mat. (Continuous press standard run)

### 5.3.2.2 Temperature predictions

The predicted cross-sectional temperature distribution along the axial centerline of the press is shown in Figure 5.15. Each mesh line connecting the press entry with the press outlet represents the temperature in one individual layer. A steep rise of the surface layer temperature is visible while the mat passes through the front zone of the press. The progressing vapor front (see section 5.2.2.2) causes the typical shape of the temperature lines shown for the intermediate layers between surfaces and central plane; main features of these lines include a time lag before the temperature begins to rise and a temperature plateau near 100°C. Predictions suggest that the second densification step does not have a significant effect on temperature. The temperature drop that appears in all layers as the panel leaves the press is a consequence of rapid evaporation of water within the panel; it is principally due to vapor escape through the panel surfaces.

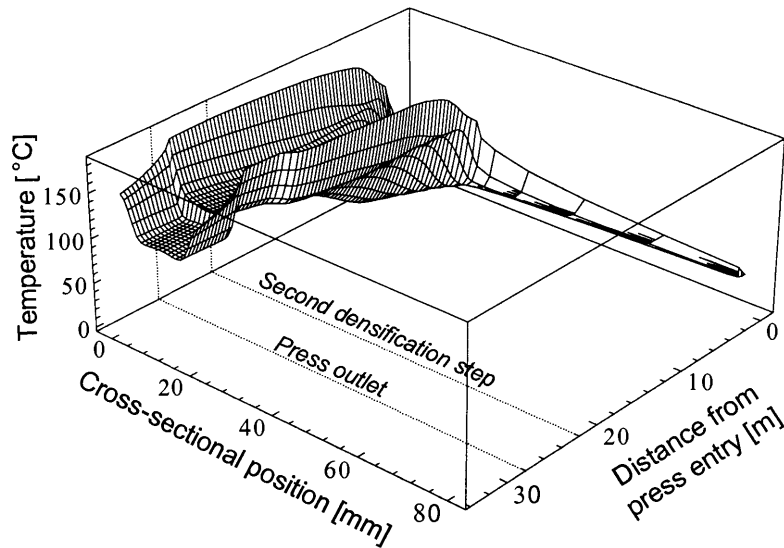


Figure 5.15. Predicted temperature distribution within the central x-z plane of the mat. (Continuous press standard run)

The solid curves in Figure 5.16 display the temperature distribution at four individual cross-sectional positions. The temperature plateau for the intermediate layer  $z = 4$  is with  $113^{\circ}\text{C}$  unusually high, compared with those temperatures observed in laboratory presses or in industrial particleboard presses. As was shown in section 5.2.2.3, at near-saturation conditions (i.e., high relative humidity values) the temperature is closely linked to the prevailing vapor pressure. Evidently, the high level of the temperature plateau results from the high gas pressure level visible in Figure 5.13.

A direct consequence of such elevated temperature levels in the intermediate layers must be that the temperature rise in the core is delayed, because more energy is required to heat the intermediate layers before the condensation front can proceed towards the central plane. To test this hypothesis, the simulation run was repeated with the in-plane permeability values artificially doubled. The effect of this manipulation was that gas escape through the edges was eased, so that a lower gas pressure built up in the mat. The temperature predictions of the new simulation run are displayed as dash-dotted lines in Figure 5.16. As expected, the temperature plateau of the intermediate layer  $z = 4$  came down, while the vapor front proceeded faster towards the central plane.



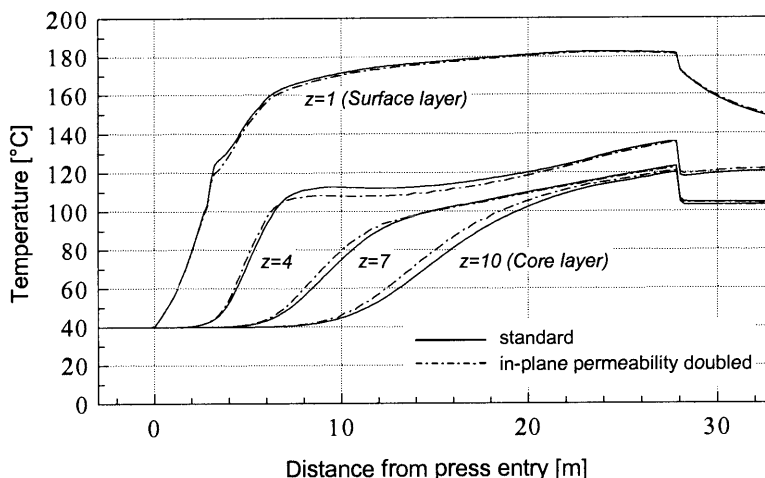


Figure 5.16. Predicted temperature distribution at four cross-sectional positions within the central  $x$ - $z$  plane of the mat. Displayed are results of runs for the continuous press, executed with two different levels of in-plane permeability.

### 5.3.2.3 Moisture content predictions

Figure 5.17 displays the development of the cross-sectional moisture profile along the axial centerline of the press. The moisture content in the surface layers declines soon after the mat has entered the press and then stays at a relatively low level. The intermediate locations between mat surfaces and central plane experience a moisture rise towards a maximum, before the moisture content drops again. By this sequence the position of maximal moisture content continuously moves forward towards the core. The simulation results presented here show that the maxima do not reach the core throughout the entire process. This prediction applies to the specific case simulated here, but should not be generalized. Under different circumstances it is entirely possible that the final moisture maximum is located in the core of the mat.

A pronounced moisture drop is predicted when the panel leaves the press. This moisture drop makes clear that not only vapor escapes that is already in existence within the voids of the mat. In fact, water evaporates rapidly due to changes of the thermodynamic conditions at the press outlet. This rapid evaporation is what causes the moisture drop as well as the temperature drop displayed in Figure 5.15.

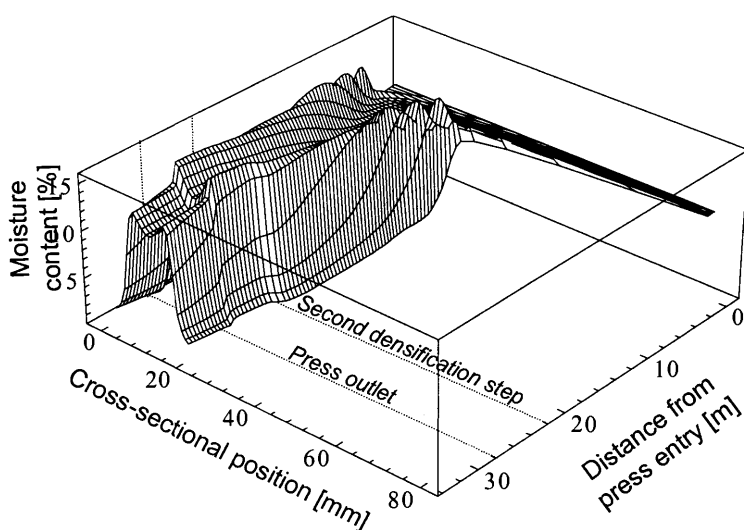


Figure 5.17. Predicted moisture distribution within the central x-z plane of the mat. (Continuous press standard run)

#### 5.3.2.4 Density profile predictions

The density profile development during continuous pressing depends on the longitudinal distribution of pressing pressure in concert with the spatial distribution of rheological mat properties. As discussed above, these mat properties are determined by temperature, moisture content and density, and change considerably throughout the pressing process. Furthermore, it can be expected that there is an impact of the adhesive cure on the mat properties. However, since adhesive cure is not considered in the present modeling approach, the following interpretations are based only upon those explanations that can be derived from the present form of the Burger-Humphrey model.

Near the press entry, high surface densities are formed, while the density of the inner layers of the mat stay at a relatively low level (Figure 10). The high surface densities are a consequence of softening during and right after the main densification. Due to the viscous-elastic component of the mat's rheological characteristics, the total thickness of the mat somewhat increases again when the pressing pressure decreases to 0.3 MPa further down the press.

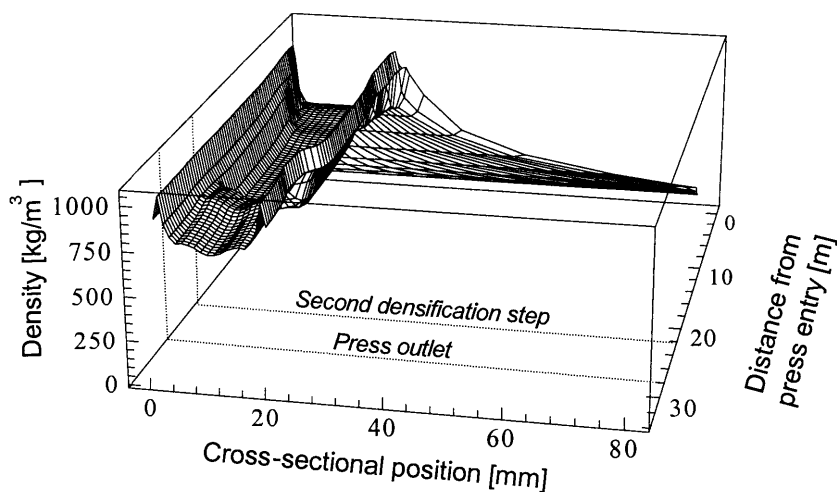


Figure 5.18. Predicted density profile development within the central x-z plane of the mat. (Continuous press standard run)

If no further densification were to take place, the density profile of the final panel would have a relatively simple shape with high densities near the surfaces and a flat density distribution across the core. However, as specified for the simulation run, the mat sustains further densification in a second step near the end of the press. At this stage, the cross-sectional distributions of rheological properties differ greatly from those near the press entry. Almost no further densification occurs in the surface layers while densification is greatest in the layers midway between surface and core. A rather complex density profile is thereby generated, with an intermediate density peak in the latter layers. After leaving the press, the panel relaxes, leading to a predicted spring-back of about 4 %.

The density profile development shown in Figure 5.18 has been predicted for the axial centerline of the press. A tendency frequently observed in continuous MDF pressing is that the density minimum in the core layer is less pronounced near the edges than at the axial centerline. Simulation results agree with this observation. Figure 5.20b shows two final density profiles, one predicted for the position 5 % inside from the edges and the other one for the axial centerline. The former profile indicates deeper intermediate density minima, but an elevated core density. These differences are a consequence of the

non-uniform temperature and moisture content distributions across the width of the mat throughout pressing.

### 5.3.3 Comparison of model predictions with measurements

In order to measure the internal gas pressure in a continuous press for MDF production, a thin steel tube was inserted into the core layer of the mat before the mat entered the press. The tube was connected to a small pressure transducer that passed through the press while lying beside the mat.

Four series of measurements were carried out (see Appendix C). Pressing conditions for trials 3 and 4 were nearly identical. The steel tube in trial 3 was inserted 90 mm (i.e., 40 % of mat width) into the mat, while the steel tube in trial 4 was inserted only 50 mm (i.e., 22 % of mat width). Both readings are displayed in Figure 5.19a.

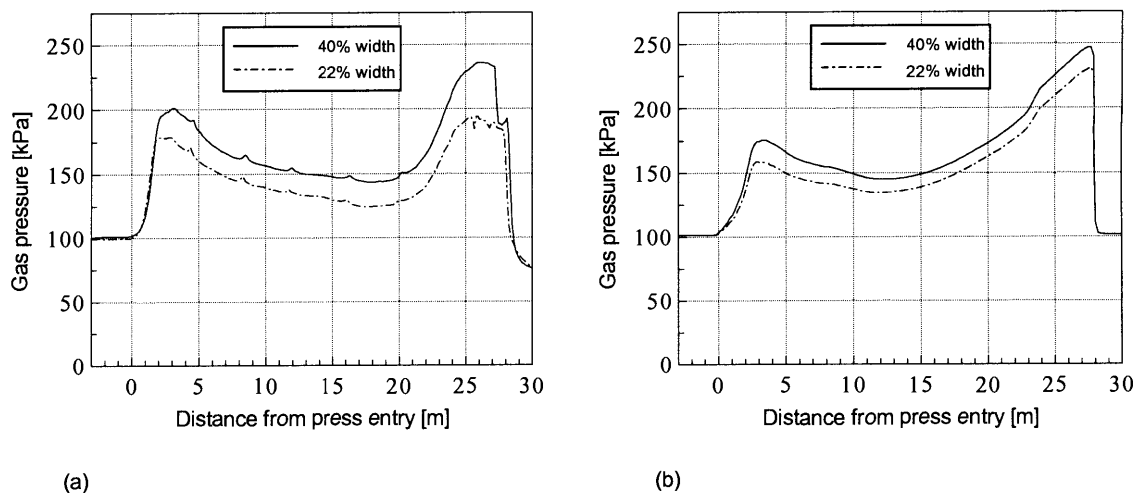


Figure 5.19. Total gas pressure distributions at two horizontal positions within the central layer of the mat during pressing in a continuous press: (a) measured in trials 3 and 4, (b) standard simulation run.

The measured gas pressure maximum near the press entry can be attributed to the compression of air during mat densification. The maximum reaches almost 1 bar above ambient for the position near the center of the mat. This value is considerably higher than those measurements reported in the literature for industrial particleboard pressing in a batch press (e.g., Denisov and Juskov 1974, Humphrey 1982). The main reasons for the

difference are the higher flow resistance of MDF, compared with particleboard, and the faster mat densification in continuous presses.

While the mat thickness stays almost constant during subsequent periods of the pressing cycle, some of the gas entrapped inside the mat escapes through the edges. The gas pressure in the center slowly drops to about 0.4 bar above ambient. Both vapor generation as well as compression of the gas during the second densification step causes the gas pressure maximum at the end of the pressing cycle. Vapor generation is clearly the main reason for the final gas pressure rise, as the void volume within the mat is only reduced by about 23 % during the second densification step. The gas pressure measured half way between the mat center and the edge stays behind the gas pressure measured at the center throughout the entire pressing cycle.

The predicted total gas pressure at two horizontal positions within the mat is shown in Figure 5.19b. Predictions and measurements agree well in trend for all features described above.

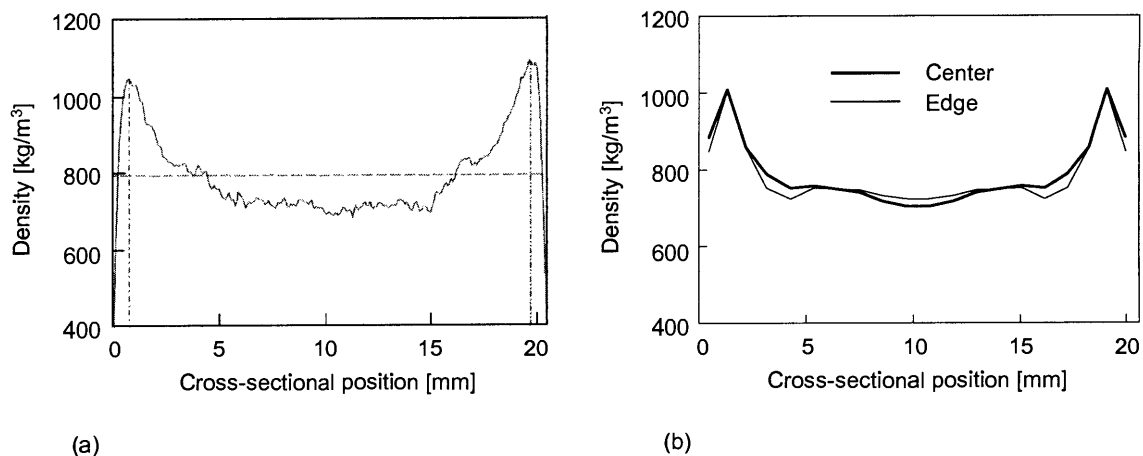


Figure 5.20. Final cross-sectional density profiles. (a) Measurement for the horizontal center of the panel. (b) Predictions for the horizontal center and the position 5 % inside from the edges. (Continuous press standard run)

The final cross-sectional density profile is highly dependent on the course of pressing pressure. Small changes in pressure at a single pressing frame may have a significant impact on the density profile. Figure 5.20a shows the measured final density profile for the center of the panel. The profile does not show a smooth transition from the

surface to the core, but rather shoulder-shaped distortions about 4 mm inside from the surfaces. Shoulders or side maxima typically develop when a pressing schedule is applied that includes two or more distinct densification steps; such effects have been described recently by Wang et al. (2000) for MDF pressing. The shoulders noticeable in Figure 5.20a are likely to be caused by the second densification step near the press outlet.

In trend, similar shoulders are predicted for the panel center, as shown in Figure 5.20b. The impact of the second densification step on the shape of the final density profile becomes clear when looking at Figure 5.18. Additional test runs of the simulation program suggest that the cross-sectional density distributions are very sensitive to changes in the magnitude and course of the second densification step.

## **5.4 SELECTED ASPECTS OF THE PHYSICS**

### **5.4.1 Heat transfer mechanisms**

Conductive and convective heat transfer are clearly the predominant mechanisms by which energy is translated from the surfaces towards the central plane of the mat. The significance of both mechanisms changes in space and time throughout the pressing cycle and can be quantified and visualized by means of model predictions. The predictions presented here are results of the simulation run for a batch press specified and discussed in section 5.2.

The conductive heat flux  $q$  perpendicular to the mat plane is displayed in Figure 5.21 and Figure 5.22. Of particular technical interest is the heat flux through the mat-platen interfaces, which determines the energy input into the wood-furnish mat. Press manufacturers need this quantity for calculating the required capacity of the heating system when designing presses. Moreover, producers of wood-based composites may use simulation results to estimate the effect of changes in pressing conditions on energy consumption and costs.

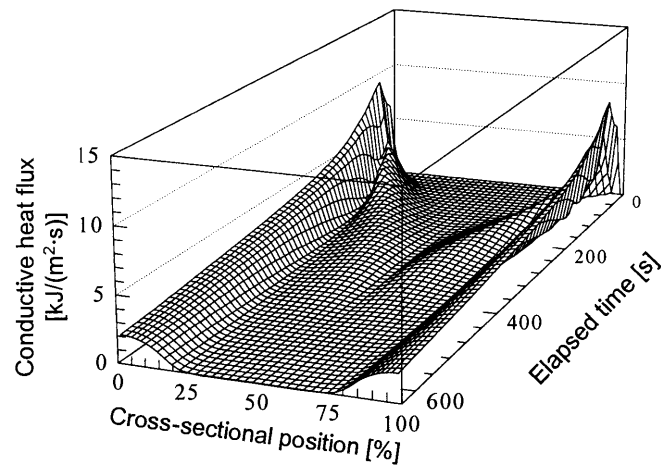


Figure 5.21. Predicted conductive heat flux perpendicular to the mat plane over time and cross-sectional position in the horizontal center of the mat. (Batch press trial 1)

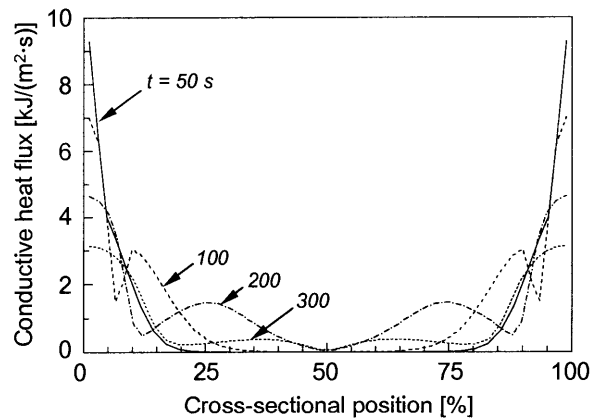


Figure 5.22. Predicted conductive heat flux perpendicular to the mat plane over cross-sectional position in the horizontal center of the mat. (Batch press trial 1)

Of academic concern are the heat transfer processes that occur *within* the mat. The contribution of conduction and convection to local temperature changes can be derived from energy balances for each control region. Suppose that  $Q_{cond}^*$  is the specific rate of conductive energy gain, i.e., the energy entering a control region through its faces by conduction during one second, divided by its dry mass. Further,  $Q_{conv}^*$  shall denote the specific rate of convective energy gain, i.e., the specific quantity of latent heat that is

freed upon condensation and absorption of water vapor during one second. It follows that  $Q_{conv}^*$  becomes negative in the case of evaporation. The specific rate of heating  $Q^* = Q_{cond}^* + Q_{conv}^*$  is the energy spent to increase the local temperature. All three variables are expressed in the units of J/(kg·s). Sensible heat transfer has only a minor effect on temperature changes, as will be shown shortly; this mechanism is therefore not accounted for in the energy balance.

In Figure 5.23 the specific rate of heating,  $Q^*$ , is plotted over time and cross-sectional position. In addition, the zones that are marked in white are those in which the contribution of condensation,  $Q_{conv}^*$ , to warming exceeds the contribution of conductive heating,  $Q_{cond}^*$ . These zones start near the surfaces as narrow layers, and progress towards the central plane of the mat, while widening. The same holds for the regions of intensive heating; the maxima of  $Q^*$  are reached at the surfaces after about 50 seconds and decline while moving inward. This pattern reflects the progressing vapor front.

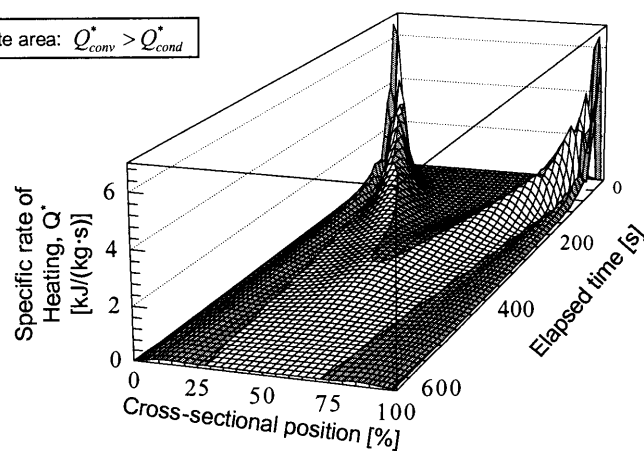


Figure 5.23. Heat energy expended to increase the local temperature in the horizontal center of the mat. The white area marks the zones in which convective heating surpasses conductive heating. (Batch press trial 1)

There are two regions in which conductive heating is of greater significance than heating due to condensation (gray shaded areas in Figure 5.23). These are the outer zones between the pressing platens and the condensation zones, and the inner zone framed by the two condensation zones until they merge at the central plane. From Figure 5.23 it



becomes clear that considerable conductive heating occurs in the inner zone before condensation becomes dominant. This conductive heating is a consequence of steep temperature gradients between intermediate and inner mat layers.

Figure 5.24 shows the contribution of both heat transfer mechanisms to warming of the central plane. Conductive and convective heating start approximately at the same time. During the subsequent period more energy enters the core layer by conduction than latent heat is released due to condensation of water vapor. Only after a core temperature of 75°C is reached in this example, does convective heating become dominant over conductive heating.

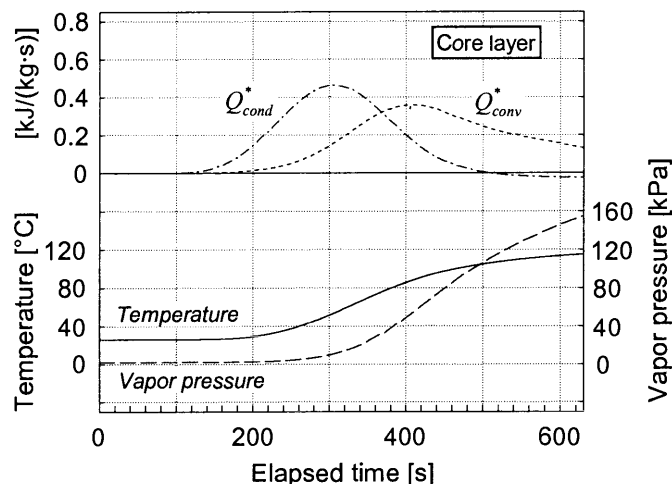


Figure 5.24. Contribution of convective and conductive heating over time at the central position of the mat.  $Q_{conv}^*$  = specific rate of convective energy gain;  $Q_{cond}^*$  = specific rate of conductive energy gain. Predicted temperature and vapor pressure development at the same location are included for reference purposes. (Batch press trial 1)

So far, heating effects due to the translation of warm gas into cooler regions and the consequent release of sensible heat carried with the gas have been neglected. To assess such effects, a routine has been built into the simulation program that accounts for sensible heat transfer. For this option the program has to be executed in the explicit mode. Running the simulation specified in section 5.2 in the explicit mode would require an execution time of several days. Therefore, a smaller grid and altered pressing conditions were chosen for the test runs.

The comparison of predictions from two simulation runs revealed that the core temperature reaches 100°C only two seconds earlier if sensible heat transfer is accounted for. Thus, neglecting this mechanism appears justified without sacrificing much of the accuracy of the predictions.

#### 5.4.2 Air inside the mat

The gas mixture inside the wood-furnish mat consists mainly of air and water vapor. Initially, air is the predominant component in the mixture. As the pressing process proceeds, vapor is generated and replaces most or all of the air inside the mat. Knowing the proportion of vapor and air in the gas mixture is important, as exact flow calculations require consideration of both vapor and air. Furthermore, a full appreciation of the physics of the hot pressing process is difficult if important features such as the composition of the gas mixture are not accounted for.

Apparently the only data reported in the literature that describe the variation of gas composition over time have been published by Denisov et al. (1975). The authors inserted a small tube 900 mm into the core layer of a mat during industrial particleboard pressing to sample the gas mixture during different stages of the pressing cycle, which they termed phases I through IV. The gas composition was analyzed by applying a chromatography method. Results of the gas analysis, summarized for these phases, are presented in Table 5.4. In addition, the condensate of the cooling gas was collected and analyzed.

Table 5.4. Composition of the gas mixture sampled from the core layer of a particle mat during consolidation in an industrial batch press. (from Denisov et al. 1975)

Phase	Time of sampling [min]	Volumetric proportion [%]	
		water vapor	air and other gases
I, II	0 ... 3.0	0	100
III	3.0 ... 3.5	71.1	28.9
IV	4.5 ... 10	99.5	0.5

Although vapor is generated in the outer mat layers as soon as the surfaces are heated, no vapor was detected by Denisov et al. in the core layer during the first three minutes (phases I and II). The onset of phase III was defined as the time when a core temperature of 100°C was reached. The volumetric proportion of vapor in the analyzed gas, averaged over the first 30 seconds of phase III, was 71.1 %. The actual proportion of vapor inside the mat must be higher during this period, as some of the vapor was reported to condense after leaving the mat. Finally, almost all air inside the mat was displaced by vapor (phase IV). Besides vapor and air, gaseous organic substances were found to exist inside the mat.

The measurements reported by Denisov et al. (1975) agree well with the simulation results presented in this work. The curve denoting the core vapor pressure in Figure 5.4 shows no noticeable increase during the first 200 seconds. After 465 seconds, that is when the core temperature has reached 100°C in this example, the volumetric proportion of vapor has risen to 74 % in the core. Towards the end of the simulated period (i.e., after 630 seconds) all air inside the mat has been displaced by vapor.

Somewhat different conclusions can be drawn from both the temperature and gas pressure measurements as well as the simulation results presented in this work for the continuous press. Measurement and prediction suggest that it is entirely possible that a considerable quantity of air may still exist in the core of the mat at the end of a typical industrial pressing cycle.

Trial 3 of the temperature and gas pressure measurements done in the continuous press (Appendix C) will be used here to prove evidence of air inside the mat during the last stage of the pressing cycle. The thermocouple was attached to the tip of the gas pressure probe so that core temperature and gas pressure were measured at exactly the same position. Core temperature and absolute gas pressure reached 114°C and 230 kPa, respectively, immediately before the mat left the press (Figure 5.25a).

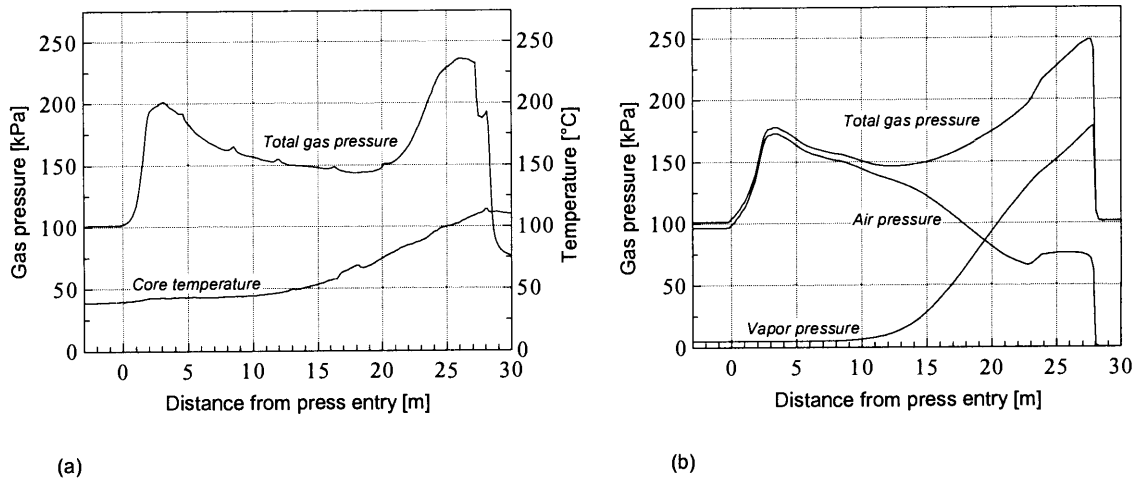


Figure 5.25. (a) Gas pressure and temperature measured in the central plane 900 mm from the edge (Continuous press trial 3). (b) Predicted total gas pressure, vapor pressure and air pressure in the middle of the central plane of the mat.

The water vapor saturation pressure at 114°C is 164 kPa. Thus, the vapor pressure cannot go beyond this value and must be lower if the vapor is not to saturate. Even when considering possible inaccuracies in the gas pressure readings, the measured gas pressure clearly exceeded the water vapor saturation pressure. The difference between measured gas pressure and actual vapor pressure must be mainly due to air. Evidently, not all air inside the mat has been displaced by vapor at the end of the pressing cycle.

Model predictions for the continuous press simulation run specified in section 5.3.1 support this finding. The predicted air pressure shown in Figure 5.25b amounts to 75 kPa before the mat leaves the press.

It is clear from thermodynamic reasoning that at least some air is present in a mat's region as long as its local temperature is below 100°C. Only after 100°C has been passed in the core of the mat, the vapor pressure in the inner region may finally exceed atmospheric pressure, and the remaining air is driven out of the core through the edges. The rapidity by which air is replaced by vapor can be expected to depend, beside others, on the size of the mat. To test this hypothesis, an additional simulation run was executed for a 400 x 400 mm<sup>2</sup> mat under otherwise identical input conditions as stated for the batch press above. The simulation results suggest that the air pressure approaches zero soon after 100°C is reached in the core, which is much faster than it was predicted for the

larger mat (see Figure 5.4). It can be concluded from this comparison that the air is replaced by vapor more rapidly in small-size laboratory presses than in industrial presses.

The terms 'vapor pressure' and 'gas pressure' are frequently found to be used synonymously in the literature when discussing gas pressure measurements. This is incorrect as long as air is still present in the mat, and may lead to wrong conclusions.

### **5.4.3 Cross-sectional gas pressure distribution**

Two alternative approaches to compute the cross-sectional convective gas flow have been described in section 3.4.5.2 and implemented within the simulation program. In both approaches total cross-sectional pressure differences are the driving force for gas convection from the surfaces toward the central plane of the mat.

In the first approach Darcy's law is applied with an explicit solution scheme for cross-sectional flow calculations. According to Darcy's law, the flux is proportional to the permeability of the material. When using this approach, extremely short time steps are required for computations to avoid reversals of pressure gradients. Results of a simulation run in which Darcy's law was applied for cross-sectional gas flow calculations are displayed in Figure 5.26a. The solid curve shown actually consists of ten individual lines, one for each layer, which lie on top of each other. Evidently, any total gas pressure difference between layers dissipates almost instantaneously, resulting in a uniform cross-sectional pressure distribution for the entire time simulated. It should be noted that, at the same time, steep partial pressure gradients for vapor and air between layers develop. Further test runs with the simulation program showed similar predictions for the entire range of pressing conditions relevant for MDF manufacture.

Following these arguments, the second approach is based on the assumption that any cross-sectional total gas pressure gradient dissipates during the short period of one time step. Instead of applying Darcy's law, a routine was implemented that directly equalizes the total gas pressure throughout the cross-section for each horizontal position. Figure 5.26b shows model predictions from a simulation run in which the second approach was used for cross-sectional flow calculations. Evidently, both approaches result in identical predictions of vapor, air (not displayed) and total gas pressure.

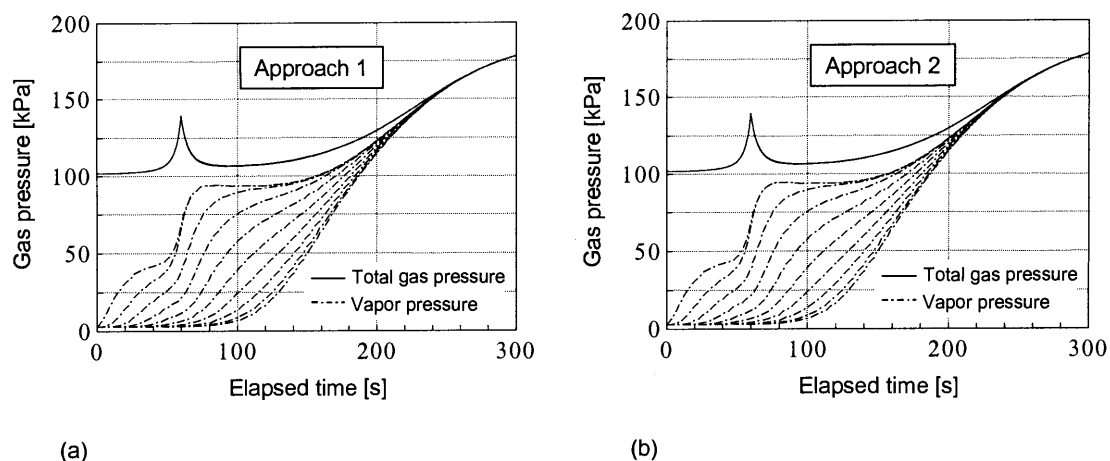


Figure 5.26. Comparison of gas pressure predictions. Displayed are results of runs executed with two different approaches for cross-sectional flow calculations. (a) Darcy's law. (b) Assumption of instantaneous cross-sectional gas pressure equalization. Platen temperature = 180°C, initial moisture content = 10 %, density = 600 kg/m<sup>3</sup>, panel thickness = 20 mm, material = MDF.

To further support the hypothesis of instantaneous cross-sectional pressure equalization, the results of the gas pressure measurements described in Appendix B are summarized in Figure 5.27. Displayed are readings recorded in the middle of the mat at the core position and the position half way between surface and core. No significant differences between the gas pressures measured at the two positions were found for the first half of the pressing cycle; this was the case for all four trial measurements. Deviations during the later stage of the pressing cycle are likely to be caused by experimental errors; this can be concluded from the fact that the curves for the core position twice exceeded and twice fall below the curves for the intermediate position.

The results agree with the model predictions (Figure 5.26a) and suggest that no significant cross-sectional gas pressure gradients prevail during pressing. In contrast to these findings are measurements reported by Kamke and Casey (1988a) and Bolton et al. (1989a). Both groups found deviations of the gas pressure measured in the core layer and an intermediate layer during the first approximately two minutes after press closure. The exact reasons for this discrepancy are not clear. The fact that the reported experiments were done on particleboard while our own measurements and predictions were made for

MDF is unlikely to explain the differences, since the flow resistance is typically lower in particleboard mats than in MDF mats.

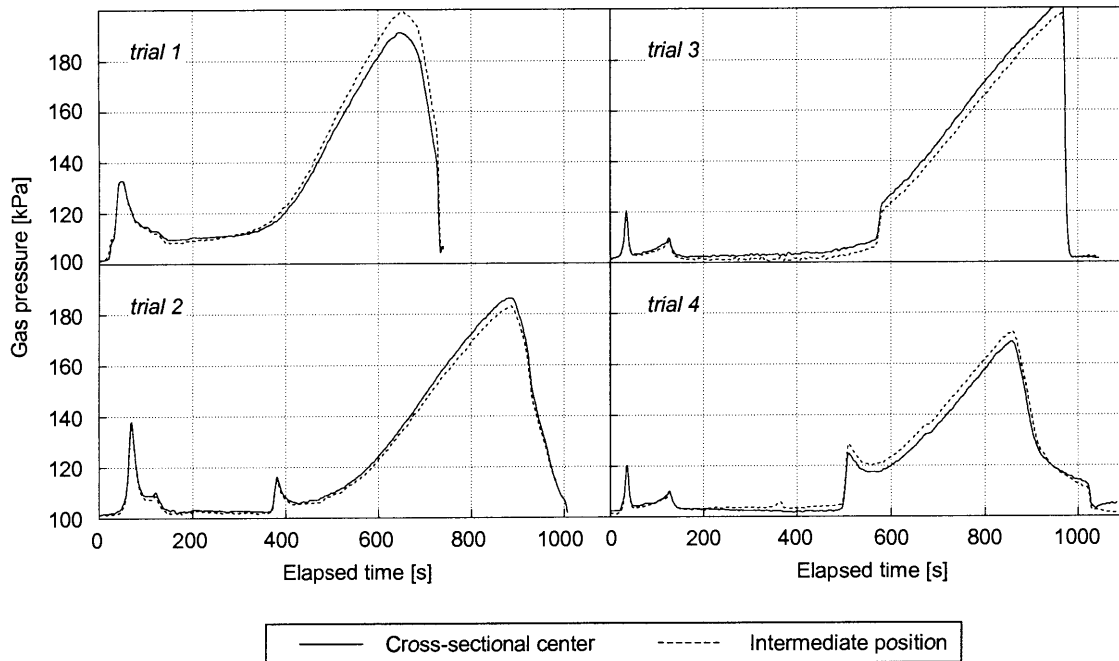


Figure 5.27. Measured gas pressure development in the horizontal middle of an MDF mat at two cross-sectional positions. (Batch press trials 1 to 4)

Our own measurements and predictions indicate that vapor translation from the surfaces towards the central plane is not restrained by the flow resistance. Evidently, the limiting factor for vertical gas flow in a hot press is not the cross-sectional permeability, as one might initially expect, but the amount of vapor that is generated, and consequently the conductive heat flow towards the regions of vapor generation and the availability of water in these regions. It is believed that gas flow from the surfaces towards the core of the fiber mat would not be accelerated significantly, even if the cross-sectional permeability approaches infinity, and that an increase in cross-sectional permeability will therefore not improve the rate of convective heat transfer towards the central plane of the mat.

It has to be emphasized that these conclusions were drawn from measurements and predictions made for fiber mats. The statement that the cross-sectional flow resistance does hardly affect the gas flow may not be valid for other wood composite

materials with considerably lower permeabilities. In particular, layered composites such as plywood with continuous sheets and glue-lines acting as barrier against gaseous flow can be expected to build up significant gas pressure differences between surface and core layer (see, for example, Zavala and Humphrey 1996).

While the rate of gas and heat convection from the surfaces towards the core is believed to be practically independent of the cross-sectional permeability, gas flow within the *horizontal* plane is clearly dictated by the flow resistance of the mat. The in-plane permeability significantly influences the build-up of vapor pressure in the mat, and consequently the development of internal mat conditions. An example of the effect of in-plane permeability on the temperature in different layers was given in Figure 5.16.



## 6. CONCLUSIONS AND OUTLOOK

The main objective of this research was to develop a model of the hot pressing process of wood-based composites, and to implement the model into a simulation program. The work presented here takes as a starting point a model developed by Humphrey (1982), which accounts for thermal conduction, vapor generation and vapor flow. Important features added in the present model are air as a component of the within-void gas mixture, molecular diffusion of vapor and air, and a structural model to predict the cross-sectional density profile. A three-dimensional grid in the Cartesian coordinate system is used instead of a circular one. This reflects the true shape of the wood-furnish mat, and thus allows account to be taken of non-isotropies of the mat in the three principle directions. Further, and most important, reflecting today's quantitative and economical importance of the continuous pressing technology, a strategy has been developed and implemented to simulate continuously working presses.

A small selection of phenomena important during hot pressing has been addressed by means of model predictions and experimental findings. Some of the more unexpected results are:

- Conductive heat transfer plays a major role not only between the surface and the progressing vapor front, but also in the inner mat regions during the first half of a typical pressing cycle.
- In large-size presses air may contribute considerably to the total gas pressure throughout the entire pressing cycle.
- Vapor flow and convective heat transfer from the surfaces towards the central plane in an MDF mat is not significantly affected by the cross-sectional permeability.

The present research was part of a larger project that included the determination of wood-furnish material properties. This circumstance permitted a quantitative comparison of model predictions with measurements that were made on mats for which the material properties were largely known. Although not all mechanisms that are important during hot pressing are considered in the present approach, the modeling

results are encouraging; they correspond well both qualitatively and quantitatively with experimental results. The ability of the model to represent the real world process not only in trend, but also in magnitude, is an important prerequisite to employ the model for a wide variety of applications in research and industry. Examples of such applications are:

- Further research those interacting mechanisms that were difficult, so far, to comprehend solely from experimental findings.
- Develop strategies to specifically manipulate the cross-sectional density profile of wood-based composites.
- Explore innovative technologies.
- Assist the design of pressing systems or components.
- Optimize individual production lines in wood-based composite manufacture.
- Visualize important physical aspects of the process for training purposes.

The modeling work has reached a stage where basically all of the applications listed above could be tackled without requiring major changes in the simulation program. However, the present model may be only an intermediate step in the evolution of more sophisticated hot pressing models. For the time being, future research should include both the refinement of the existing model to further improve the accuracy of predictions, as well as the expansion of the model to simulate additional features of existing and new processes. Work appears to be needed in the following areas:

- Some of the material properties used in the present approach are only known for solid wood (e.g., hygroscopicity). Sensitivity studies may be carried out to quantify the effect of differences between solid wood and composite mats on model predictions. If necessary, those material property data used so far should be substituted with improved data.
- Within-particle moisture gradients and the possible presence of free water are not accounted for in the model. Neglecting these effects may lead to unrealistic predictions, particularly when moving on to simulate wood-furnish materials with larger wood constituents such as OSB. Experimental studies

and possibly a revision of the numerical approach appear to be necessary to incorporate moisture gradients and free water within the model.

- Research about the kinetics of adhesive polymerization and associated bond-strength development is on its way. Considering adhesive cure in the model may improve the accuracy of cross-sectional density profile predictions. Perhaps even more important, accounting for adhesion will provide a basis upon which to simulate the development of mechanical panel properties, and to assess the minimum pressing time required to avoid panel failure upon press opening.

The computational power will certainly further increase during the coming years, and this will reduce the execution time of simulation runs and/or improve the spatial resolution of the computations. Although the accuracy of model predictions is most important, factors such as execution time and user-friendliness of the program will clearly have a significant impact on the acceptance and usage of hot pressing simulation models in the future.

**BIBLIOGRAPHY**

- Avramidis, S., and P. Lau. 1992. Thermal coefficients of wood particles by a transient heat-flow method. *Holzforschung* 46(5): 449-453.
- Avramidis, S., and J.F. Siau. 1987. An investigation of the external and internal resistance to moisture diffusion in wood. *Wood Sci. Technol.* 21: 249-256.
- Bodig, J., and B.A. Jayne. 1982. *Mechanics of wood and wood composites*. Van Nostrand Reinhold Company, New York. 712 pp.
- Boehme, C. 1991. Rohdichteprofil und Dickenquellung von Spanplatten. *Holz-Zentralblatt* 125: p. 1984.
- Boehme, C. 1992. Die Bedeutung des Rohdichteprofiles für MDF. *Holz als Roh- und Werkstoff* 50: 18-24.
- Boehme, C. 1994. Wasserdampf-Diffusionswiderstandszahlen von dünnen und dicken Spanplatten, senkrecht, schichtweise und parallel zur Plattenoberfläche ermittelt. WKI Short Report No. 10, Braunschweig, Germany.
- Bolton, A.J., and P.E. Humphrey. 1988. The hot pressing of dry-formed wood-based composites. Part I. A review of the literature, identifying the primary physical processes and the nature of their interaction. *Holzforschung* 42: 403-406.
- Bolton, A.J., and P.E. Humphrey. 1994. The permeability of wood-based composite materials. Part I. A review of the literature and some unpublished work. *Holzforschung* 48 (Suppl.): 95-100.
- Bolton, A.J., P.E. Humphrey, and P.K. Kavvouras. 1989a. The hot pressing of dry-formed wood-based composites. Part III. Predicted vapour pressure and temperature variation with time compared with experimental data for laboratory boards. *Holzforschung* 43(4): 265-274.
- Bolton, A.J., P.E. Humphrey, and P.K. Kavvouras. 1989b. The hot pressing of dry-formed wood-based composites. Part IV. Predicted variation of mattress moisture content with time. *Holzforschung* 43(5): 345-349.
- Bowen, M.E. 1970. Heat transfer in particleboard during pressing. Ph.D. Thesis, Colorado State Univ., U.S.A.
- Bramhall, G. 1979. Mathematical model for lumber drying. Part 1. Principles involved. *Wood Sci.* 12(1): 22-28.
- Cai, L., and F. Wang. 1994. Steady and unsteady state moisture movement in particleboards. *Holz als Roh- und Werkstoff* 52: 304-306.

- Cammerer, J.S. 1956. Bezeichnungen und Berechnungsverfahren für Diffusionsvorgänge im Bauwesen. *Kältetechnik* 8: 339-343. (in Niemz 1993).
- Cammerer, W.F. 1970. Wärmeleitfähigkeit und Diffusionswiderstand von Holzwerkstoffen. *Holz als Roh- und Werkstoff* 28(11): 420-423.
- Christensen, G.N., and K.E. Kelsey. 1959. Die Geschwindigkeit der Wasserdampfsorption durch Holz. *Holz als Roh- und Werkstoff* 17(5): 178-188.
- Crank, J. 1975. *The mathematics of diffusion*. 2nd ed. Clarendon Press, Oxford. 414 pp.
- Cunningham, R.E., and R.J.J. Williams. 1980. *Diffusion in gases and porous media*. Plenum Press, New York. 275 pp.
- Cussler, E.L. 1984. *Diffusion. Mass transfer in fluid systems*. Cambridge Univ. Press. 525 pp.
- Dai, C., and P.R. Steiner. 1993. Compression behavior of randomly formed wood flake mats. *Wood and Fiber Sci.* 25(4): 349-358.
- Denisov, O.B. 1973. Überwachung des Preßvorgangs bei der Spanplattenherstellung. *Holztechnologie* 14(1): 43-46.
- Denisov, O.B., P.P. Anisov, and P.E. Zuban. 1975. Untersuchung der Permeabilität von Spanvliesen. *Holztechnologie* 16(1): 10-14.
- Denisov, O.B., and M.S. Sosnin. 1967. [Besonderheiten der Veränderung von Temperatur und Dampfdruck in großformatigen Holzspanplatten während der Pressung.] *Derev. Prom.* 16(8): p. 11. (in Russian).
- Denisov, O.B., and V.V. Juskov. 1974. Die Berechnung der Preßzeit bei der Herstellung von Spanplatten aus Holz. *Holztechnologie* 15(3): 168-172.
- Deppe, H.-J., and K. Ernst. 1964. *Technologie der Spanplatten: ein Ratgeber für die Praxis*. Holz-Zentralblatt Verl.-Ges., Stuttgart. 283 pp.
- Deppe, H.-J., and K. Ernst. 1996. *MDF - Mitteldichte Faserplatte*. DRW-Verlag, Leinfelden-Echterdingen. 200 pp.
- DIN Deutsches Institut für Normung e.V. 1987. *Bestimmung der Wasserdampfdurchlässigkeit von Bau- und Dämmstoffen*. DIN 52615.
- Engelhardt, F. 1979. Untersuchungen über die Wasserdampfsorption durch Buchenholz im Temperaturbereich von 110°C bis 170°C. *Holz als Roh- und Werkstoff* 37: 99-112.
- Fahrni, F. 1956. Das Verpressen von Spanplatten bei gefeuchteten oder feuchteren Deckspänen. *Holz als Roh- und Werkstoff* 14(1): 8-10.

- F.A.O. Food and Agriculture Organization of the United Nations. 2000. "FAOSTAT Forestry Data", wood-based panels. Web-based database. Last updated 20th January 2000.
- Flowers, B.H., and E. Mendoza. 1970. Properties of matter. John Wiley & Son, London. (in Humphrey and Bolton 1989a).
- Frühwald, A., A. Steffen, P.E. Humphrey, G. von Haas, and H. Thömen. 1999. Entwicklung und Überprüfung eines Modells des thermodynamischen und des rheologischen Verhaltens von Fasermatten für MDF während der Heißpressung in Taktpressen und Ansätze zur Modellierung von Endlospressen. Final report submitted to the AIF, project no. 10359 N. Ordinariat für Holztechnologie, Univ. Hamburg, Germany. 214 pp.
- Fuller, E.N., J.C. Giddings, and P.D. Schettler. 1966. A new method for prediction of binary gas-phase diffusion coefficient. *Jour. of Industrial and Engineering Chemistry* 58(5): 19-27.
- Gefahrt, J. 1977. Zur Spänevorwärmung mit Hochfrequenzenergie - Modell zur Berechnung des Temperaturverlaufes in Vliesmitte bei der Heißpressung. *Holz als Roh- und Werkstoff* 35: 183-188.
- Goring, D.A.I. 1963. Thermal softening of lignin, hemicellulose and cellulose. *Pulp and Paper Magazine of Canada* 64(12): T517-T527.
- Graser, M. 1962. Temperaturverlauf in industriell gefertigten Spanplatten. *Holz-Zentralblatt* 137.
- Grumach, M. 1951. The equilibrium moisture content of wood in superheated steam. C.S.I.R.O., Division of Forest Products, Int. Rep. Proj. p. 17.
- von Haas, G. 1998. Untersuchungen zur Heißpressung von Holzwerkstoffmatten unter besonderer Berücksichtigung des Verdichtungsverhaltens, der Permeabilität, der Temperaturleitfähigkeit und der Sorptionsgeschwindigkeit. Dissertation, Univ. Hamburg, Germany. 264 pp.
- von Haas, G., A. Steffen, and A. Frühwald. 1998. Untersuchungen zur Permeabilität von Faser-, Span- und OSB-Matten für Gase. *Holz als Roh- und Werkstoff* 56(6): 386-392.
- Hailwood, A.J., and S. Horrobin. 1946. Absorption of water by polymers: analysis in terms of a simple model. *Trans. Faraday Soc.* 42B: 84-92.
- Hann, R.A. 1965. An investigation of the drying of wood at temperatures above 100 degrees centigrade. Ph.D. Thesis, North Carolina State Univ., U.S.A.
- Hänsel, A., and G. Kühne. 1988. Untersuchungen zur Mechanik der Spanplatte. *Holzforschung und -verwertung* 40(1): 1-5.

- Harless, T.E.G., F.G. Wagner, P.H. Short, R.D. Seale, P.H. Mitchell, and D.S. Ladd. 1987. A model to predict the density profile of particleboard. *Wood and Fiber Sci.* 19(1): 81-92.
- Haselein, C.R. 1998. Numerical simulation of pressing wood-fiber composites. Ph.D. Thesis, Oregon State Univ., U.S.A. 244 pp.
- Hata, T., S. Kawai, and H. Sasaki. 1990. Production of particleboard with steam-injection. Part II. Computer simulation of temperature behavior in particle mat during hotpressing and steam-injection pressing. *Wood Sci. Technol.* 24: 65-78.
- Hata, T., S. Kawai, T. Ebihara, and H. Sasaki. 1993. Production of particleboards with a steam-injection press. Part V. Effects of particle geometry on temperature behaviors in particle mats and on air permeabilities of boards. *Mokuzai Gakkaishi* 39(2): 161-168.
- van der Held, E.V.M., and F.G. van Drunen. 1949. A method of measuring the thermal conductivity of liquids. *Physica* 15: 865-881. (in Avramidis and Lau 1992).
- Heller, W. 1995. *Die Spanplatten-Fibel*. Hameln. 366 pp.
- Holman, J.P. 1980. *Thermodynamics*. 3rd ed. McGraw-Hill, Inc., New York. 770 pp.
- Horn, J. 1969. Untersuchungen über die Wasserdampfdiffusion durch Holzspanplatten in Abhängigkeit von einigen technologischen und klimatischen Einflußfaktoren. Dissertation, Univ. Hamburg, Germany. 147 pp.
- Hubert, P., and C. Dai. 1998. An object-oriented finite element processing model for oriented strand board wood composites. Proc. of the 13th Int. Conf. on Composite Materials, Paris, France.
- Humphrey, P.E. 1982. Physical aspects of wood particleboard manufacture. Ph.D. Thesis, Univ. of Wales, U.K.
- Humphrey, P.E. 1991. Pressing issues in panel manufacture: Internal behavior during pressing and its impact on time minimization, properties and profit. Proc. of the 25th Particleboard and Composite Materials Symp., Washington State Univ., Pullman, U.S.A. 99-108.
- Humphrey, P.E. 1994. Engineering composites from oriented natural fibres: A strategy. Proc. of the 2nd Pacific Rim Bio-Based Composites Symp., Vancouver, Canada. 2-8.
- Humphrey, P.E., and A.J. Bolton. 1989a. The hot pressing of dry-formed wood-based composites. Part II. A simulation model for heat and moisture transfer. *Holzforschung* 43(3): 199-206.

- Humphrey, P.E., and A.J. Bolton. 1989b. The hot pressing of dry-formed wood-based composites. Part V. The effect of board size: comparability of laboratory and industrial pressing. *Holzforschung* 43(6): 401-405.
- Jones, R.L. 1963. The effect of fiber structural properties on compression response of fiber beds. *Tappi* 46(1): 20-27.
- Kamke, F.A., and L.J. Casey. 1988a. Gas pressure and temperature in the mat during flakeboard manufacture. *Forest Prod. J.* 38(3): 41-43.
- Kamke, F.A., and L.J. Casey. 1988b. Fundamentals of flakeboard manufacture: internal mat conditions. *Forest Prod. J.* 38(6): 38-44.
- Kamke, F.A., and M.P. Wolcott. 1991. Fundamentals of flakeboard manufacture: wood-moisture relationships. *Wood Sci. Technol.* 25: 57-71.
- Kauman, W.G. 1956. Equilibrium moisture content relations and drying control in superheated steam drying. *Forest Prod. J.* 6(9): 328-332.
- Kavvouras, P.K. 1977. Fundamental process variables in particleboard manufacture. Ph.D. Thesis, Univ. of Wales, U.K. 156 pp.
- Kayihan, F., and J.A. Johnson. 1983. Heat and moisture movement in wood composite materials during the pressing operation - a simplified model. *Numerical Methods in Heat Transfer* 2: 511-531.
- Kehr, E., and S. Schölzel. 1965. Untersuchungen über das Preß-Diagramm zur Herstellung von Spanplatten. *Drevarsky Vyskum* 10(3): 133-147.
- Kelsey, K.E. 1957. The sorption of water vapour by wood. *Australian Jour. of Applied Sci.* 8: 42-54.
- Kelsey, K.E., and L.N. Clarke. 1956. The heat of sorption of water by wood. *Australian Jour. of Applied Sci.* 7(2): 160-175.
- Keylwerth, R. 1949. Grundlagen der Hochtemperaturtrocknung des Holzes. *Holz-Zentralblatt* 75: 953-954.
- Keylwerth, R. 1958. Zur Mechanik der mehrschichtigen Spanplatte. *Holz als Roh- und Werkstoff* 16(11): 419-430.
- Keylwerth, R. 1969. Praktische Untersuchungen zum Holzfeuchtigkeits-Gleichgewicht. *Holz als Roh- und Werkstoff* 27(8): 285-290.
- Kollmann, F. 1951. *Technologie des Holzes und der Holzwerkstoffe. Erster Band.* 2nd ed. Springer-Verlag, Berlin. 1050 pp.



- Kollmann, F. 1955. Technologie des Holzes und der Holzwerkstoffe. Springer-Verlag, Berlin. (in von Haas 1998).
- Kollmann, F. 1957. Über den Einfluß von Feuchtigkeitsunterschieden im Spangut vor dem Verpressen auf die Eigenschaften von Holzspanplatten. Holz als Roh- und Werkstoff 15(1): 35-44.
- Kollmann, F. 1959. Über die Sorption von Holz und ihre exakte Bestimmung. Holz als Roh- und Werkstoff 17(5): 165-171.
- Kollmann, F. 1961. Rheologie und Strukturfestigkeit von Holz. Holz als Roh- und Werkstoff 19(3): 73-80.
- Kollmann, F., and L. Malmquist. 1952. Untersuchungen über die Trocknung von Kiefernholz mit erhöhten Temperaturen. Svenska Traforsk., Tratekn. Avd. 23.
- Koponen, H. 1984. Dependences of moisture diffusion coefficients of wood and wooden panels on moisture content and wood properties. Paperi ja Puu - Papper och Tra 12: 740-745.
- Krischer, O. 1963. Die wissenschaftlichen Grundlagen der Trocknungstechnik. 2nd ed. Springer-Verlag, Berlin. 491 pp.
- Küch, W. 1943. Der Einfluß des Feuchtigkeitsgehaltes auf die Festigkeit von Voll- und Schichtholz. Holz als Roh- und Werkstoff 6(5): 157-161.
- Kühlmann, G. 1962. Untersuchungen der thermischen Eigenschaften von Holz und Spanplatten in Abhängigkeit von Feuchtigkeit und Temperatur im hygroskopischen Bereich. Holz als Roh- und Werkstoff 20: 259-270.
- Kull, W. 1954. Die Erwärmung von parallelfächigen Stoffen zwischen Heizplatten und die Bestimmung der Heizzeit bei der Holzverleimung, insbesondere bei der Spanplattenherstellung. Holz als Roh- und Werkstoff 12(11): 413-418.
- Kull, W. 1963. Die Dichte von Holz und Holzwerkstoffen. Holz-Zentralblatt 89: 125-131.
- Kunesh, R.H. 1961. The inelastic behavior of wood: A new concept for improved panel forming processes. Forest Prod. J. 11(9): 395-406.
- Lang, E.M., and M.P. Wolcott. 1996. A model for viscoelastic consolidation of wood-strand mats. Part II. Static stress-strain behavior of the mat. Wood and Fiber Sci. 28(3): 369-379.
- Lehmann, W.F. 1972. Moisture-stability relationships in wood-base composition boards. Forest Prod. J. 22(7): 53-59.

- Lenth, C.A., and F.A. Kamke. 1996. Investigations of flakeboard mat consolidation. Part II. Modeling mat consolidation using theories of cellular materials. *Wood and Fiber Sci.* 28(3): 309-319.
- León-Méndez, R., and H. Thömen. 1996. Untersuchungen zur Optimierung eines Prozeßleitsystems in einem Spanplattenwerk. Diplomarbeit, Univ. Hamburg, Germany. 240 pp.
- Liiri, O. 1969. Der Preßdruck bei der Spanplattenherstellung. *Holz als Roh- und Werkstoff* 27(10): 371-378.
- Lindsay, J.D. 1989. The physics of impulse drying: New insights from numerical modeling. IPC Technical Paper Series No. 330, Appleton, Wis., U.S.A. 51 pp.
- Lobenhoffer, H. 1990. Qualitätsbedingte Regelung eines Spanplattenformstrangs. Dissertation, Georg-August-Univ. Göttingen, Germany.
- Luikov, A.V. 1975. Systems of differential equations of heat and mass transfer in capillary porous bodies. *Int. Jour. of Heat and Mass Transfer* 18: 1-14.
- Lutz, J.F. 1974. Drying veneer to a controlled final moisture content by hot pressing and steaming. USDA For. Serv. Res. Pap. FPL 227, Forest Prod. Lab., Madison, Wis., U.S.A.
- Maku, T. 1954. Studies on the heat conduction in wood. *Wood Res. Bulletin*, Kyoto Univ., Japan, 13: 1-80. (in von Haas 1998).
- Maku, T., and R. Hamada. 1955. Studies on the chipboard. Part I. Mechanical properties. *Wood Research* 15: 38-52.
- Maku, T., R., Sasaki, and H. Hamada. 1959. Studies on the particle board. Report IV. Temperature and moisture distribution in particle board during hot-pressing. *Wood Research* 21: 34-46.
- Marrero, T.R., and E.A. Mason. 1972. Gaseous diffusion coefficients. Reprint No. 1 from *Journal of Physical and Chemical Reference Data* 1(1). 118 pp.
- May, H.-A. 1970. Einflüsse der Pressenregelung auf Wirtschaftlichkeit und Qualität der Spanplattenherstellung. *Holz als Roh- und Werkstoff* 28(10): 391-396.
- May, H.-A. 1977. Zur Mechanik der Holzspanplatten unter besonderer Berücksichtigung der Rohdichte-Differenzierung und Rohstoffzusammensetzung. *Holz als Roh- und Werkstoff* 35: 385-387.
- May, H.-A. 1983. Zusammenhänge zwischen Eigenschaften, Rohstoffkomponenten und dem Dichteprofil von Spanplatten. Teil 5. Einflüsse der Dichteprofile und Rohstoffe auf Biege-E-Modul und Biegefestigkeit. *Holz als Roh- und Werkstoff* 41: 271-275.

- May, H.-A. 1985. Untersuchungen über den Einfluß der alkalischen Bestandteile phenolharzverleimter Spanplatten auf Hygroskopizität und mechanisch-technologische Eigenschaften des Werkstoffes. Teil 1. Zusammenhänge zwischen mechanisch-technologischen Eigenschaften und dem Alkaligehalt. *Adhäsion* 9: 12-15.
- May, H.-A., and L. Mehlhorn. 1969. Verbesserung der Preßbedingungen durch die Anwendung von Regelsystemen anstelle von Programmsteuerungen. *Holz-Zentralblatt* 86: 1342-1348.
- Meyer, W., and U. Reinhardt. 1976. Beitrag zur Konstantenermittlung für den Temperaturverlauf im Spänevlies während des Preßvorganges. Abschlußarbeit an der Fachhochschule Rosenheim. Abschlußarbeit, Fachhochschule Rosenheim, Germany. (in Gefahrt 1977).
- Munson, B.R., D.F. Young, and T.H. Okiishi. 1990. *Fundamentals of fluid mechanics*. Wiley, New York. 843 pp.
- Nasrallah, S.B., and P. Perre. 1988. Detailed study of a model of heat and mass transfer during convective drying of porous media. *Int. J. Heat Mass Transfer* 31(5): 957-967.
- Niemz, P. 1993. *Physik des Holzes und der Holzwerkstoffe*. DRW-Verlag, Leinfelden-Echterdingen. 243 pp.
- Nketiah, K.D. 1982. Within board variation of particleboard permeability. M.Sc. Thesis, Univ. of Wales, U.K.
- Noack, D. 1959. Beitrag zur Sorption des Holzes im Bereich höherer Temperaturen und Wasserdampfdrücke. *Holz als Roh- und Werkstoff* 17(5): 205-212.
- Oblivin, A., and A. Dolgintsev. 1976. [Permeability of chip mat.] *Lesnoi Zhurnal* 19(2): 77-81. (in Russian).
- Ozisik, M.N. 1993. *Heat conduction*. 2nd ed. John Wiley & Son, New York. 692 pp.
- Patankar, S.V. 1980. *Numerical heat transfer and fluid flow*. McGraw-Hill, Inc., New York. 197 pp.
- Pierce, C.B., and J.M. Dinwoodie. 1977. Creep in chipboard. Part I. Fitting 3- and 4-element response curves to creep data. *Jour. of Material Sci.* 12: 1955-1960.
- Plath, E. 1971. Beitrag zur Mechanik der Holzspanplatten. *Holz als Roh- und Werkstoff* 29(10): 377-382.
- Plath, E., and E. Schnitzler. 1974. Das Rohdichteprofil als Beurteilungsmerkmal von Spanplatten. *Holz als Roh- und Werkstoff* 32: 443-449.

- Rackwitz, G. 1954. Ein Beitrag zur Kenntnis der Vorgänge bei der Verleimung von Holzspänen zu Holzspanplatten in beheizten hydraulischen Pressen. Dissertation, Technische Hochschule Braunschweig, Germany.
- Rackowski, J. 1969. Der Einfluß von Feuchtigkeitsänderungen auf das Kriechverhalten des Holzes. *Holz als Roh- und Werkstoff* 27(6): 232-237.
- Rajman, V., J. Jahic, and I. Horman. 1992. [Heat and moisture content transfer in the mat during particleboard pressing.] *Drvna ind.* 43(1): 7-12. (in Serbo-Croat).
- Rauch, W. 1984. Temperature- und Dampfdruckverlauf bei der Herstellung von Spanplatten und ihr Einfluß auf die technologischen Eigenschaften. *Holz als Roh- und Werkstoff* 42: 281-286.
- Ren, S. 1991. Thermo-hygro rheological behavior of materials used in the manufacture of wood-based composites. Ph.D. Thesis, Oregon State Univ., U.S.A. 226 pp.
- Resch, H., M.L. Hoag, and H.N. Rosen. 1988. Desorption of yellow-poplar in superheated steam. *Forest Prod. J.* 38(3): 13-18.
- Ritter, C., W. Landmesser, P. Niemz, and A. Hänsel. 1990. Vergleichende Untersuchungen zur Anwendbarkeit verschiedener Methoden für die Modellierung der Spanplattenfertigung. *Holztechnologie* 30(1): 23-25.
- Roffael, E., and A. Schneider. 1978. Zum Sorptionsverhalten von Holzspanplatten. Teil 1. Einfluß des Bindemitteltyps und des Bindemittelaufwands auf die Gleichgewichtsfeuchtigkeit. *Holz als Roh- und Werkstoff* 36: 393-396.
- Roffael, E., and A. Schneider. 1979. Zum Sorptionsverhalten von Holzspanplatten. Teil 2. Einfluß der Holzart auf die Gleichgewichtsfeuchtigkeit. *Holz als Roh- und Werkstoff* 37: 259-264.
- Roffael, E., and A. Schneider. 1980. Zum Sorptionsverhalten von Holzspanplatten. Teil 3. Untersuchungen an mit Phenolformaldehydharzen gebundenen Spanplatten. *Holz als Roh- und Werkstoff* 38: 151-155.
- Roffael, E., and A. Schneider. 1981. Zum Sorptionsverhalten von Holzspanplatten. Teil 4. Einfluß von Zusatzstoffen auf die Gleichgewichtsfeuchtigkeit. *Holz als Roh- und Werkstoff* 39: 17-23.
- Schulte, M., and A. Frühwald. 1996. Some investigations concerning density profile, internal bond and relating failure position of particleboard. *Holz als Roh- und Werkstoff* 54: 289-294.
- Schweitzer, F. 1992. Modellierung des Heißpreßvorgangs zur Herstellung von Spanplatten in diskontinuierlich arbeitenden Pressen. Dissertation, Technische Univ. Dresden, Germany.

- Schweitzer, F., and P. Niemz. 1991. Untersuchungen zum Einfluß ausgewählter Strukturparameter auf die Porosität von Spanplatten. *Holz als Roh- und Werkstoff* 49: 27-29.
- Sekino, N., and M.A. Irlé. 1996. Particleboard hygroscopicity: Its prediction and the influence of hot-pressing. *Mokuzari Gakkaishi* 42(1): 43-50.
- Shao, M. 1989. Thermal properties of wood fiber networks. M.S. Thesis, Oregon State Univ., U.S.A. 95 pp.
- Siau, J.F. 1984. Transport processes in wood. Springer-Verlag, Berlin. 245 pp.
- Simpson, W.T. 1973. Predicting equilibrium moisture content of wood by mathematical models. *Wood Fiber Sci.* 5(1): 41-49.
- Simpson, W.T., and H.N. Rosen. 1981. Equilibrium moisture content of wood at high temperatures. *Wood and Fiber Sci.* 13(3): 150-158.
- Sitkei, G. 1994. Die Pressung von Staub und Spänen. Unpublished summary of a research project carried out at Sopron Univ., Hungary. 10 pp.
- Skaar, C. 1972. Water in wood. Syracuse Univ. Press, New York. 218 pp.
- Smith, D.C. 1982. Waferboard press closing strategies. *Forest Prod. J.* 32(3): 40-45.
- Sokunbi, O.K. 1978. Aspects of particleboard permeability. M.Sc. Thesis, Univ. of Wales, U.K.
- Stamm, A.J., and W.K. Loughborough. 1935. Thermodynamics of the swelling of wood. *Jour. Phys. Chem.* 39: 121-132.
- Stamm, A.J., and M. Wilkonson. 1965. Effect of structure upon drying of insulating board. *Tappi* 48(10): 578-583.
- Steffen, A., G. von Haas, A. Rapp, P.E. Humphrey, and H. Thömen. 1999. Temperature and gas pressure in MDF-mats during industrial continuous hot pressing. *Holz als Roh- und Werkstoff* 57: 154-155.
- Strickler, M.D. 1959. Effect of press cycles and moisture content on properties of douglas-fir flakeboard. *Forest Prod. J.* 9(7): 203-215.
- Strickler, M.D. 1968. High temperature moisture relations of grand fir. *Forest Prod. J.* 18(4): 69-75.
- Suchsland, O. 1959. An analysis of the particle board process. Quarterly bulletin, Michigan State Univ., Agricultural Experiment Station, 42: 350-372.
- Suchsland, O. 1962. The density distribution in flake boards. Quarterly bulletin, Michigan State Univ., Agricultural Experiment Station, 45: 104-121.

- Suchsland, O. 1967. Behavior of a particleboard mat during the press cycle. *Forest Prod. J.* 17(2): 51-57.
- Sunds Defibrator Industries AB, Sweden. 1997. MDF industry update '97.
- Suo, S., and J.L. Bowyer. 1994. Simulation modeling of particleboard density profile. *Wood and Fiber Sci.* 26(3): 397-411.
- Thunell, B. 1941. Über die Elastizität schwedischen Kiefernholzes. *Holz als Roh- und Werkstoff* 4(1): 15-18.
- VDI Verein Deutscher Ingenieure. 1988. VDI Wärmeatlas: Berechnungsblätter für den Wärmeübergang. 5th ed. VDI-Verlag Düsseldorf.
- Wang, S., P.M. Winistorfer, W.W. Moschler, and C. Helton. 2000. Hot-pressing of oriented strandboard by step-closure. *Forest Prod. J.* 50(3): 28-34.
- Ward, R.J., and C. Skaar. 1963. Specific heat and conductivity of particleboard as functions of temperature. *Forest Prod. J.* 13(1): 31-38.
- Weichert, L. 1963. Untersuchungen über das Sorptions- und Quellungsverhalten von Fichte, Buche und Buchen-Preßvollholz bei Temperaturen zwischen 20°C und 100°C. *Holz als Roh- und Werkstoff* 21: 290-300.
- Winistorfer, P.M., S. Wang, and W.W. Moschler. 1998. Dynamics of wood composite mats during consolidation: Monitoring density development during pressing with an in-situ density monitoring system. *Proc. of the 2nd European Panel Products Symp., Llandudno, Wales, U.K.* 12-23.
- Wolcott, M.P. 1989. Modeling viscoelastic cellular materials for the pressing of wood composites. Ph.D. Thesis, Virginia State Univ., U.S.A.
- Xu, W., and P.M. Winistorfer. 1995. Layer thickness swell and layer internal bond of medium density fiberboard and oriented strandboard. *Forest Prod. J.* 45(10): 67-71.
- Zavala, D., and P.E. Humphrey. 1996. Hot pressing veneer-based products: The interaction of physical processes. *Forest Prod. J.* 46(1): 69-77.

## APPENDICES

## INTRODUCTION TO APPENDICES A, B AND C

The series of tests to determine the obstruction factor of medium density fiberboard (MDF) as it is summarized in Appendix A is part of a larger experiment conducted at the Ordinariat für Holztechnologie (Universität Hamburg, Germany). The pilot trial measurements described in Appendices B and C were carried out jointly with the project partners Universität Hamburg and the machine-building company Siempelkamp GmbH & Co. (Krefeld, Germany). Methods and results of these measurements have been reported to the research sponsor AIF (Frühwald et al. 1999). Acknowledgement should certainly be given to Dr. A. Steffen for organizing the experiments.



## APPENDIX A

### MEASUREMENT OF THE OBSTRUCTION FACTOR FOR MOLECULAR DIFFUSION

#### MATERIAL AND METHODS

A series of tests has been carried out to determine the obstruction factor of MDF for different material densities. The obstruction factor for molecular diffusion through a porous material can be obtained by dividing the diffusion coefficient of air by the effective diffusion coefficient measured for the material. A slightly modified procedure as outlined in the German standard DIN 52615 (1987) was used. Test specimens were prepared from urea-formaldehyde bonded MDF panels (11 % resin solids based on the oven-dry fiber weight) with homogeneous cross-sectional density profiles, consolidated in a laboratory press. A detailed description of the panel making procedure is given in von Haas (1998).

Diffusive flow rates for steady-state water vapor movement perpendicular to the panel surface were determined by applying the dry-cup method. In order to ensure only one-directional flow, the edges of the round test specimens (diameter 35 mm, thickness 20 mm) were coated with epoxy. Diffusion cups, partially filled with silica gel as the desiccating absorbent, were covered by the test specimens and sealed against gas flow around the specimens. The relative humidity inside the diffusion cup was considered to be 0 %. The samples were placed in a climatic chamber at temperature 23°C and relative humidity of 50 % at atmospheric pressure. Over a period of about 100 days, the flow rates were determined by weighing the covered diffusion cups periodically on a laboratory scale to an accuracy of  $10^{-3}$  grams.

#### RESULTS

Fourteen specimens were tested in the density range between  $650 \text{ kg/m}^3$  and  $1200 \text{ kg/m}^3$ . The specimens had average moisture contents of 3 % to 5 % after equilibrium conditions had been reached. In Figure A.1 the obstruction factor versus

oven-dry density is displayed. Within the observed density range, the resistance of the material to diffusion increases towards higher densities. In order to obtain an expression for the relationship between obstruction factor and density, an exponential equation was fitted to the data points.

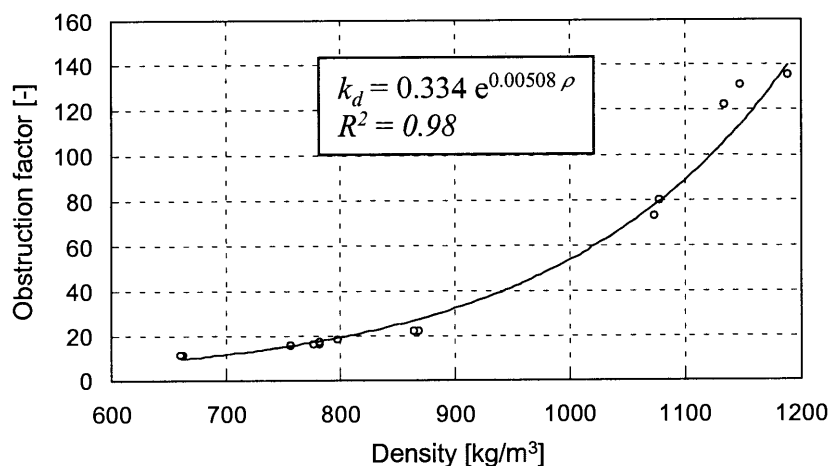


Figure A.1. Obstruction factor for molecular diffusion perpendicular to the panel surface,  $k_d$ , versus density  $\rho$  for MDF.

Molecular gas diffusion through the inter-particle void system has been assumed to be the only transfer mechanism when deriving the obstruction factor from the measured data. Indeed, following those arguments stated in section 3.2.1.2 of this dissertation, it is likely that this mechanism plays the major role in moisture transport through a wood-furnish material under isobaric conditions. However, bound-water diffusion through the cell wall material and movement of water due to capillary forces through small passageways between the wood particles may also contribute to steady-state moisture diffusion.

Cammerer (1970) therefore stated that a more accurate term would be 'apparent' obstruction factor, instead of simply obstruction factor, since the measured obstruction factor does not describe the true resistance of the porous material to pure molecular gas diffusion. For a more fundamental treatment of water transport mechanisms within wood-based composites it would be desirable to obtain separate transfer coefficients for gas diffusion, bound water diffusion and capillary moisture movement. Such an undertaking was, however, beyond the scope of this work.

## APPENDIX B

### MEASUREMENTS IN A LARGE-SIZE LABORATORY PRESS

#### MATERIAL AND METHODS

Measurements of internal temperature and gas pressure during pressing of MDF in a 4 x 8 ft. laboratory press were carried out to provide experimental data that can be used to validate the simulation model. The resinated fiber mats used for the experiments were produced in an industrial MDF plant from pine chips (8.2 bar digester pressure). A melamine supplemented urea-formaldehyde resin (UFm) was used as the adhesive. Four fiber mats were taken from the conveyor belt between pre-press and hot press and then transported within 4 hours to the laboratory to be pressed. Mat 1 was consolidated about eight hours and mats 2, 3 and 4 twenty-six to thirty hours after mat forming.

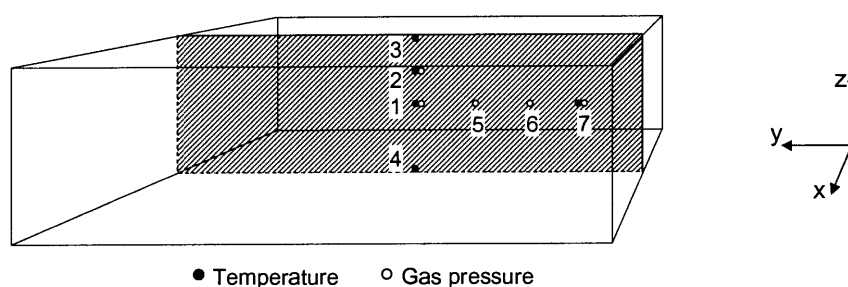


Figure B.1. Schematic of mat with positions of temperature and gas pressure probes.

The mat's dimensions were about 1350 x 2300 x 295 mm<sup>3</sup>, and moisture contents prior to pressing were measured as 9.4 % to 11.1 %. Five thermocouples and five thin stainless steel tubes (inside diameter 0.5 mm, outside diameter 1.0 mm) were inserted from the right side into the loose mat, following the scheme shown in Figure B.1. The tubes were connected to small pressure transducers. The exact positions of the measuring points were determined after pressing by dissecting the panel; they are listed, together with the measured mat dimensions, in Table B.1. About 5 minutes after press opening, 50 x 50 mm<sup>2</sup> samples were cut from the center and the edge of each panel to determine

cross-sectional density and moisture profiles. A commercial x-ray densitometer was used for the density profile measurements. The samples for the moisture content measurements were immediately sub-divided into five or six slices parallel to the panel surface and put into plastic bags to avoid further moisture changes.

Table B.1. Positions of temperature (T) and gas pressure (P) probes as well as mat dimensions in mm for batch press trials 1 to 4. Coordinates and numbering are used as specified in Figure B.1. The x-positions for panels 2 to 4 corresponded closely to those for panel 1 and were therefore not measured.

	Panel 1			Panel 2			Panel 3			Panel 4		
	x	y	z	x	y	z	x	y	z	x	y	z
T1	1130	660	20		660	23		660	17		665	10
T2	1155	660	34		660	32		660	30		665	34
T3	1100	710	top	1030	630	top	1160	700	top	1150	650	top
T4	1150	660	bottom	1210	670	bottom	1100	680	bottom	defective		
T7	1030	170	20		85	17		160	21		160	16
P1	1180	660	20		660	23		660	32		665	10
P2	1155	660	34		660	24		660	25		665	15
P5	1270	500	23		500	20		500	22		500	15
P6	defective				340	21		330	18	defective		
P7	1030	180	20		160	20		160	22		160	16
Size:	2300	1330	295	2300	1350	295	2250	1370	290	2300	1350	295

The laboratory batch press was operated in position control mode. The pressing cycle was the only parameter that was specifically varied between the four trial measurements. All panels were pressed to a target thickness and density of 39 mm and 700 kg/m<sup>3</sup>, respectively. For clarity, the recorded courses of platen position and pressing pressure are displayed together with the results of the internal temperature and gas pressure measurements. The target platen temperature was 190°C; actual temperatures varied between 186°C and 192°C.

## RESULTS

The results of the temperature and gas pressure measurements, together with the pressing schedules, are displayed in Figure B.2 to Figure B.5. Platen positions and pressing pressures (upper charts) are averaged over the readings at the two pressing pistons of the press. In trial 1, between 50 and 100 seconds, the maximum pressing pressure was reached (limited by the press hydraulics); during this period the pressing pressure dictated the platen position. The press was opened gradually in trials 1, 2 and 4 to allow the internal gas to escape slowly; only in trial 3 did a defect in the press control system lead to a sudden opening of the press, evident in steep gas pressure and temperature drops.

In all trials panels with pronounced cross-sectional density profiles were produced, with density maxima near the surfaces above  $1150 \text{ kg/m}^3$  and relatively low core densities. The most extreme profile, measured for trial 1 (maxima  $1240 \text{ kg/m}^3$ , core density  $450 \text{ kg/m}^3$ ), was caused by the particular pressing cycle chosen for this trial, e.g., rapid consolidation to target thickness. The core density was highest in trial 3 with approximately  $600 \text{ kg/m}^3$ .

Moisture content values, averaged over all samples of one panel, varied between 4.5 % (trials 1 and 2) and 4.9 % (trial 3). The lowest values were measured at the surfaces (1.9 % to 3.0 %), the highest for the core slices (8.3 % to 9.8 %).

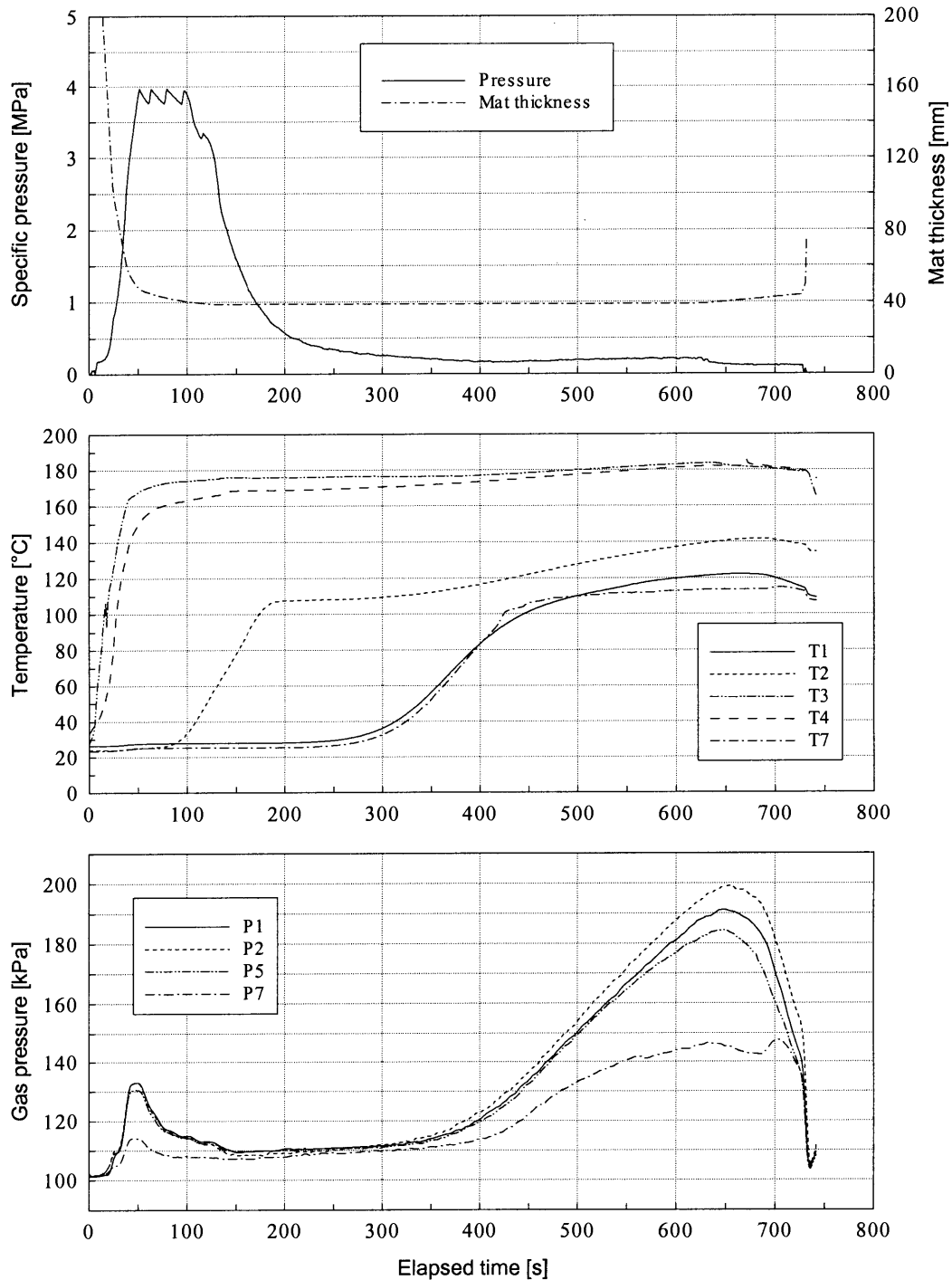


Figure B.2. Pressing pressure, mat thickness, internal temperature and gas pressure, measured for batch press trial 1.

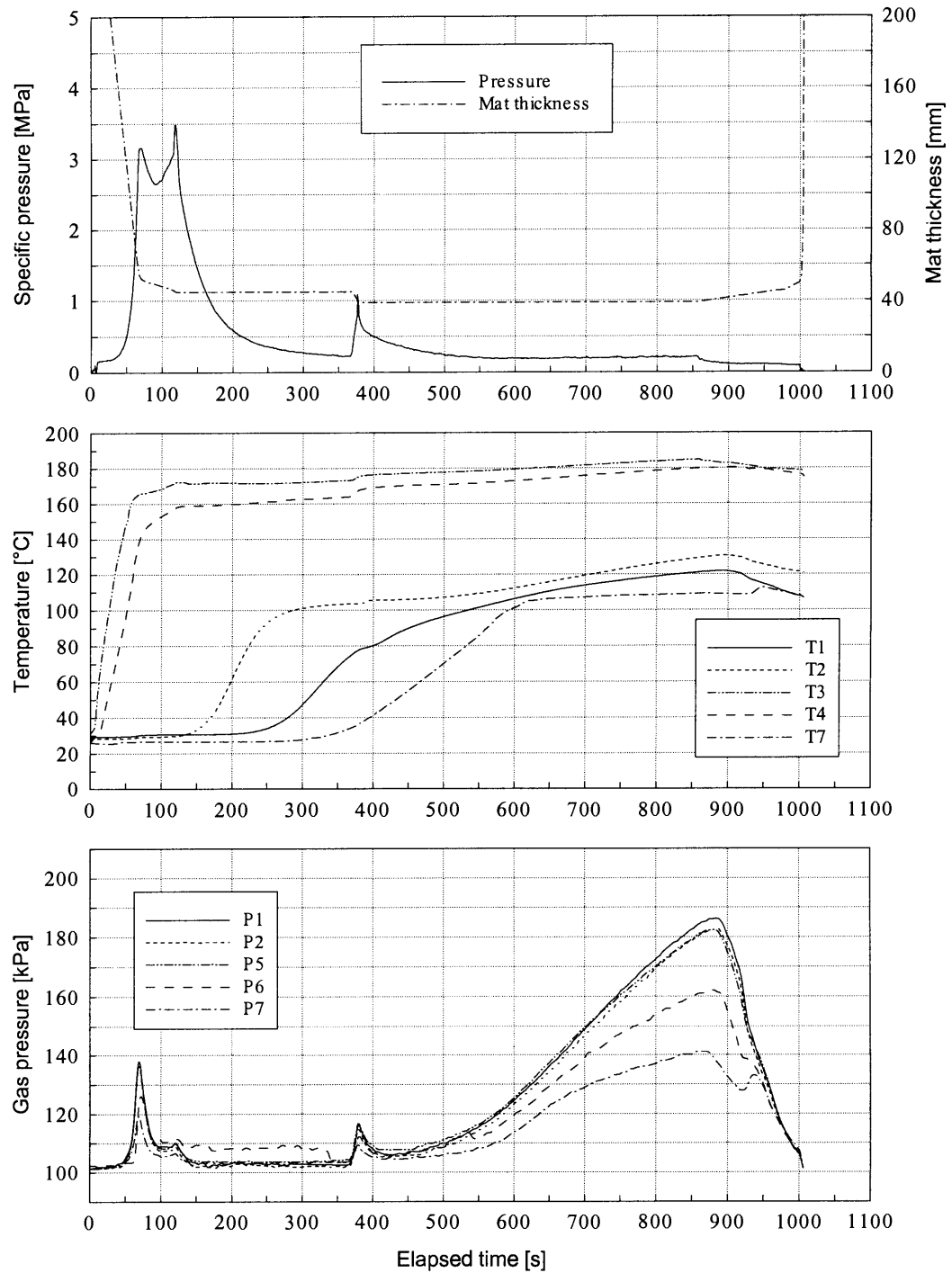


Figure B.3. Pressing pressure, mat thickness, internal temperature and gas pressure, measured for batch press trial 2.

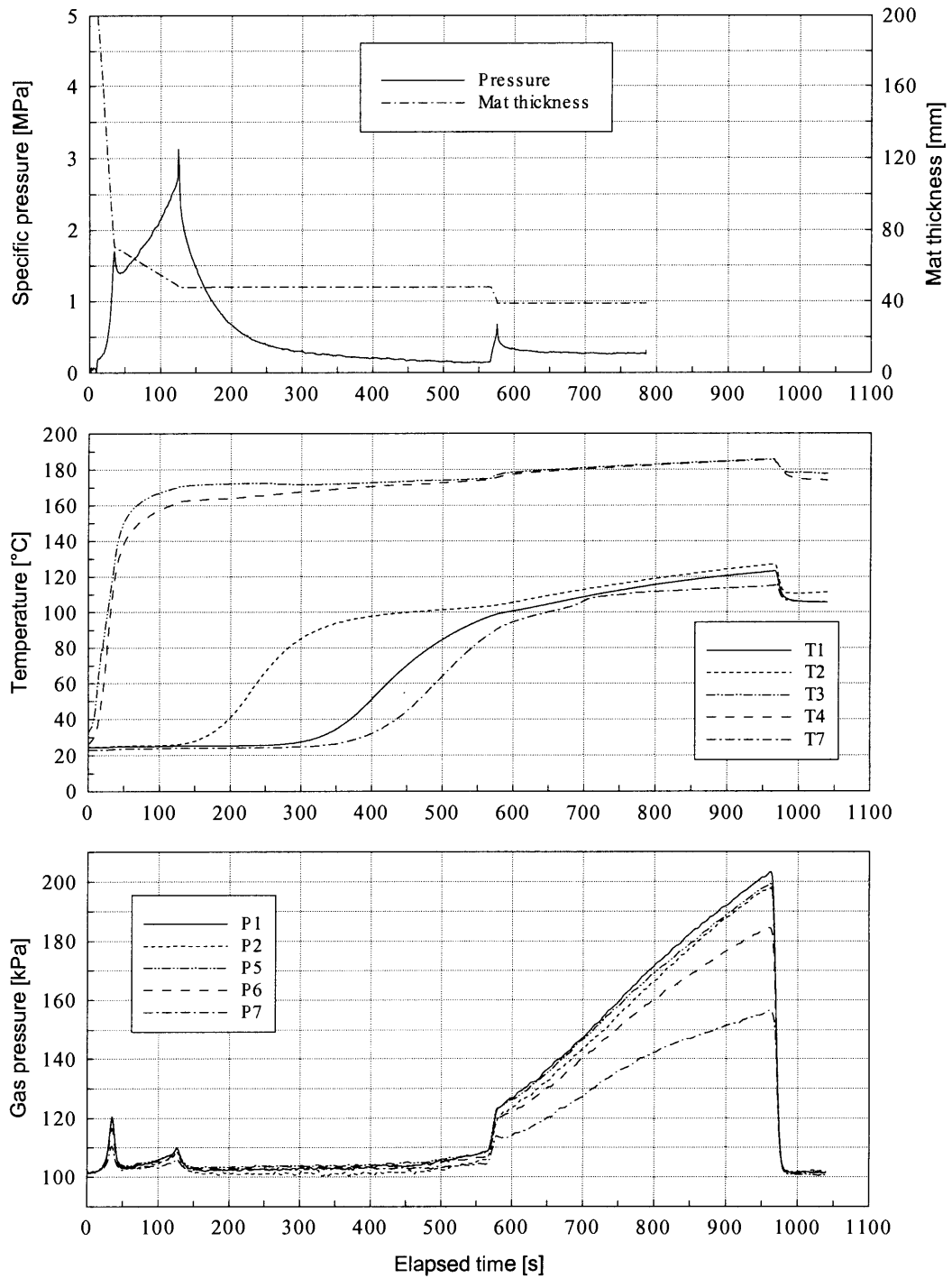


Figure B.4. Pressing pressure, mat thickness, internal temperature and gas pressure, measured for batch press trial 3.



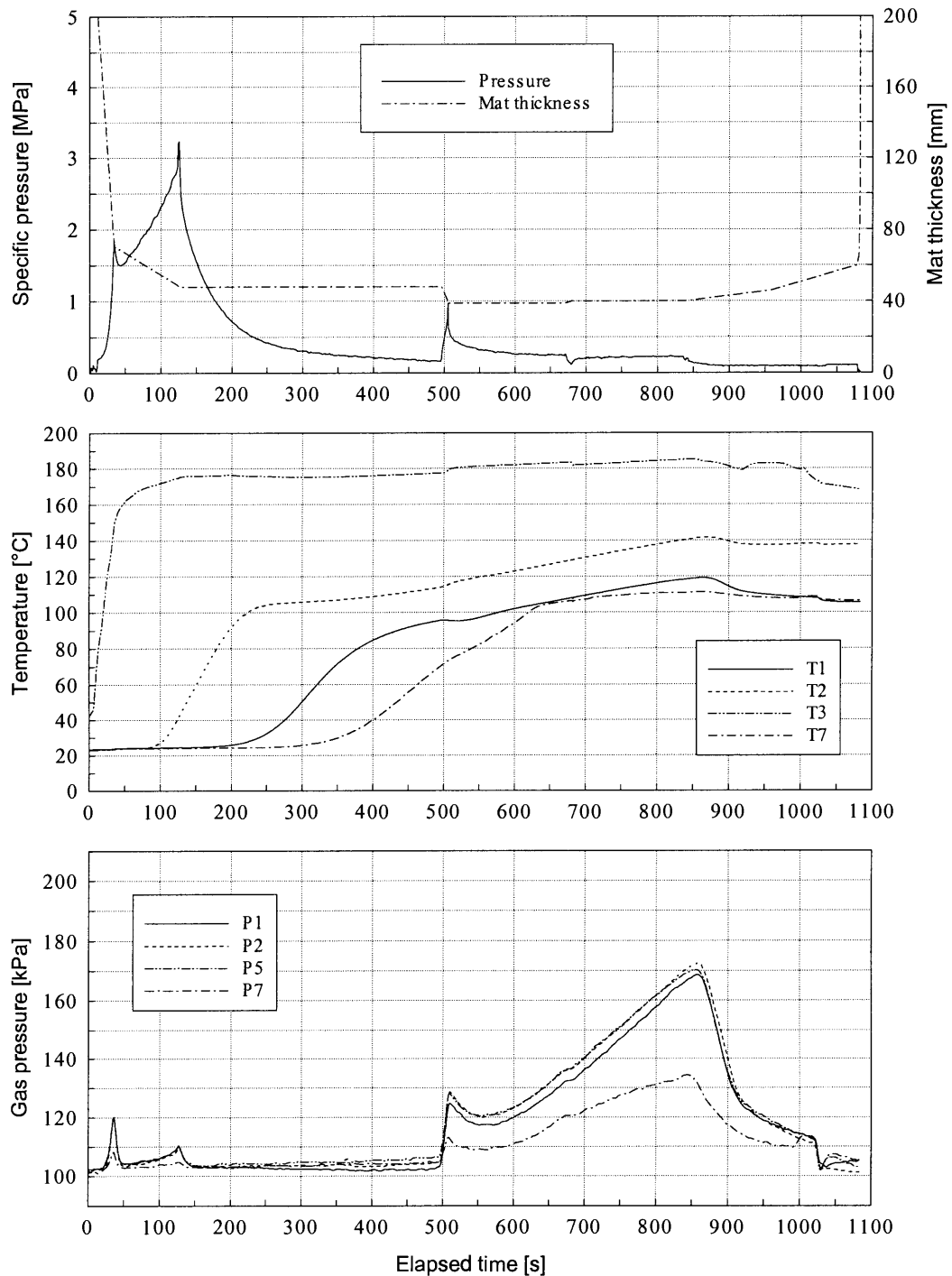


Figure B.5. Pressing pressure, mat thickness, internal temperature and gas pressure, measured for batch press trial 4.

## APPENDIX C

### MEASUREMENTS IN AN INDUSTRIAL CONTINUOUS PRESS

#### MATERIAL AND METHODS

A series of four trial measurements was conducted in order to determine temperature and gas pressure developments in fiber mats during MDF pressing in an industrial continuous press. Part of the results has been published (Steffen et al. 1999).

Wood chips (90 % softwoods, 10 % hardwoods) were disintegrated in a refiner (digester pressure 7.5 bar), adhesive (urea-formaldehyde) was applied to the fiber material, it was dried, formed to a 2.3 meter wide mat and condensed in a pre-press. The moisture content of the mat prior to hot pressing was approximately 9.6 %. The fiber mat was then consolidated in a 28-meter continuous press (Siempelkamp, ContiRoll). Pressing conditions as they prevailed during trial 3 are displayed in Figure C.1. The pressing conditions were similar for the other three trials. Only some parameters deviated from those in trial 3, the most important of which are listed in Table C.1. The mat was pressed to a raw panel thickness and density of about 20.5 mm and 780 kg/m<sup>3</sup> to 800 kg/m<sup>3</sup>, respectively.

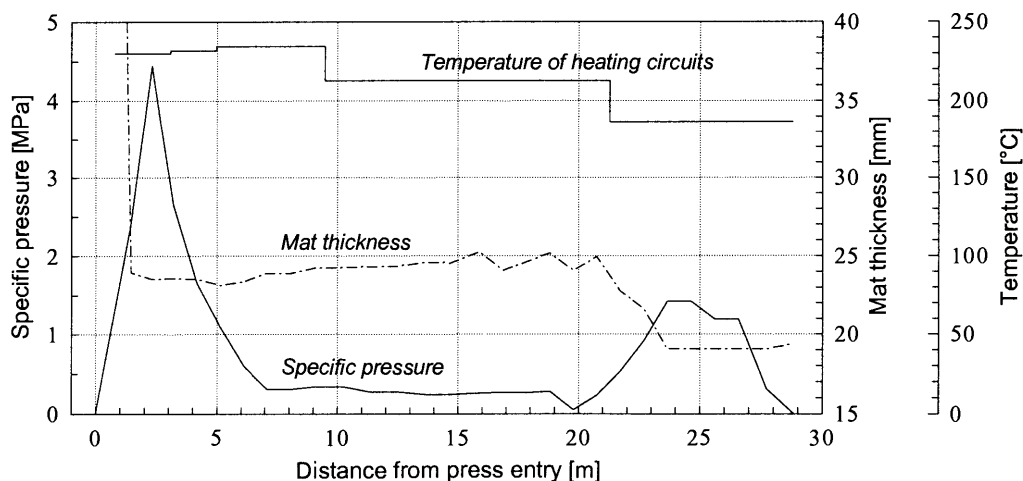


Figure C.1. Pressing conditions that prevailed during continuous press trial 3.

Between pre-press and hot press, an air-filled stainless steel tube with an outside diameter of 2.0 mm was inserted from the edge into the mat. The lengths of the tubes and cross-sectional positions varied among the trials, as given in Table C.1. The tube was attached to a small insulated pressure transducer (measurement range 0 to 7 bar), that passed through the press while lying beside the mat. The temperature compensation of the transducer covered a range from 20°C to 80°C. A heat resistant cable linked the pressure transducer to the power supply and the data acquisition system that was placed near the press entry.

A thermocouple was connected to the tip of the steel tube; two additional thermocouples recorded the temperature at the upper mat surface and inside the insulation case of the pressure transducer. The tip of the thermocouple positioned at the mat surface was covered with epoxy to avoid direct steel belt contact.

Table C.1. Some pressing conditions and positions of probes for continuous press trials 1 to 4.

	Trial 1	Trial 2	Trial 3	Trial 4
Feed speed [mm/s]	111		129	
Temperature heating circuits	≈ 10°C below trial 3		see Figure C.1	
Belt temperature press entry [°C]	127		132	
Tube length [cm]	90			50
Tube position from surface [mm]	11	6	11	

## RESULTS

The temperature development at the three measurement points, e.g., inside the mat, at the mat surface and at the pressure transducer, together with the internal gas pressure readings, are summarized in Figures C.2 to C.5 for each of the measurement trials. Noticeable is the pronounced gas pressure maximum of about 1 bar above atmospheric pressure near the press entry, caused by the compression of air trapped in the mat, and the relatively slow gas pressure decline following.

Inaccuracies in gas pressure readings are likely to be the reason for the drop below atmospheric pressure at the press outlet. Shortcomings in temperature compensation of the pressure transducer or condensation effects inside the steel tube and the transducer may have caused these inaccuracies. Still, the results of these measurements provide important information about the internal mat conditions during pressing of wood-furnish mats in a continuous press, the more so as internal gas pressure measurements in this type of process have not been published before.

Four samples of  $50 \times 50 \text{ mm}^2$ , distributed over one half of the width of the final panel, were prepared for each of the trials, and the cross-sectional density profiles of the samples were measured using a commercial x-ray densitometer. All samples tested showed similar density profiles: The density maxima near the panel's surfaces reached  $1000 \text{ kg/m}^3$  to  $1100 \text{ kg/m}^3$ , and core densities of approximately  $700 \text{ kg/m}^3$  were measured. Furthermore, distinct shoulders halfway between surface and central plane were recognizable on most of the samples tested, whereas the inner one-third of the samples showed relatively flat density distributions.

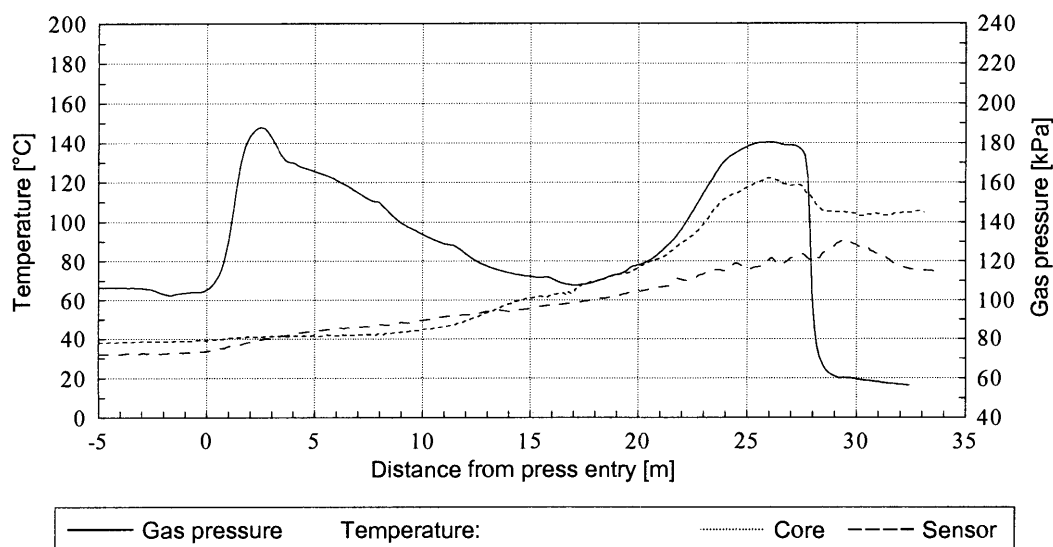


Figure C.2. Absolute gas pressure inside the mat and temperatures, measured at two positions, for continuous press trial 1.

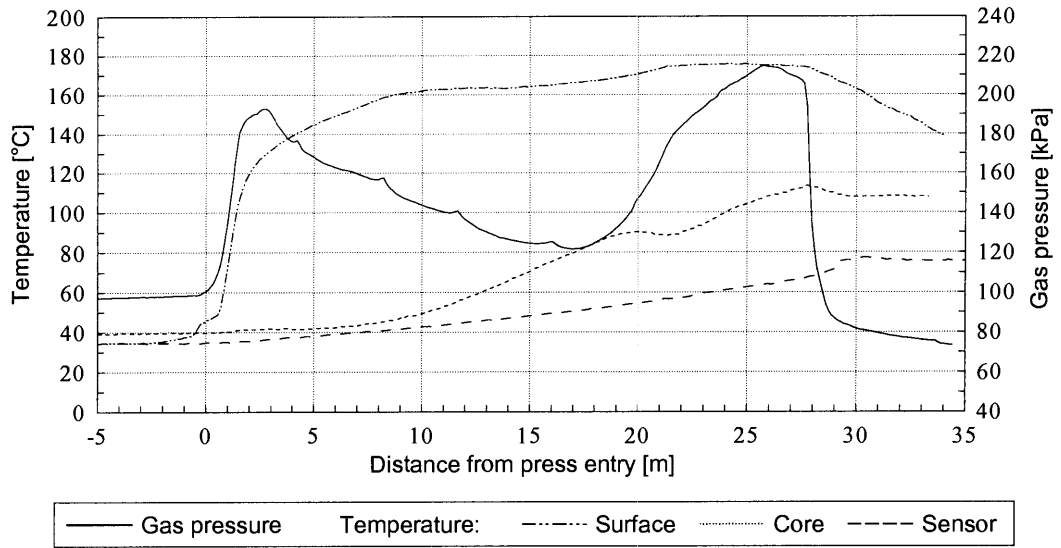


Figure C.3. Absolute gas pressure inside the mat and temperatures, measured at three positions, for continuous press trial 2.

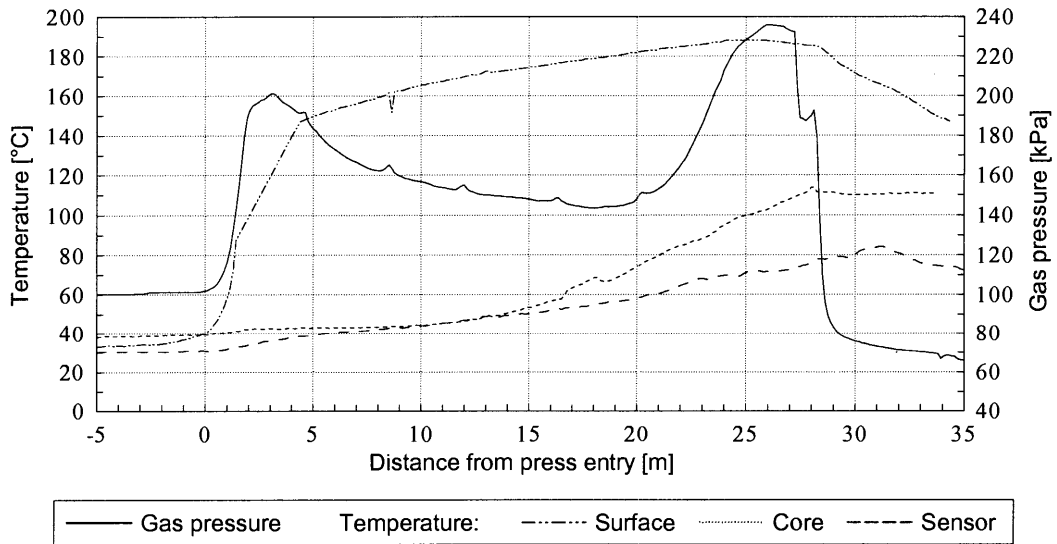


Figure C.4. Absolute gas pressure inside the mat and temperatures, measured at three positions, for continuous press trial 3. Erratic temperature readings at the surface between 1.5 and 4.5 m have been replaced by interpolated values.

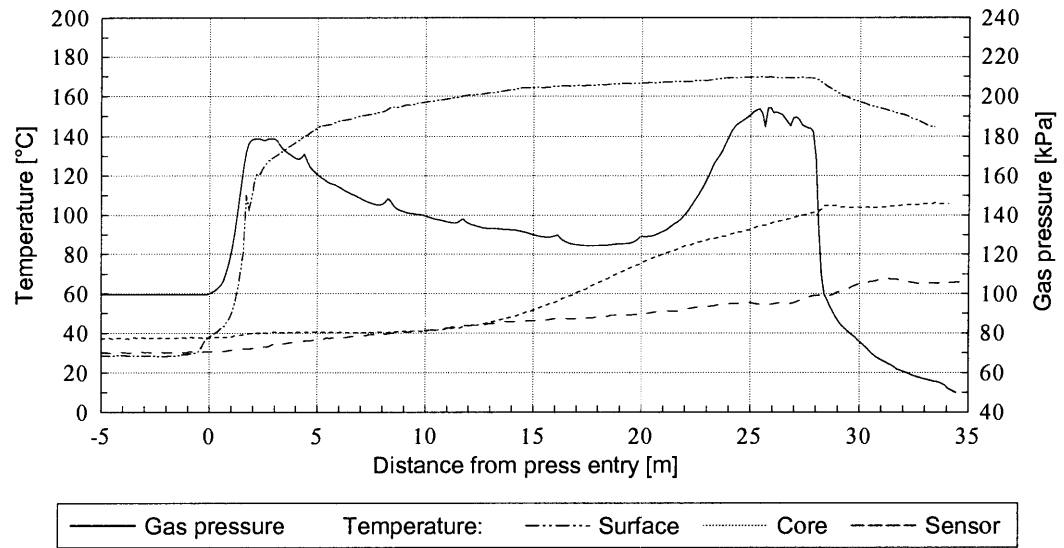


Figure C.5. Absolute gas pressure inside the mat and temperatures, measured at three positions, for continuous press trial 4.

## APPENDIX D

### DERIVATION OF CONSERVATION EQUATIONS

#### MASS CONSERVATION EQUATION

The mass conservation equation for water vapor within a porous hygroscopic material will be derived here. The simpler mass conservation equation for dry air has a similar form, except that the generation term becomes zero. In a general form, the mass balance for water vapor on a differential volume element of dimension  $V = \Delta x \Delta y \Delta z$  may be written as:

$$(\text{input}) - (\text{output}) + (\text{generation}) = (\text{accumulation})$$

or:

$$(\Delta y \Delta z \Delta t \cdot j_x|_x - \Delta y \Delta z \Delta t \cdot j_x|_{x+\Delta x} + \dots - \dots) + V \cdot \Delta t \cdot m_{ev} = m|_{t+\Delta t} - m|_t$$

where the expression within the brackets contains the fluxes  $j$  in the directions of all three coordinates. The variables  $t$ ,  $m_{ev}$  and  $m$  denote time, evaporation rate and mass of vapor, respectively. Dividing by  $V$  and  $\Delta t$ , and writing the equation in its differential form, we get:

$$-\nabla \cdot j + m_{ev} = \frac{1}{V} \frac{\partial m}{\partial t}$$

If the gas within the porous material is supposed to be an ideal mixture of perfect gases, then the ideal gas law  $pV_{eff} = \frac{m}{M}RT_{abs}$  relates the vapor mass  $m$  within the void volume of the material,  $V_{eff}$ , to the prevailing partial vapor pressure  $p$  and absolute temperature  $T_{abs}$ .  $M$  is the molecular mass of vapor and  $R$  is the gas constant. Substituting

$m = \frac{pV_{eff}}{T_{abs}} \frac{M}{R}$  into the previous equation yields:

$$-\nabla \cdot j + m_{ev} = \frac{M}{R} \frac{1}{V} \frac{\partial}{\partial t} \left( \frac{pV_{eff}}{T_{abs}} \right)$$

Applying the relationship  $\phi = \frac{V_{eff}}{V}$ , where  $\phi$  is the void fraction of the porous material, this equation may be written as:

$$-\nabla \cdot j + m_{ev} = \frac{M}{R} \frac{\partial}{\partial t} \left( \frac{p\phi}{T_{abs}} \right)$$

Differentiation with respect to  $t$  on the right hand side yields:

$$-\nabla \cdot j + m_{ev} = \frac{M}{R} \left[ \frac{1}{T_{abs}} \frac{\partial(p\phi)}{\partial t} - \frac{p\phi}{T_{abs}^2} \frac{\partial T_{abs}}{\partial t} \right] = \frac{M}{RT_{abs}} \left[ p \frac{\partial \phi}{\partial t} + \phi \frac{\partial p}{\partial t} - \frac{p\phi}{T_{abs}} \frac{\partial T_{abs}}{\partial t} \right]$$

Multiplying with  $R$  and  $T_{abs}$ , and dividing by  $M$  gives:

$$-\frac{RT_{abs}}{M} \nabla \cdot j + \frac{RT_{abs}}{M} m_{ev} = p \frac{\partial \phi}{\partial t} + \phi \frac{\partial p}{\partial t} - \frac{p\phi}{T_{abs}} \frac{\partial T_{abs}}{\partial t}$$

After rearranging the terms, the equation may be written in its final form:

$$-\frac{RT_{abs}}{M} \nabla \cdot j - p \frac{\partial \phi}{\partial t} + \frac{p\phi}{T_{abs}} \frac{\partial T_{abs}}{\partial t} + \frac{RT_{abs}}{M} m_{ev} = \phi \frac{\partial p}{\partial t}$$

The mass conservation equation for dry air has the same form, except that the term  $\frac{RT_{abs}}{M} m_{ev}$  is zero, as no air is generated or expended within the volume element.

## HEAT CONSERVATION EQUATION INCLUDING TRANSFER OF SENSIBLE HEAT

The governing equation for heat transfer derived in this section accounts for conductive and convective heat transfer. The latter mechanism includes both the transport of sensible heat as well as changes in heat energy due to phase change. In a general form, the heat balance on a differential volume element may be written as:

$$(\text{input}) - (\text{output}) + (\text{generation}) = (\text{accumulation})$$

The input and output terms account for energy flow through the faces of the volume element. This includes the conductive heat flux  $q$  and that share of the convective heat flux that results from the transport of sensible heat,  $q_{sens}$ . The generation term has to account both for the liberation or consumption of latent heat due to phase change, as well



as for the change of internal energy due to differences in specific heat  $c$  of bound water and water vapor.

The energy balance for the volume element of dimension  $V = \Delta x \Delta y \Delta z$  may be written as:

$$\begin{aligned}
 & (\Delta y \Delta z \Delta t \cdot q_x|_x - \Delta y \Delta z \Delta t \cdot q_x|_{x+\Delta x} + \dots - \dots) \\
 & + (\Delta y \Delta z \Delta t \cdot q_{sens,x}|_x - \Delta y \Delta z \Delta t \cdot q_{sens,x}|_{x+\Delta x} + \dots - \dots) \\
 & - V \cdot \Delta t (H_v m_{ev} + (c_b - c_v) T \cdot m_{ev}) \\
 & = Q|_{t+\Delta t} - Q|_t
 \end{aligned} \tag{D.1}$$

where the expressions in the first and second brackets contain the heat fluxes in the directions of the three coordinates. The variables  $T$ ,  $H_v$  and  $m_{ev}$  in the generation term are respectively the temperature, the latent heat of sorption from the vapor to the bound water state, and the evaporation rate. The subscripts  $w$ ,  $b$ ,  $v$  and  $a$  denote the four components dry wood, bound water, water vapor and air. The right hand side of this equation describes the change in total internal energy  $Q$  during a small time interval  $\Delta t$ .

Dividing by  $V$  and  $\Delta t$ , and writing the equation in its differential form, yields:

$$-\nabla \cdot q - \nabla \cdot q_{sens} - H_v^\circ m_{ev} = \frac{1}{V} \frac{\partial Q}{\partial t}$$

where  $H_v^\circ$  is defined by  $H_v^\circ = H_v + (c_b - c_v)T$ . Applying the relationships

$Q = \sum_{i=w,b,v,a} (c_i m_i T)$  and  $q_{sens} = \sum_{i=v,a} (c_i j_i T)$ , the equation may be written in the form:

$$-\nabla \cdot q - \nabla \cdot \sum_{i=v,a} (c_i j_i T) - H_v^\circ m_{ev} = \frac{1}{V} \frac{\partial}{\partial t} \sum_{i=w,b,v,a} (c_i m_i T)$$

Defining the mass content of component  $i$  as  $u_i = m_i / m_w$  and the density of dry wood as  $\rho_w = m_w / V$ , the equation may be written in its final form:

$$-\nabla \cdot q - \nabla \cdot \sum_{i=v,a} (c_i j_i T) - H_v^\circ m_{ev} = \rho_w \frac{\partial}{\partial t} \sum_{i=w,b,v,a} (c_i u_i T) \tag{D.2}$$

## SIMPLIFIED HEAT CONSERVATION EQUATION

A simplified heat conservation equation is derived here, utilizing the fact that the mass of the gas within the void system of the wood-furnish material is relatively small compared to the mass of solid cell wall substance and bound water. Again, the starting point is Equation (D.1); its right hand side may be expressed as:

$$\Delta Q = \sum_{i=w,b,v,a} (c_i m_i) \Delta T$$

where  $c_i$  and  $m_i$  denote the values for specific heat and mass, respectively, of each component in the system, averaged over the small time interval  $\Delta t$ . According to this notation, the energy content of the volume element is related to temperature changes only. Such a formulation of the right hand side requires that the term  $(c_b - c_v) T m_{ev}$  on the left hand side of Equation (D.1) has to be dropt.

Now, two important simplifications are made. First, the amount of energy required to change the temperature of the gas is negligible, since the mass of the gas within the pore spaces is much smaller than the mass of dry wood and bound water. Then:

$$\sum_{i=w,b,v,a} (c_i m_i) \approx (c_w m_w + c_b m_b) = c_u m_u .$$

Here,  $c_u$  and  $m_u$  are specific heat and mass, respectively, of the cell wall material at current moisture content. The second assumption made is that the transfer of sensible heat associated with the gas flow (which is the expression in the second bracket of Equation (D.1)) is neglected.

Considering the above, Equation (D.1) may be written in the following form:

$$(\Delta y \Delta z \Delta t \cdot q_x \Big|_x - \Delta y \Delta z \Delta t \cdot q_x \Big|_{x+\Delta x} + \dots - \dots) - V \cdot \Delta t (H_v m_{ev}) = c_u m_u (T \Big|_{t+\Delta t} - T \Big|_t)$$

Dividing by  $V$  and  $\Delta t$ , and writing the equation in its differential form, we get the final simplified heat conservation equation:

$$-\nabla \cdot q - H_v m_{ev} = c_u \rho_u \frac{\partial T}{\partial t} \tag{D.3}$$

where  $\rho_u$  denotes the density of wood at current moisture content. Equation (D.3) has been derived using Equation (D.1) as a starting point. However, it can also be derived from Equation (D.2) when applying the respective assumptions.



## APPENDIX F

Table F.1. Constants for Equations 3.62 and 3.65 for fiber mats presented by von Haas (1998).

Temperature [°C]	Moisture content [%]			
	0	5	10	14
<b>Constant <i>a</i></b>				
20	1.28E-06	1.55E-06	9.60E-07	8.64E-07
50	3.41E-06	3.60E-06	2.43E-06	1.92E-06
80	3.47E-06	1.72E-06	3.59E-06	1.01E-06
110	3.40E-06	2.50E-06	1.13E-07	7.33E-07
140	2.68E-06	1.18E-06	4.27E-08	2.15E-08
190	4.23E-06	3.53E-05		
<b>Constant <i>b</i></b>				
20	2.38	2.35	2.38	2.38
50	2.23	2.2	2.23	2.25
80	2.22	2.3	2.13	2.28
110	2.21	2.2	2.54	2.22
140	2.26	2.25	2.64	2.71
190	2.14	1.58		